UPTEC W 23002
Examensarbete 30 hp
June 2023

UPPSALA UNIVERSITET

SLU

Characterization of Landscape Structures and Precipitation in relation to Flooding events in Pampa Deprimida

A Minor Field Study in Argentina

Linnea Svärd

Civilingenjörsprogrammet i miljö- och vattenteknik

Abstract

The purpose of the thesis is to characterize flood events within the agricultural fields of flooding Pampa in Argentina. The characterization divides the flat landscape into flood prone areas and endeavour at linking driving factors to flood response based on past events. The characterization is based on information freely available from remote sensing (satellite images, digital elevation, and estimated rain data), from precipitation data from a weather station and from field measurements carried out with Universidad Nacional de La Plata. The main research question is: Which are the driving factors contributing to the flooding?

Data from remote sensing was used to visualize previous areal water extents, to calculate the topographic wetness index, the upslope areas for the field study sites and for a precipitation trend analysis. Furthermore, data from remote sensing was used to replace missing days of rain data from the weather station. The complemented rain data was compared with the water extent for the events. Relationships between event precipitation, previous precipitation, land-use, and surface runoff was evaluated with the Soil Conservation-Curve Number method, SCS-CN, and the runoff coefficients for different antecedent conditions were calculated. The precipitation data and the satellite images showing water extents were also used to calculate the 100-year and 20-year storm- and flood event. The measured infiltration capacity was used as input data in the SCS-CN-method to calculate the surface runoff and the measured soil moisture was used to verify results from the Topographic Wetness Index, TWI, map.

The flood risk areas are visualized with satellite images and the calculated Modified Normalized Difference Water Index. The TWI also visualizes the more flood prone or wetter areas and delineates the lower depressions where soil moisture was also measured to be higher, however not significantly. With the available satellite images within the study results indicate that floods are more common wintertime and that great flood events cannot be foreseen with only antecedent precipitation and event precipitation with the SCS-CN method. However, the events in the study with larger water extents, had high precipitation. No clear correlation between water extents from satellite images calculated by Instituto Nacional de Tecnología Agropecuaria, and estimated surface runoff from the SCS-CN method could be seen. However, the obtained runoff coefficients from the SCS-CN method can be used for estimating surface runoff for future storm events were higher Antecedent Moisture Condition, AMC, and low infiltration capacities increases surface runoff. The infiltration capacity of the studied fields is approximately 16 mm/hour and hence not alone a driving factor causing inundation since the soil can absorb, for example, a 20-year storm event of 125 mm/day. However, that is not the case since a 20-year storm flood has covered 9 % of the area around Don Joaquin and El Amanecer with water. No seasonal precipitation trends can be seen in Punta Indio during the last 40 years analysing precipitation data from remote sensing.

In flooding Pampa the agricultural fields inundate almost on yearly basis in the depressions due to the gentle slopes and high intense precipitation (yearly maximum daily precipitation is always higher than 60 mm/day). To decrease the flood risk the management should ensure high vegetative cover which increases infiltration and balances the hydrological responses.

Key words: Pampeana hydrology, flood risk mapping, runoff, infiltration, precipitation, SCS-CN, remote sensing

Department of Earth Sciences, Uppsala University. Villavägen 16, SE 752 36 UPPSALA

Referat

Syftet med studien är att karakterisera översvämningar inom jordbruket på Argentinska Pampas. Det platta landskapet mest översvämningsutsatta områden pekas ut och arbetet har fokuserat på att koppla landskapets utformning och regnmönster till översvämningarna. Karakteriseringen utgår ifrån information från satellitbilder och digitala höjddata, från nederbördsdata från den närmaste väderstationen som kompletterats med regndata från fjärranlyser och från fältmätningar utförda tillsammans med Universidad Nacional de La Plata. Den huvudsakliga frågan är: Vilka är de bidragande faktorerna till översvämningarna?

Information från fjärranalyser användes för att visualisera tidigare översvämningar, för att beräkna det topografiska fuktighetsindexet, tillrinningsområdet för fältstudieplatserna och för en nederbördstrendanalys. Regndatan jämfördes med vattenarean under tidigare översvämningar. Sambanden mellan nederbörd, markanvändning och ytavrinning utvärderades med Soil Conservation-Curve Number metoden, SCS-CN, och avrinningskoefficienterna för olika nederbördsförhållanden beräknades. Nederbördsdata och satellitbilder som visar vattnets utbredning användes också för att beräkna magnituden av ett 100-årsregn och 20-årsregn samt utbredningen av en 100-årsöversvämning. Den i fält uppmätta infiltrationskapaciteten användes som indata i SCS-CN-metoden för att beräkna ytavrinning och den i fält uppmätta markfuktigheten för att verifiera resultat från GIS-analysen av det topografiska fuktighetsindexet.

Översvämningsriskområden visualiserades i studien med satellitbilder och det modifierade normaliserade differens vattenindexet. Även det topografiska fuktighetsindexet visualiserar de mer översvämningsbenägna områdena och markerar vattnets väg där markfuktigheten också uppmättes vara högre, dock inte signifikant blötare än ovan liggande punkter. Analys av de tillgängliga satellitbilderna i studien visar att översvämningar är vanligare vintertid och att stora översvämningshändelser inte kan förutses enbart med de senaste dagarnas regnmängd och eventregnet med SCS-CN-metoden. Alla satellitbilder i studien med större vattentäckning kunde dock kopplas till stora regnmängder. Ingen tydlig korrelation mellan vattenutbredningen och uppskattad ytavrinning med SCS-CN-metoden kunde ses. De erhållna avrinningskoefficienterna från SCS-CN-metoden kan dock användas för att uppskatta risken för ytavrinning vid framtida regn där större regnmängder och låg infiltration ökar ytavrinningen. Fältens infiltrationskapacitet är cirka 16 mm/timme och därmed inte ensamt en drivande faktor till översvämningarna eftersom infiltrationskapaciteten är högre än exempelvis ett 20-årsregn (125 mm/dygn). Dock kan 20-årsregn täcka 9 % av området runt Don Joaquin och El Amanecer med vatten. Inga nederbördstrender kan ses i Punta Indio under de senaste 40 åren genom analys av nederbördsdata från fjärranalyser.

I Pampa deprimida översvämmar jordbruksfälten nästan årligen i sänkorna på grund av den platta topografin och den höga intensiva nederbörden (den årliga maximala dagliga nederbörden är nästan alltid högre än 60 mm/dag). För att minska översvämningsriskerna bör lantbrukare säkerställa en hög vegetativ täckning som ökar infiltrationen, skyddar marken och balanserar de hydrologiska reaktionerna.

Nyckelord: Hydrologi på Pampas, kartläggning av översvämningsrisker, avrinning, infiltration, nederbörd, SCS-CN, fjärranalys

Institutionen för Geovetenskaper, Uppsala universitet. Villavägen 16, 752 36 UPPSALA

Resumen

El propósito de la tesis es analizar los posibles eventos de inundación en un sector de la Pampa Deprimida en Argentina, dada la importancia productiva de la región. Se trabajó en los campos de la Universidad Nacional de La Plata con la dirección del curso de Edafología, de la Facultad de Ciencias Agrarias y Forestales. Se caracterizó la región en general y los campos en particular, utilizando información de acceso gratuito en la web, tales como imágenes satelitales, mapas de elevación digital e información meterologíca.

Se utilizaron técnicas geomáticas para definir la evolución de agua en superficie mediante un análisis de la precipitación y coberturas de agua en imágenes satelitales obtenidas entre el 2000 y 2022 con la finalidad de calcular el Indice de Humedad Topográfico (TWI). Se establecen relaciones entre la precipitación, el manejo de los campos, la escorrentía superficial y las cuberturas de aguas. Se analizó la occurrencias de eventos de excesos hídricos. Se efectuaron ensayos de infiltración y el método Soil Conservation Service-Curve Number (SCS-CN) a fin de estimar la escorrentía superficial y las medidas de la humedad del suelo para verificar los resultados del mapa con el TWI.

Las imágenes satélitales y el Modified Normalized Differential Water Index (MNDWI) calculado, permiten estimar las áreas más expuestas a inundaciones. El TWI permitió distinguir los sectores más altos y bajos mediante la medición de la humedad del suelo. Con los datos disponibles en este estudio, los resultados indican que las inundaciones son más frecuentes en invierno, y que los grandes eventos de inundación no se pueden predecir solo con registros de precipitación y el uso del método SCS-CN. No se pudo observar una correlación entre las extensiones de agua de las imágenes satelitales calculadas por Instituto Nacional de Tecnología Agropecuaria (INTA Clima y Agua, Castelar), y la escorrentía superficial estimada por el método SCS-CN. Sin embargo es possible encontrar una correspondencia entre las precipitaciones muy elevadas y la cobertura de agua. La occurencia de altas precipitaciones luego de un periodo lluvioso en un suelo con baja infiltración debido a una baja cobertura vegetal, aumenta la escorrentía superficial. La capacidad de infiltración del campo estudiado es de aproximadamente 16 mm/hora y un evento de lluvia extrema que se produce cada 20 años puede ser de 125 mm/día. Consecuentemente, no sería la baja infiltración la principal causa de la inundacion. No obstante, se aprecia que effectivamente un evento de 125 mm/día cubre 9 % del área en Don Joaquín y del El Amanecer. Con precipitaciones normales la cobertura es de aproximadamente 2 %. Cabe indicar que las precipitaciones registradas en la estación de Punta Indio durante los últimos 40 años, no manifiestan un comportamiento diferente en su occurencia y cantidad.

En Pampa deprimida los campos se inundan frecuente, no solo debido a las precipitaciones locales y el amabiente de muy bajas pendientes. Los flujos de agua subterranea, aunque no se las pudo analizar en este estudio, también afuectuan las coberturas de agua. A fin de disminuir los riesgos de inundación, el manejo debe garantizar una alta cobertura vegetal que aumente la infiltración y proteja al suelo y, de este modo, contribuir a controlar la natural dinámica hidrológica de la región en estudio.

Palabras claves: Hidrología de la Pampa Deprimida, cartografía del riesgo de inundaciones, escorrentía, infiltración, precipitación, SCS-CN, sensores remotos

Preface

This thesis is a Minor Field Study founded by SIDA and the final part of the master's Programme in Environmental and Water Engineering at Uppsala University and the Swedish University of Agricultural Sciences. The thesis includes 30 Swedish academic credits and thanks to the scholarship which covers travels and accommodation, the thesis was conducted in Argentina in collaboration with the National University of La Plata, UNLP.

The supervisors were Abraham Joel from the Swedish University of Agricultural Sciences, at the Department of Soil and Environment, and Margarita M. Alconada-Magliano at the National University of La Plata, at the Faculty of Agricultural and Forestry. Thanks for making this possible!

The subject reviewer was Benjamin Fischer at Uppsala University, the Department of Earth Science. Thank you for all the advice and support!

Prefacio

Esta tesis se realizo en el marco de proyecto: *Estudio del suelo, agua subterránea y vegetación, como base para definir ambientes de manejo en el partido de Magdalena.*

Proyecto Código:11A/360. 2021-2025.

Dirección: M M Alconada Magliano.

Codirección: A.V. Carbone.

Facultad de Ciencias Agrarias y Forestales, Universidad Nacional de La Plata.

Este trabajo se realiza con información recopilada por el INTA, Instituto Nacional de Tecnología Agropecuaria para el proyecto de referencia, y con la información obtenida en el sitio por diversas fuentes. Se contó para la interpretación de información y estudios de campo, con la colaboración de profesionales involucrados en el mencionado proyecto: Esteban Baridon, Federico Fernandez, Adrián Rodríguez Guiñazú, Barbara Novillo, Marco D Amico, Juan Vitale, Ariel German, Natalia Noemí Gattinoni, y especialmente a Margarita M. Alconada Magliano que hizo todo posible organizando y acompañandome en las activitades que posibiltaron la culminación de este estudio.

Agradesco entonces a todos ellos, así como, a mis amigos, familiares y a los argentinos en genereal por tener siempre una buena actitud y predisposición para ayudarme en todo momento.

Popular Scientific Summary

Pampas is the name of the fertile agricultural lands of central-eastern Argentina which produces and exports large quantities of meat and crops. The eastern part of the region, flooding Pampa, Pampa deprimida in Spanish, is characterized by a flat landscape, which frequently accumulates water due to the slow transportation of water in the fields with small slopes and the heavy precipitation. The inundations are problematic for the farmers and the whole country is affected by its destructive power.

It is of importance to analyse past flooding events, the landscape and precipitation patterns to reduce damages and foresee future floods. Instead of costly advanced modelling, freely available data from past floods can be used to produce reliable maps which marks areas with higher risk of inundation. Furthermore, how often, when, and during which conditions the floods occur is relevant information that can be obtained with *remote sensing.* Remote sensing data is for example gathered from satellites which uses sensors to obtain information about physical features on the earth's surface. Information about the terrain, precipitation, and images from the past and present are available almost globally for anyone.

More intense rainfall can lead to more devastating flood events in the future, analysing rain data is important to discover precipitation changes over time. The magnitude of overland flow of water, called surface runoff, due to storm precipitation also depend on the preceding precipitation. If the soil is saturated with water from heavy precipitation, the storm rainfall will cause more overland flow of water. Furthermore, overland flow depends on the management of the lands. Soils with high vegetative cover and soils with higher infiltration can absorb water faster.

Within the field study measurements were realized in Don Joaquín and El Amanecer, in Pampa Deprimida, to calculate how fast the water transports through the topsoil. The soil moisture was also measured to find differences in soil moisture between dates with different antecedent precipitation and different topologies. Elevation data from remote sensing was used to identify wetter spots in the landscape and the area which transports water to the two field study sites. Remote sensing data was further used to visualize flooding extents in maps from satellite images and to complement missing precipitation data from the closest weather station. The rain data was used combined with the local knowledge about the fields to estimate the overland flow for events. The estimated overland flow was compared to past events for which the flood extent and precipitation records were known. The rain data was also used to calculate the size of a 100-year storm event, which is a high precipitation event with only 1 % risk of occurrence every year. The same analysis was done to calculate the extent of a 100- year storm flood.

The produced maps from the analysis are based on two indices; the Modified Normalized Difference Water Index, the MNDWI, which shows the water extent in the area around the two field study sites and the Topographic Wetness Index, the TWI, which visualize where soil moisture is likely to be higher considering the topography and slopes of the fields. The upslope areas of the fields are relatively small and on the ridge of the basin to Río Samborombón, the floods are not as widespread in the studied fields as they are closer to the river Río Sambormobón. No clear relation was found between the area of earlier flooding extents, the soil moisture due to previous days precipitation or event precipitation for the selected events studied. However, an estimated correlation between surface runoff, previous

days precipitation and soil characteristics was found which can be used to forecast surface runoff for storm precipitation. Depending on the previous precipitation, if the soil moisture is dry, normal, or wet, 30 %, 60 %, or 80 % of the storm precipitation turns into surface runoff which affect plant growth. Results indicate that flooding is more common wintertime. The biggest flood since the start of the satellite programme covered almost 16 % of the land surface which is bigger than a 20-year flood event. However, the method for estimating direct runoff could not forecast such an event from the preceding conditions and the event rainfall.

The landscape of Pampa deprimida is frequently flooded and so it has been through generations. Whether inundations are more sever now than before is hard to tell from this study's precipitation analysis and flood extents from past events. However, as climate change is more likely to change precipitation patterns the soil´s resilience to overland flow must be strengthen. Therefore, it is important with proper rangeland management where soils are covered with protective vegetation that increases the infiltration, stops the rain drops from destroying the soil structure and holds some of the water back from reaching the ground in the canopy, so called interception. By halting overland flow, the vegetation evens out the water flow since the water is kept in the soil, as in a sponge, and decreases soil erosion and the degradation of rangelands. Proper land management can therefore reduce the risks linked to intense rainfall and reduce the risk of droughts as water is kept in the landscape.

Table of Contents

1. Introduction

Floods are the most frequent natural hazard worldwide (Farhadi *et al.*, 2021) and cause great economical losses (Awadallah and Tabet, 2015). These hydrological alternations are ones of the many processes that will affect the supply of food and water in the future and they are strongly affected by how humans manage and use their lands (Alconada-Magliano, 2021).

Depending on how climate change is tackled, and what management and implementations are made to adapt, the impacts on water resource systems will differ. According to the Intergovernmental Panel on Climate Change report, agricultural- and livestock-lands will be highly affected by climate change since they have sensible water regimes (Bruce, 2017). In Argentina, one of the primary industries is the agricultural and its related products is Argentina´s biggest exports. The agricultural sector is dependent on water resources, and during droughts and floodings the whole country's economy is affected by the decreased yield. Floods are the worst natural disasters in Argentina, however, the periods of water shortage is affecting the agriculture worse (OECD, 2019). The land-use and associated soil characteristics, influenced by the management, affect runoff and flood formations in agricultural landscapes. Certain land-use changes cause compaction of the layers in the soil which can decreases the grounds ability to prevent floods (Hümann *et al.*, 2011).

The Buenos Aires region in Argentina has been affected by both flooding and drought historically, see Figure 1. To deal with the periods of inundations drainage channels were constructed. However, during dry periods the plain grass lands, the *Pampas,* is left barren without vegetation, and the ranger's cattle is left with the few fields that still has some vegetation left. The drainage channels functionality is therefore questioned as it may lead to more severe droughts (Ameghino, 1884). Climate change in Argentina will affect agriculture more than any other sector due to its sensitivity to changes in water resources, and so it is for many other countries as well. It is probable that the damages caused by alternations in the water cycle, as droughts and floods, will accelerate since the ecosystem vulnerability increases as the ecosystems degrades (OECD, 2019).

Figure 1a) Flooding in General Guido, Province of Buenos Aires (Unknown, 2022). b) Drought in Don Joaquín, Province of Buenos Aires, around a water tank 22nd of April 2022 (Juan Vitale, INTA, 2022).

Hydrological droughts, in comparison to floods, are not as easy to quantify, but can be estimated in other ways. For example, droughts can be identified as when there is a lack of water in a hydrological system, as in waterways or when groundwater tables are lower than usual (Bruce, 2017). Droughts can be divided into groups and soil moisture drought is one of them which can lead to plant death. Within dry regions the mismanagement resulting in decreased plant cover, desertification, is getting more common. Desertification has similar symptoms as soil moisture droughts, however it is only caused by human activities (Van Loon, 2015).

Water saturated soil also have bad impacts on the yield in agricultural lands as it causes anoxic environments which stresses the roots and affect the transportation of nutrients to other parts of the plant. Water saturation can occur for natural reasons because of heavy precipitation and inefficient draining but also due to poor management practices (Herzog *et al.*, 2016). The poor management practice of for example keeping too many grazing animals can lead to uncovered soils with impermeable soil layers. This occur since the grazers consumes plants selectively and since they cause soil compaction by their trampling (Marteinsdóttir, Barrio and Svala Jónsdóttir, 2017). The vegetation cover has major impact on the topsoil's ability to infiltrate water. Raindrops falling on barren ground decreases the infiltration capacity of the soil since the force from the falling raindrops destroys the aggregated structure. This can create dry crusts on the surface which stops vegetation growth or cause layers that during wet condition have very low water permeability. Uncovered soils can therefore cause surface runoff with soil erosion as a result which also increases the risk of drought since water is transported away faster and not retained longer in the system (Alconada-Magliano, 2021).

In 2016 Argentina's National Water Plan was approved with the objective, among others, to prevent the hazardous consequences of floods. The necessity of early flood warnings systems is mentioned along with a wider irrigation system (OECD, 2019). Flood models require gauged systems. These models require discharge data from the waterways network and high-resolution topographic maps. Additionally, precipitation records containing information about rain depth and its intensity are needed for these hydraulic and hydrologic models. Within areas of less data availability models can be replaced by estimating and characterizing earlier events with free open-source data for frequency analysis and water extent. Available global flood detection systems (GFDS) can be used within basins where the lack of data prevents flood modelling. However, in rural and flatter areas it can underestimate the water extent compared to results from optical images (Awadallah and Tabet, 2015).

1.1 Rain Analysis

During the many years of floods in Argentina no correlation can be observed with annual total precipitation. However, it is the seasonal trends, as well as the frequency and intensity of the rainfall that are the interesting parameters for flood analysis (D'Andrea *et al.*, 2019). Problems in estimating flood events in the future are due to difficulties in predicting the intensity of the rainfall (Bruce, 2017) and the duration of storm events, which are important to consider for construction of safe urban water control (Hosseinzadehtalaei, Tabari and Willems, 2020).

How climate change is affecting the hydrology of the landscape by altering temperature, runoff, and precipitation, is of high relevance when planning for flood prevention. Therefore,

it is important to analyse changes and trends with time. Different tests exists with the purpose of finding trends over time, the Mann-Kendall test is one of them (Güçlü, 2018). When analysing trends in time series the seasonal and short term variations are diminished to find the long-term changes (Bergendal, Håstad and Råde, 1967).

During the last century the mean yearly precipitation increased overall in Argentina and according to climate models the precipitation will increase this century as well in the eastern parts of Argentina (Carter *et al.*, 2000). Until recently there were no modern precipitation trend analysis done within the fertile lowlands of Argentina, the Pampas. New studies based on station data has not found any significant trends in yearly precipitation within this important agricultural area (D'Andrea *et al.*, 2019). Models and predictions vary, and some models see decreasing precipitation trends in in the subtropic areas. The hydrological balance is mostly affected by precipitation patterns over longer scales. However, the flood frequency depends on variation in the intensity of the precipitation and on yearly alternations in rainfall. Even though the total annual precipitation might decrease in areas, extreme rainfall events are more likely to occur globally with climate change (Bruce, 2017).

1.2 Runoff

Flood extents in a basin and flood occurrence are dependent on the precipitation, both earlier precipitations stored in the soil and the event precipitation (Kim *et al.*, 2019). Water flows and inundations can arise from precipitation in other basins, as water follow hydrogeological paths (Alconada-Magliano, 2021). Studies has been carried out to investigate the relationship between flood frequency, Antecedent Moisture Condition (AMC) and precipitation frequency. The AMC is an indication of how moist the soil in a system is before an event. It has been shown that within a basin a rainfall event with 7-year return period can cause a 100-year flood if the soil is water saturated from previous rainfall, and therefore has high antecedent moisture conditions (Kim *et al.*, 2019).

How the precipitation and the landscape characteristics affects the runoff patterns within a basin is often expensive to estimate within ungauged systems and within gauged systems it can be problematic as well since continuous measurements of streamflow needs to be maintained (Arreghini *et al.*, 2007). Meanwhile, methods for estimating the runoff are necessary for the managements of watersheds (Parvez and Inayathulla, 2019). When the data availability is sparse but precipitation records are available, the AMC can be used with more simple methods to estimate the response runoff of storms (Gray and Burke, 1983). However, more reliable runoff results can be obtained if discharge data is available for calibration and if various rain gauges can be used to obtain a rainfall distribution over the basin (Arreghini *et al.*, 2007). Antecedent Rainfall, or antecedent moisture condition, is the total amount of rain fallen within one location five days before an event. It is divided into classes depending on the rain depth (mm/5-days) and the season. The classes are 1, 2 and 3 or more and if an event has a lower AMC class it means that it has rained relatively little before the event. During the vegetative growing season the AMC class criteria are higher (Gray and Burke, 1983). The criteria for the AMC class are defined in

Table *1* and the growing season is defined as the days with a daily mean temperature higher than 6 °C (De Paola, Ranucci and Feo, 2013).

Table 1: AMC classes (De Paola et al., 2013)

AMC Classes *	Vegetative dormant season	Vegetative growing season
I Drier soils *	<12.7 mm	<35.5 mm
II Normal conditions *	12.7-28.0 mm	35.5-53.3 mm
III Heavy rainfall *	>28.0 mm	>53.3 mm

* (Parvez and Inayathulla, 2019)

The surface runoff is also an important factor within e.g., hydrology, to assess flooding risks. Surface runoff differs from runoff as it only includes waterflow on the ground while runoff is the whole discharge from an area in a stream or in other waterways (Parvez and Inayathulla, 2019).

In Argentina runoff is usually estimated since discharge data from basins is unusual (Arreghini *et al.*, 2007). However, in an event-based study of a smaller basin in the Pampas, available discharge has been used to investigate the interacting factors causing runoff response. The study was based on past events and the relation between the surface runoff and the following factors were analysed: groundwater depth, erosion, vegetative cover, antecedent moisture condition, rainfall intensity, and formed rills acting as waterways created by soil erosion in wetter periods. The drainage network's fluctuation was visually interpreted with satellite data and other data was collected in field. Rainfall data was obtained from a station 5 kilometres away. The study found non-linear relationships between precipitation and surface runoff. They concluded that the hydrological response is a combined effect of various factors and the culmination of them. The greatest hydrological responses occur if they coincide. Furthermore, the study found that land-use changes upstream impact the runoff response downstream (Ares *et al.*, 2020).

1.2.1 Surface Runoff with the SCS-CN method

The Soil Conservation Service (SCS) has developed a method to calculate the direct runoff from storm events in catchments. The direct runoff is the runoff excluding the baseflow in a system and the term includes surface runoff and channel runoff. The method is called the *curve number runoff equation* (SCS-CN) (USDA-NRCS, 2019). The Curve Number (CN) is based on site-specific soil characteristics and the Antecedent Moisture Conditions classes (soil moisture) to estimate surface runoff from storm precipitation with curves. The characteristics used for the determination of the curve number is the hydrologic "soil group" determined by the infiltration capacity, the soil texture, and the land-use or land cover controlled by the management. The SCS-CN is widely used and appropriate for bigger watersheds (Parvez and Inayathulla, 2019). The obtained runoff can then be used for constructing hydrographs (USDA-NRCS, 2019) and also for simulation models (Soulis and Valiantzas, 2012).

The method aims at estimating the catchment's direct runoff response to storm precipitation where no runoff is generated for smaller events, and where the runoff response increases

almost linearly with precipitation. The following relationship derived by Victor Mockus fulfils the demands of such a relationship (USDA-NRCS, 2019), see Equation 1.

$$\frac{F}{S} = \frac{Q}{P} \qquad (1)$$

The runoff, Q (mm), is the water generated from a rain event, P (mm) with the possible retention of water in the system, S (mm), and the actual retention of water, F (mm).

The formula is then transformed by including an initial abstraction, I_a, of 20 % of the possible retention factor of water in the soil, S, which is related to the soil's characteristics. The initial abstraction is the part of the precipitation that never becomes direct runoff. This includes the processes of interception of water in canopies, initial infiltration, and surface depression storage. The water abstraction of interception depends on vegetation cover and so does the infiltration. The infiltration at the beginning of the storm depends on the intensity of the rainfall which affect the soil surface permeability, but also on soil moisture since initial infiltration rates are higher in unsaturated soils. The magnitude of the I_a of the system decides when a storm results in direct runoff, and when no runoff occurs (USDA-NRCS, 2019).

The relation between the considered parameters results in Equation 2, for all storm events where storm precipitation exceeds the initial abstraction, I_a.

$$Q\ (mm) = \frac{(P - 0.2S)^2}{P + 0.8S} \qquad (2)$$

With the curve number for the site of interest the surface runoff for a certain rainfall event can be estimated with graphs based on the National Engineering Handbook (USDA-NRCS, 2019), or it can be calculated by first calculating S with the formula in Equation 3. The 2.54 factor in the equation is the conversion from inches to millimetres and CN is the curve number.

$$S(mm) = \frac{25400}{CN} - 254 \qquad (3)$$

The SCS has determined 13 different land-use categories and four hydrologic soil groups to help determine the curve number for a site, see Table 2. The curve number is then adjusted after the antecedent soil moisture, the AMC classes. The curve number for AMC class II (normal conditions) are presented in Table 2, and the curve numbers for AMC class 1 and 3 are adjusted according to Equation 4 and Equation 5 (Parvez and Inayathulla, 2019).

$$CN_1 = \frac{CN_2}{2.281 - 0.01281CN_2} \qquad (4)$$

$$CN_3 = \frac{CN_2}{0.427 + 0.00573CN_2} \qquad (5)$$

CN_1, CN_2 and CN_3 are the curve numbers for AMC class 1, 2 and 3 respectively.

The four hydrological soil groups: A, B, C and D depend on the soil's infiltration rate (Parvez and Inayathulla, 2019). There are various ways of measuring the infiltration in the field where the most accurate trials demand larger areas of investigation where water is being ponded. However, large experiments are costly (Johnson, 1963) and an easier infiltration rate experiment can be conducted with a double ring infiltrometer (Eijkelkamp, 2015). Soils with

lower infiltration rates have higher direct runoff potential which in general gives these kinds of soil higher curve numbers in the evaluation, hence, more runoff. The soil groups are described like this (Parvez and Inayathulla, 2019):

Group A

These soils have high infiltration rates due to its texture even during wetter conditions. These soils are typically sands or gravel.

Group B

Soils categorized in the B group are not as well-drained as in Group A and possess somewhat finer textures.

Group C

These soils can have impermeable layers or consist of finer material which decreases the water transmission rate downwards. Soils of group C has slower infiltration rates during wet conditions.

Group D

Soils categorized as group D have very low infiltration rates for different reasons. For example soils with clay in the top layers, shallow groundwater tables or shallow soils with impermeable materials under.

Table 2: Curve numbers for SCS-CN method for AMC II (Parvez and Inayathulla, 2019).

Land-use	Hydrologic Soil Group			
	A	B	C	D
Agricultural land without conservation (Kharif)	72	81	88	91
Double crop	62	71	88	91
Agricultural Plantation	45	53	67	72
Land with scrub	36	60	73	79
Land without scrub (stony waste/rock outcrops)	45	66	77	83
Forest (degraded)	45	66	77	83
Forest Plantation	25	55	70	77
Grass land/pasture	39	61	74	80
Settlement	57	72	81	86
Road/railway line	98	98	98	98
River/Stream	97	97	97	97
Tanks without water	96	96	96	96
Tank with water	100	100	100	100

1.2.2 Runoff Coefficient

The runoff coefficient is commonly used to describe the hydrological response within catchments. The runoff coefficient is calculated by dividing the runoff by the rainfall, see Equation 6. The runoff coefficient, which also goes under many other terms, could either consider the event runoff following a certain storm event, or the total runoff including the baseflow (Blume, Zehe and Bronstert, 2007).

$$Runoff\ Coefficient = \frac{Q\ (mm)}{Rainfall\ (mm)} \qquad (6)$$

The runoff coefficient in a smaller basin in Argentinian Pampas is around 1.6 % (as a median value), this considering only the event water as runoff (Ares *et al.*, 2020). For flat agricultural landscapes the runoff coefficient is usually between the values of 10-50 % (Goel, 2011).

1.3 Remote Sensing

Considering that the measured locally produced data needed for runoff generation and flood risk analysis often is not available, *Remote sensing* is a convenient tool since it collects data almost globally and fast while it is also accessible for anyone. Remote sensing is informative collection of physical features on earth by analysing reflected and emitted radiation from, for example, satellites (Farhadi *et al.*, 2021). These big sets of information are available through Google Earth Engine, GEE, a web-based platform free to use for academics and researchers enabling satellite images and datasets such as topography, rainfall and surface water for analysis and downloading. GEE provides a code editor with JavaScript which enables fast processing analysis for anyone with a Google account (*Google Earth Engine,* n.d).

1.3.1 CHIRPS Rainfall Estimates

Monitoring precipitation both spatially and temporally is vital for flood risk analysis. When rainfall data is lacking, either because of too few rain gauges in an area, missing measurements or too short time series for analysis; satellite derived rainfall data can be used (Paredes Trejo *et al.*, 2016). Climate Hazards Group InfraRed Precipitation with Stations (CHIRPS) is a precipitation dataset compiled by algorithms combining observed precipitation, information from satellite imagery and global climatology. It is one of various remote sensing tools used for environmental monitoring. The precipitation data is estimated with satellites and is based on different methods, where the cloud coverage is correlated to rainfall. The precipitation data from CHIRPS covers great surfaces of earth's land and has records from 1981 up until today for different time intervals (Rivera, Hinrichs and Marianetti, 2019).

The CHIRPS dataset's efficiency has been compared with rain gauges rainfall data in South America. Studies have shown that its performance is better in flatter and wider landscapes (Paredes Trejo *et al.*, 2016) and that the product works well for longer timescales (Rivera, Hinrichs and Marianetti, 2019). Since CHIRPS rainfall data is the average rainfall over an area, high intensity rainfall events are underestimated (UC Santa Barbara, 2021).

1.3.2 Digital Elevation

In the processes of producing flood risk maps that can visualize how extreme rainfall events affect the area of interest, digital elevation is often used to analyse how water flows and effect the landscape depending on the terrain (Farhadi *et al.*, 2021).

Digital elevation is available for download from the Shuttle Radar Topography Mission (SRTM). SRTM is a collaboration project between NASA and the German and Italian Space Agencies to collect digital elevation data of the world. The mission collected the data during the year of 2000 using two antennas and the data can be used within various fields, for example for hydrological modelling. The resolution is about 30 meters, but most industrial countries have higher resolution national digital elevation models (Farr *et al.*, 2007).

In Argentina various national forms of digital elevation data are available for download. For some areas around the country, they have developed Digital Terrain Models with high resolution, which excludes buildings and tree canopies. The data available nationwide is a digital elevation model that relays on the SRTM and the Advanced Land Observing Satellite (ALOS) (Instituto Geográfico Nacional, n.d).

1.3.3 Flood Risk Indices

Based on the digital elevation and remote sensing various information can be extracted from great areas. Water accumulating depressions and steep slopes can be spotted and classified as higher risk areas for flooding and erosion respectively (Farhadi *et al.*, 2021).

There are many characteristics of the landscape that affect the degree of flood risk within the landscape. The study by (Farhadi *et al.*, 2021) was done to evaluate the relevance of different indices that can be derived from remote sensing data as flood risk factors. The information used for calculation of different indices can be retrieved from databases with land-use, topography, satellite imagery and rainfall through GEE. GEE was used in the study to produce indices representing the land-use, slopes, the slopes aspect, Topographic Wetness Index, TWI, elevation, River Distance, Soil texture and Waterway & River Distances. The Normalized Differential Vegetation Index, NDVI, and the Normalized Difference Water Index, NDWI, were calculated within the code editor interface using the Near Infrared band, the green band, and the red band from satellite imagery to discover the density of the vegetation's canopy, the 'greenness', and the extent of superficial water. The indices relevance for flood risk mapping were evaluated in ArcGIS and in this particular basin the indices Elevation, Waterway river Distance, River Distance and Maximum 1Day precipitation index were the most valuable (Farhadi *et al.*, 2021).

The Topographic Wetness Index, TWI, relates the topography on a local scale with the slopes to approximate the spatially distributed wetness conditions (Pourali *et al.*, 2016) and is shown to be accurate in smaller basins (Haas, 2010) and commonly used within a watershed scale (Grabs *et al.*, 2009). The topographic wetness index is a concept that is more easily available during flood risk assessment than the more expensive hydrodynamic models since it can be derived from any Geographical Information System with a digital elevation model (Pourali *et al.*, 2016). But the TWI has limitations that other more advance dynamic distributed hydrological models are better at solving for. For instance, the TWI assumes that the waterflow follow the slope gradient of the ground surface, which is not always true. Especially in flatter landscapes the TWI is not as good as dynamic models in defining the spatial wetness conditions since the groundwater flow depends on other factors than surface slopes. Furthermore, the static TWI relay on the calculated flow direction which could change with time (Grabs *et al.*, 2009).

The original TWI equation takes the following form, see Equation 7 (Beven, Kirkby and Kirkby, 1979):

$$TWI = \ln \frac{a}{\tan \beta} \qquad (7)$$

The TWI gives a steady-state value to each point in a landscape where higher values indicate higher wetness condition and lower value's indicate drier locations in the landscape. The variable a in Equation 7 is the specific contributing area, in other words the upslope area per

unit contour length (Pourali *et al.*, 2016). The β is the angle of the slope at that point, where a greater angle symbolizing a steeper slope gives lower TWI, hence less moisture in the soil (Beven, Kirkby and Kirkby, 1979). Throughout the years the original formula has been developed, taking into account various other factors, for instance the properties of the soil (Pourali *et al.*, 2016).

Analysing past events is another way of using remote sensed data to produce flood risk maps. With synoptic information from remote sensing water extents can be monitored and quantified. The Landsat collection is an archive of images and with the collection it is possible to detect changes in the landscape and flood affected areas over time (Soltanian, Abbasi and Riyahi Bakhtyari, 2019) due to its many years of collecting (Awadallah and Tabet, 2015). The Landsat images are composed of bands with different wavelength which can be combined to classify different features in the landscape such as vegetation and water.

To distinguish water from other surfaces as vegetation and soil different indices have been defined, for example, the Modified Normalized Difference Water Index, MNDWI, which is a variant of the Normalized Difference Water Index. They both separate the grids with water from grids without water with the calculations given in Equation 8 and Equation 9 (Soltanian, Abbasi and Riyahi Bakhtyari, 2019).

$$MNDWI = \frac{Green\ band - SWIR}{Green\ band + SWIR} \qquad (8)$$

$$NDWI = \frac{Green\ band - NIR}{Green\ band + NIR} \qquad (9)$$

Where NIR is the near-infrared band, and SWIR the shortwave infrared band.

The two indices give distinct water extents. However, they both uses the green band to increase the reflectance of water while the infrared waves are minimized since water does not reflect well in the infrared spectrum. The MNDWI classify inundated fields as water bodies while the NDWI does not and the NDWI can, instead of soil moisture, show values of vegetation moisture which is misleading when assessing superficial water (Soltanian, Abbasi and Riyahi Bakhtyari, 2019).

1.3.4 Flood Mapping

Remote sensed data has been used in studies (Farhadi *et al.*, 2021) aiming at producing flood risk maps using available databases and satellite image band composites to obtain indices that divides the landscape into informative mosaics. Flood risk mapping is essential for land-use planning. However, it is often a costly and advanced process since it usually demands hydrodynamic modelling (Pourali *et al.*, 2016). The idea of flood risk mapping is to reduce the risk of hazardous events for humans and buildings. Reliable flood risk maps are therefore important for decision-making. Flood risk assessments based on fixed characteristics in the landscape (Farhadi *et al.*, 2021) demand less time, money and data since it considers fewer parameters, such as topography (Pourali *et al.*, 2016), soil texture, land-use and rainfall of the basin (Farhadi *et al.*, 2021).

2. Research Questions

The integrated analysis aims at explaining the temporal and spatial variability of the hydrological response in flooding Pampa based on topography, precipitation and soil properties using various tools. Information from the Instituto Nacional de Tecnología Agropecuaria, Punta Indio's weather station, field measurements with Universidad Nacional de La Plata and information gathered with remote sensing is used for the flood risk analysis and to answer the following research questions:

- Which are the driving factors contributing to the flooding?
- What are the precipitation trends in flooding Pampa?
- How does precipitation relate to surface runoff within ungauged basin Río Samborombón?
    - How is the superficial water extent affected by soil characteristics within the two field sites, Don Joaquín and El Amanecer?
    - How does the land-use affect surface runoff within the basin of Río Samborombón?

3. Study Site

The study's field measurements are conducted at the two field study sites Don Joaquín and El Amanecer in the north-eastern Buenos Aires province within the Pampean region.

3.1 Pampas

The grasslands of Argentina, the Pampas, *La Pampa*, is extended across several provinces; the Buenos Aires province, Santa Fé, Córdoba, and La Pampa and takes various forms and are named thereafter. The Pampas is known for its plain monotone landscape with insufficient slopes. Within the subdivisions of the Pampas the landscape differs and can for example be wavy, *La Pampa ondulada,* or with hills and dunes (Ameghino, 1884). The Pampas is one of the most productive agricultural regions in the world and its surface is covered with cereal and oilseed plantations (Cicore *et al.*, 2015).

Flooding Pampa, *Pampa deprimida o inundable* or just *Pampa deprimida* in Spanish (*De Frente al Campo*, 2021), is one of the subregions of Pampas and less productive compared to the other parts of Pampas due to its floodings caused by its flat slopes which inhibit drainage, but also its alkalinity (Cicore *et al.*, 2015). Pampa deprimida, see Figure 2, is within the province of Buenos Aires and belongs to the humid region of the Pampas with drainage systems to the sea. In the depression Pampa deprimida, surrounded by the mountain range of Tandil and Pampa ondulada, el Río Salado is the most important drainage. However, it does not drain the abnormal rain events which cause inundations, why the channel network was built from west to east. However, the channel network cannot drain all flood water (Ameghino, 1884).

There exist various definitions of the size of Pampa deprimida depending on what factors are chosen for its distinction. INTA delineates the region deprimida as shown in Figure 2 (Bellati et al., 1978). Due to the big variety of soils and chemical properties found within the region, investigators attempt to incorporate different management to different environments within the region Pampa deprimida to correlate the elevation to the soils chemical status (Cicore *et al.*, 2015). The soils of Pampa deprimida are of finer material as clay and silt, which is why it

has lower permeability in the topsoil (Auge, 2004). The flat landscapes of Pampas prevents high speed surface runoff and flash floods in the landscape and most of the water from the precipitation drains via infiltration or evapotranspiration (Ares *et al.*, 2020), and can therefore be ponding for several days in the fields of Pampa deprimida before it retreats. The shallower groundwater table (1 meter to 1,5 meters of depth) also cause ponding as it frequently emerges (Auge, 2004)

In the Pampas there is an ongoing land-use intensification, where the former grasslands are converted into pastures and different cultivations, altering the runoff pattern (Ares, Varni and Chagas, 2020). However, keeping livestock is still common in the Buenos Aires province and the most common is cattle (INDEC, 2019). Almost half of Argentina´s cultivated land is found within the province (Bona, 2021).

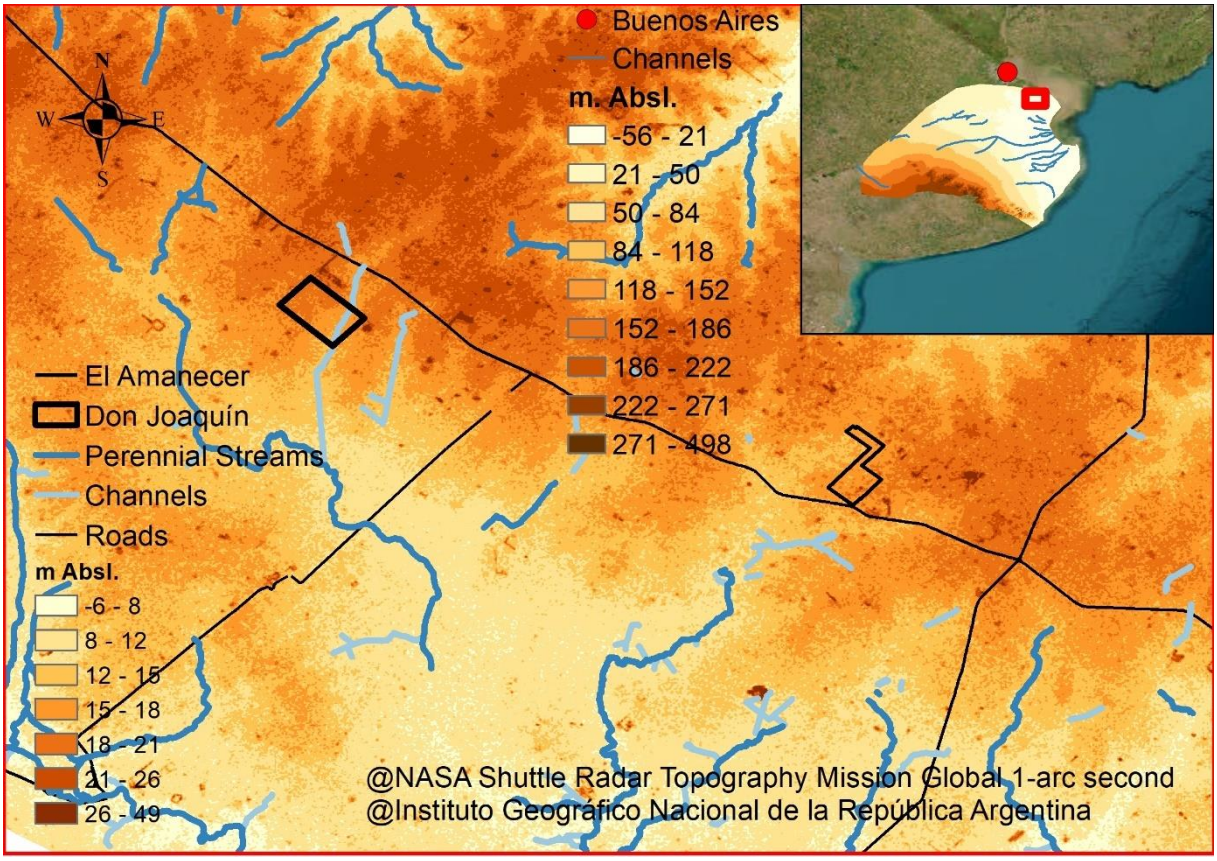

Figure 2: Digital elevation over Pampa deprimida (inset map) in eastern Argentina and digital elevation from the area around the two field sites Don Joaquín and El Amanecer.

3.1.1 The Two Field Sites: Don Joaquín and El Amanecer

The Faculty of Agricultural and Forestry Sciences of the National University of La Plata has two field sites, Don Joaquin and El Amanecer, see location in Figure 3. The two study sites, called "c*ampos*" in Spanish, which means "ranch" or "fields", are located within the region *Pampa deprimida o inundable* (Abba *et al.*, 2015). According to some definition this region could also be part of Pampa Ondulada (Pereyra and Ragas, 2021).

Don Joaquín

El Amanecer

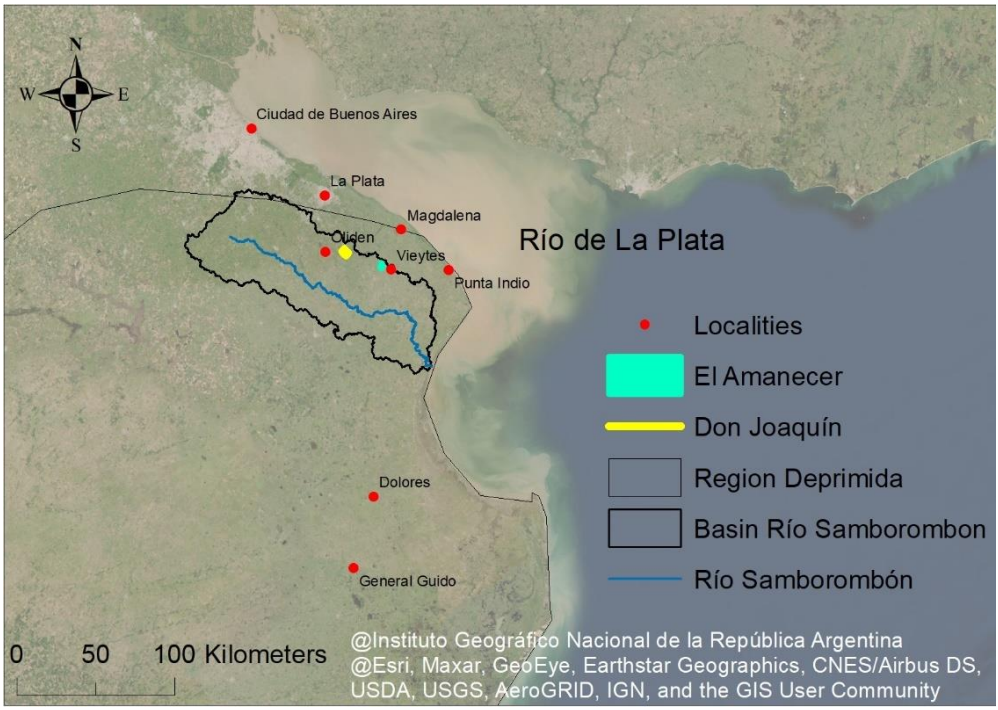

Figure 3: Map of the north-eastern parts of the province Buenos Aires where Río de La Plata flows out into the South Atlantic Ocean. The bigger cities Buenos Aires and La Plata as well as other villages close to the field sites are marked with red dots. The village Punta Indio, where the weather station is, is on the north-eastern edge of Pampa Deprimida. The entrances for the two campos are shown to the left.

3.1.2 Climate

The area of study is within the humid subtropical climate, which means that climate is temperate with no dry season and hot summers (*National Geographic Society*, n.d.) and on a more local scale within the subhumid-humid part of Pampas. The growing season affects plant characteristics (Degano *et al.*, 2021) and in central Argentina growing seasons are limited by the drought (Palmero *et al.*, 2022). The average temperature variability through the year in Punta Indio, which is the closest weather station of the two field sites, is presented in Figure 4.

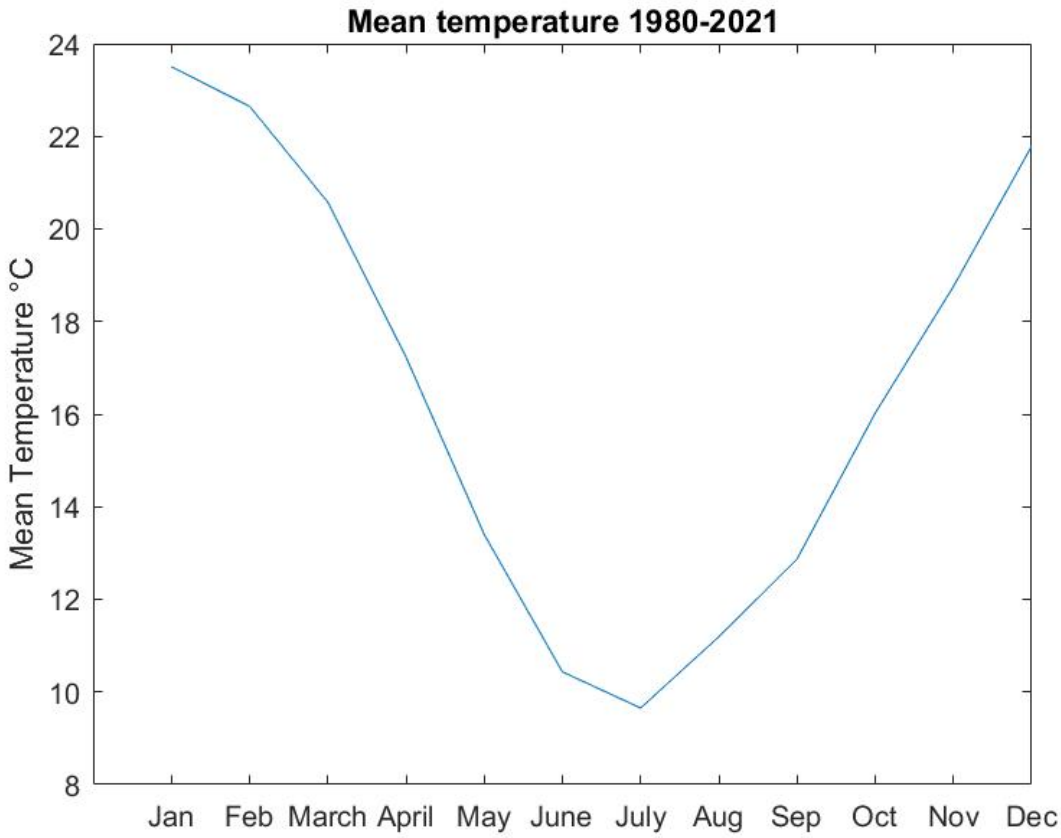

Figure 4: Mean monthly temperatures in Punta Indio calculated from data from the 1st of January 1980 to the 15th of June 2021. There are several days/months with no data which are excluded from the calculation of the mean.

The yearly mean maximum temperature is increasing overall in Pampas. However, no such trend has been discovered in Punta Indio. This is thought to be explained by the proximity to Río de La Plata, the sea, which due to its high heat capacity regulate the temperature. Evapotranspiration is increasing in Punta Indio which is also located in the east and most rainy parts of Pampa with average annual precipitation of 1200 mm/year (D'Andrea *et al.*, 2019). About 80 % of the rainfall is lost due to evapotranspiration in Argentina (Degano *et al.*, 2021).

4. Material and Method

The data and general method used for the characterization of landscape structures and precipitation in relation to flooding in flooding Pampa is shown below, see Figure 5. The workflow of the thesis relay on data collected from remote sensing, field measurements and the closest weather station. The geographic data from satellite images with previous floods and digital elevation are combined to visualize the flood prompt areas. The precipitation's effect on the water extent and runoff is investigated through graphs using data from past events and the Soil Conservation Service-Curve Number method. The calculation of a 100-year storm and the precipitation trends in the area are for quantifying worst case scenarios and future risks. The field measurements are used to estimate runoff generation through the SCS-CN method and to verify to compare the calculated wetness from digital elevation to field values.

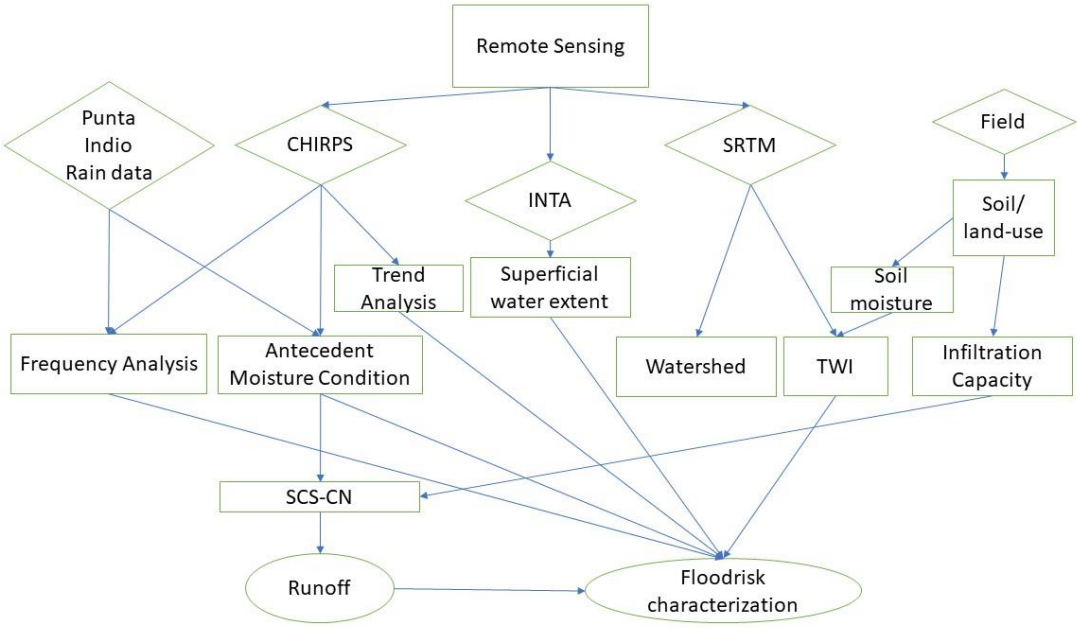

Figure 5: The flowchart starts from the top with data sources (diamonds), then follows the interaction of methods/measurements (squares) resulting in the catchment's hydrological response (ovals).

4.1 Rain Data

4.1.1 Punta Indio and CHIRPS

The weather station in Punta Indio, see Figure 3, collects daily rainfall data with a Pluviometer type B and is handled by the *Servicio Meteorológico Nacional*. The rainfall is measured every 24 hours at 9am and corresponds to the date before the measurement (*personal communication, N N Gattinoni 2022*). Punta Indio is located on the coast of Río de La Plata, about 40 kilometres from El Amanecer and 67 kilometres from Don Joaquín.

For the years and days no precipitation data was available from Punta Indio weather station (see the difference between the two datasets in Figure 6) mean daily precipitation data was recovered from CHIRPS for the Punta Indio area. Daily mean precipitation data from 1981 (since the start of the collection) was downloaded from Climate Engine. The yearly sums of the daily data from Punta Indio complemented with CHRPS is shown in Figure 6 along with the yearly precipitation from only the CHIRPS data.

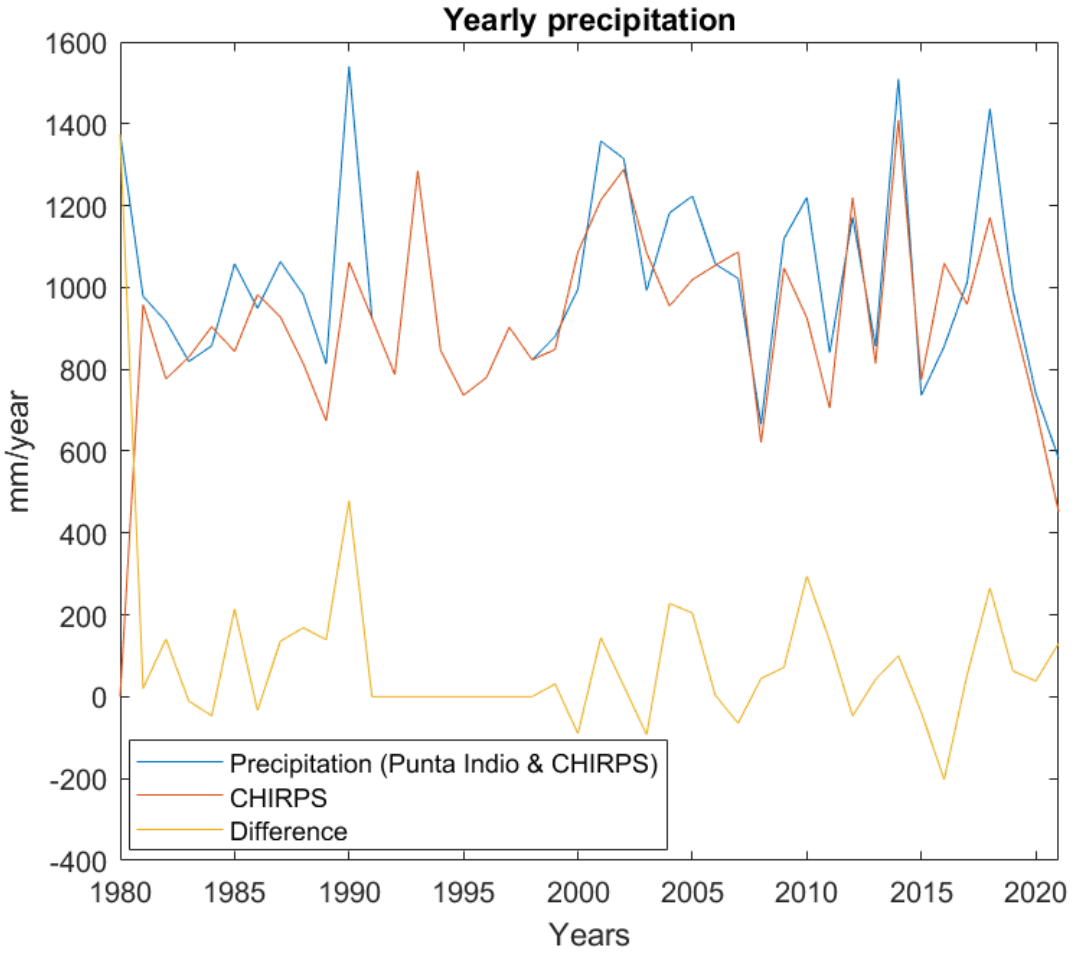

Figure 6: The yearly precipitation in Punta Indio based on Punta Indio weather station's daily precipitation complemented CHIRPS daily rainfall estimates. The yearly precipitation from only CHIRPS is also shown along with the difference between the two data sets (from 1981).

The mean daily precipitation from CHIRPS was inserted into Excel for plotting the seasonal precipitation. A seasonal trend analysis was done using an Excel macro with an implemented Mann-Kendall test. The four seasonal precipitation sums were input raw data. From the year of 1981 (start of the CHIRPS rainfall collection) to 2021 the data were analysed through the Excel-macro to find temporal trends in the seasonal precipitation pattern.

4.1.2 100-year Storm Event

The 100-year storm event is calculated to estimate a worst-case scenario and to be able to classify event rainfalls as heavier and less likely or lighter and less destructive. The highest daily precipitation (data from weather station Punta Indio and CHIRPS) for each year (1980-2021) was sorted in descending order, see Appendix A, and MATLAB's *normplot()*-function was used to obtain a normal probability plot. The 100-year daily precipitation event was spotted as the precipitation-value were the fitted line reached 0.99 (1 % exceedance probabilty every year) on the y-axis. The magnitude of a 20-year precipitation event was also estimated from the same graph where the fitted line from MATLAB's normplot-function reached the 0.95 value on the y-axis.

The size of a 100-year flood was estimated with the same method but using the data from INTA with information about the water extent in the area (in %) around Don Joaquín and El Amanecer, see Appendix B. 22 years of water extent data is available since the start of the Landsat programme in 2000. All events, or images, are not flood events.

4.1.3 Antecedent Moisture Condition

Previous precipitation can have great effect on the extent of floods after a storm. Higher antecedent soil moisture result in greater floods as the soil is more water saturated. The Antecedent Moisture Condition for each event, see Appendix B, was calculated in MATLAB as the cumulative sum of precipitation five days prior the event rainfall, which is standard for AMC calculations, using precipitation data from Punta Indio weather station complemented by CHIRPS data. In this study the event rainfall is the largest daily rainfall among the four days preceding the capturing of the satellite image or the same date. Each event was divided into AMC classes, 1, 2 or 3 depending on antecedent moisture conditions. Only the vegetative growing season limits were used for the division since mean temperature is seldom under 6 °C in Punta Indio, see Figure 4. The AMC for each event was plotted against the water extent in the area around Don Joaquin and El Amanecer.

4.1.4 Surface Runoff with SCS-CN method

The calculation of the estimated surface runoff was done in MATLAB, see Appendix C. The estimated surface runoff can be used to foresee how much water a storm will result in. In this study the surface runoff is estimated based on the land-use “grass land” and the hydrologic soil group C, which corresponds to soils with lower infiltration capacities and finer particles (according to field measurements and observations). The curve number for the Don Joaquín and the El Amanecer area is chosen to be 74, see Table 2. The curve number for AMC class 1 and 3 were calculated in MATLAB according to Equation 4 and Equation 5. The retention factor, S, was also calculated for each event. This was used to estimate the surface runoff for each event using Equation 2. For AMC class 1, 2 and 3 all surface runoff results with event precipitations bellow 33 millimetres, 15 millimetres, and 5 millimetres respectively where set to zero millimetres runoff since precipitation events lower than that does not cause surface runoff according to the SCS-CN method. The runoff coefficient for the different AMC classes was then estimated from the curves, see Appendix D.

4.2 Field Measurements

In Don Joaquín three spots were chosen for the field measurements using a transect with a slope through the field, crossing the three piezomenters for groundwater measurements, see Figure 7, Figure 8 and Figure 9. The piezometers are plastic wells with a diameter about six centimetres. The groundwater levels were measured several times from February to April in Don Joaquín with measuring tapes.

Figure 7: The field measurements around the groundwater well **bajo** in Don Joaquín the 8th of February 2022. In the centre of the photo is the groundwater well (grey with a white lid) surrounded by a protecting fence and to the right an on-going soil sampling.

Figure 8: The groundwater well **media loma.** The placement of this groundwater well is in between bajo and loma, in the middle of the transect.

Figure 9: The groundwater well **loma**. In the foreground there is a corn field left to rest. The ground is almost barren. The groundwater well is to the right in the photo in front of the smaller trees and the "callejón" (not visible) where the cows go between the fields.

4.2.1 Infiltration Capacity Measurements

To discover if the soil surface had impermeable layers infiltration measurements were carried out using a double ring infiltrometer in Don Joaquín next to the groundwater wells bajo and media loma on the same day, and at loma another day. The rings were knocked about two centimetres into the ground, see Figure 10, with a hammer and to attempt perpendicular penetration into the soil a wooden plank was used as driving plate. Water was added and measured with a glass measuring cylinder. The experiment was carried out for least two hours at each location. The placement of the rings was chosen considering the vegetation and the distance to the groundwater wells. At media loma the rings were inserted at a spot with intermediate vegetation, between the high vegetation plot and the plot with poor vegetation cover, see Figure 9. At bajo the vegetation cover was more homogenous, and the rings were

inserted at a flat surface near the groundwater well. At loma the rings were inserted on grass next to the corn field.

Figure 10: Experimental set-up at “media loma”. In the inner ring the line is marking 4,5 cm, that is the hight of the water column at each addition of water. In the photo water had only been added to the outer ring. Soil was added to the borders of the outer ring since water leaked out.

The infiltration rate was then calculated in Excel by dividing the volume added water by the area of the inner ring, the soil surface, and dividing that by the time passed since the last addition. At the end of the trial the infiltration rate reached a steady state, that is the soils infiltration capacity. It was estimated as the mean infiltration rate after two hours of adding water to the soil.

No infiltration measurements were done in El Amanecer due to logistical restrains.

4.2.2 Soil moisture measurements

To see whether water is retained in the soil after rain and whether the soil moisture mapping with the TWI were reliable, soil samples to measure the soil moisture were collected with a soil sampler (a hollow iron bar) stuck in the ground, shown closely in Figure 11, the 8th of February 2022 and the 19th of February. The samples were collected next to the groundwater wells from 0-10 centimetres and 10-20 centimetres. Three soil samples from each depth were collected at each groundwater well in smaller plastic tubes and later placed in a styrofoam compartment to reduce evapotranspiration losses due to the warm weather.

Figure 11: The soil sampler used to collect the moisture samples. This particular sample is from “bajo” and the measuring tape is inverted, the top soil layer is to the left.

The 19th of February the same procedure was done, except samples were taken from holes made with a shovel since the soil moisture sampler could not enter the soil as the soil was too dry.

After a night in the fridge, the soil samples from Don Joaquín were divided into small metal cupcake forms and weighted on a scale (humid soil) the day after the collections. Then they were put in the oven for three days in 40 °C. Then they were all weighed again, and the soil moisture were calculated in percentage.

No soil moisture measurements were done in El Amanecer due to logistical constrains.

The analysis of significant differences in the soil moisture between the two different days with different antecedent moisture conditions were then calculated in Microsoft Excel with the data analyst tool t-test: Paired two Sample for Means with the mean values. The difference in soil moisture between the elevations (bajo, media loma and loma) was also calculated with the t-test. The paired t-test is a commonly used statistical test to analyse if mean values from two paired samples are significantly different, paired meaning that the samples are coupled. The paired t-test relay on the null-hypothesis, where two mean values from two dependent samples are assumed to be the same, and if the null-hypothesis can be rejected, the two samples are significantly different. According to the paired t-test two dependent observations are significant different if the p-value is smaller than, depending on confidence interval but usually, 0.05 (95 % confidence interval). (Xu *et al.*, 2017). To discover if the antecedent precipitation affected the soil moisture it was assumed that that it rained in Don Joaquín as well as in Punta Indio and that no other changes (e.g., irrigation) had occurred between the two measurements.

4.3 Digital Elevation

Digital elevation was used for the calculation of the upslope areas and the calculation of the TWI. The digital elevation is from the SRTM with a resolution of 1-ArcSecond.

4.3.1 Delineation of the Upslope area for Don Joaquín and El Amanecer

The delineation of the watersheds for Don Joaquin and El Amanecer was performed in ArcGis 10.8.1 with the help of tools from the ArcToolbox and the SRTM digital elevation with approximate 30 meters resolution downloaded from Google Engine. Shapefiles from the Nacional University of La Plata (plots/fields) and satellite images files from INTA were used for the location of the fields and to display water accumulation sites.

Satellite images, Landsat-8, processed by INTA was used to locate the outlet points. The Satellite Images selected for the upslope area analysis are from 20th of June 2014 and the 4th of October 2018. During these dates there were superficial water within the campos of Don Joaquín and El Amanecer and their surroundings.

The digital elevation covering a large portion of the Province of Buenos Aires coastal area was first cut in ArcGIS to reduce its size. A polygon covering both Don Joaquín and El Amanecer and their surroundings down to Río Samborombón were used as mask in the *extract by mask* tool. The extracted digital elevation was prepared for the watershed analysis by filling ‘sinks’ in the digital terrain using the *fill* tool. To calculate the direction of the flow the *flow direction* tool was used with the filled digital elevation model as input. The *flow accumulation* tool was used to calculate how many cells that are upstream a grid. Comparison between shapefiles of stream networks from IGN (*Capas SIG | Instituto Geográfico Nacional*,

n.d.) and the flow accumulation grid was made to see how well they overlapped. Comparisons were also made between the satellite images of the water extent and the flow accumulation grid. A point shapefile was created and named outlet. For Don Joaquín the outlet was placed on a cell with a higher flow accumulation value and close to an actual water accumulation site according to the placement of the stream rinsing through Don Joaquín (dry during visit in February – April 2022) and where water accumulates according to satellite photos. The stream was drawn in Google Earth pro according to the placement of the "arroyo" (eng. *Stream*). The outlet for El Amanecer was placed similarly, however the outlet point was chosen further away from the field so that a bigger part of the field would be within the watershed.

The areas of the watersheds were then calculated by first creating a new field in the Attribute table for the watershed polygon. Then, using Calculate Geometry in Editing mode, the area was calculated. The slopes were calculated in ArcGIS with the tool *slope*.

The basin of Río Samborombón was calculated in the same way as the upslope areas, the outlet point was selected at a grid cell with high flow accumulation and close to the real outlet of the river to the sea.

4.3.2 TWI in ArcGIS

The Topographic Wetness Index was calculated in ArcMAP using the filled digital elevation. The digital elevation raster with a resolution of about 30 meters was used as input raster to produce a slope-raster with the slope in degrees with the *slope*-tool. The tangent of the slope for each grid cell was calculated in radians the following Equation 10 The conversion factor from degrees to radians 1.570796/90 is used instead of the conversion factor π /180.

$$Tan\frac{(' slope\ in\ degrees' * 1.570796\ )}{90} = Tangent\ of\ slope\ [rad] \quad (10)$$

To remove the grid cells without any slope in the raster, a condition statement was used in the Raster Calculator replacing 0 radians by 0.001 radians, see Equation 11.

$$Con\ (\text{"Tangent of slope"} == 0\ ,\ 0.001,\ "Tangent\ of\ slope") \quad (11)$$

The flow accumulation raster was then used to calculate the upslope area to each grid cell per unit contour length, the SCA, see Equation 12. The flow accumulation raster (calculated with multiple flow direction) is the amount of grid cells draining to a grid, the plus 1 in the formula is to include that cell too. By multiplying it with the cell size you get the specific contributing area, SCA surface.

$$Specific\ Contributing\ Area = (flow\ accumulation\ raster + 1) * cell\ size \quad (12)$$

The cell size depends on the resolution of the digital elevation and in this case, it was 26.949458 meters.

Finally, the Topographic Wetness Index was calculated in the Raster Calculator by Equation 13.

$$TWI = ln\ \frac{Specific\ Contibuting\ Area}{Tangent\ of\ slope} \quad (13)$$

The flood the 7th of September 2014, see Figure 13, has a great extent and was therefore chosen for the evaluation of the TWI as a soil moisture indicator along with the soil moisture measurements in the field. The calculated TWI from for each grid cell was imported into QGIS and reclassified. Lower TWI values (4-15) indicating the theoretically driest parts of the landscape were deleted to highlight the wetter grids, higher values (15-27) were categorized so that the TWI would delineate with the perennial-, and intermittent streams and channel network (*Capas SIG | Instituto Geográfico Nacional*, n.d.) and the 2014 flood event. The flood extent from the 7th of September 2014 were visualized with QGIS Python console, see code in Appendix E.

4.4 Water extent in Pampas

The dates of satellite images used in the study are presented in Appendix B or presented in the corresponding section. The images show different water extent, and not all are floods. The images show areas where water accumulates during wetter periods, and conclusions can be drawn about when and where floods occur. Images has been obtained through the Python console in QGIS.

4.4.1 Satellite Images with Water Extent from INTA

Data from the Landsat programme has been collected by INTA since the year of 2000. These images are non-cloudy and for each image the area of the water extent has been calculated with the MNDWI. The area selected of INTA is shown in the images bellow, see Figure 12 and Figure 13.

Figure 12: False colour composite processed by INTA from the 7th of September 2014. Source: Landsat-8 image courtesy of the U.S. Geological Survey. The code for the image is in Appendix F.

Figure 13: The area of the flood is calculated as the blue area from MNDWI-calculations in Google Earth engine. This map is from the 7th of September 2014. Source: Landsat-8 image courtesy of the U.S. Geological Survey, processed by INTA. The code for the image is in Appendix F.

The calculated water extent, done by INTA, is plotted against the precipitation data from Punta Indio to discover possible relations between antecedent precipitation, event precipitations, the season of the year and the water extent or flood. The code for the MATLAB script is in Appendix C.

4.4.2 Mosaic of Environments

INTA (2022) has mapped environments that are based on the satellite images showing the water extent during past floods. These are shown as mosaics, see Figure 14 and Figure 15. The mosaic represents how frequently different parts of the fields are flooded and the water extent of flooding. The wetter environments are frequently flooded (however not on every year basis), while the spots that are sometimes wet have been flooded during the years of observation from optical images but are more rarely covered with water (personal communication INTA, 2022). The streams during the period February – March 2022 are dry and there are no free water surfaces in the surroundings.

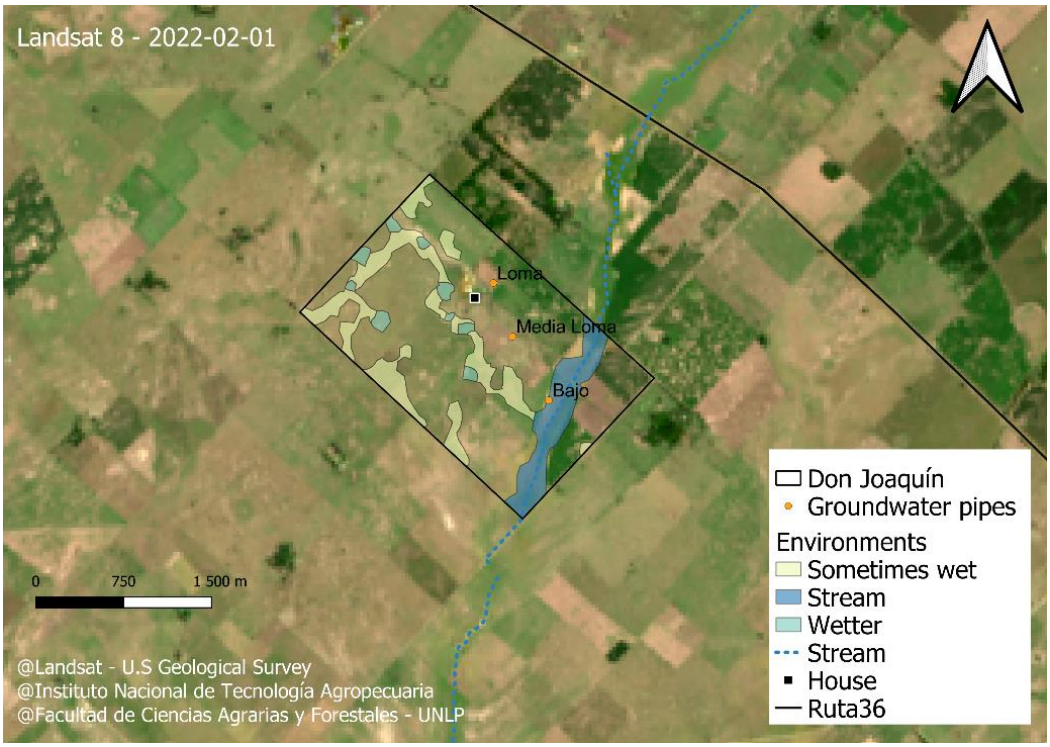

Figure 14: Don Joaquín and the field's predefined environments. The environments are based on INTA's analysis of satellite images of floods. The different colours marks wetter and drier environments within the field. The parts of Don Joaquín which does not flood has not got any assigned colour. The yellow areas are not as often submerged as the blue marked area. The yellow areas reveal the water's flow path and are not visible unless flooded.

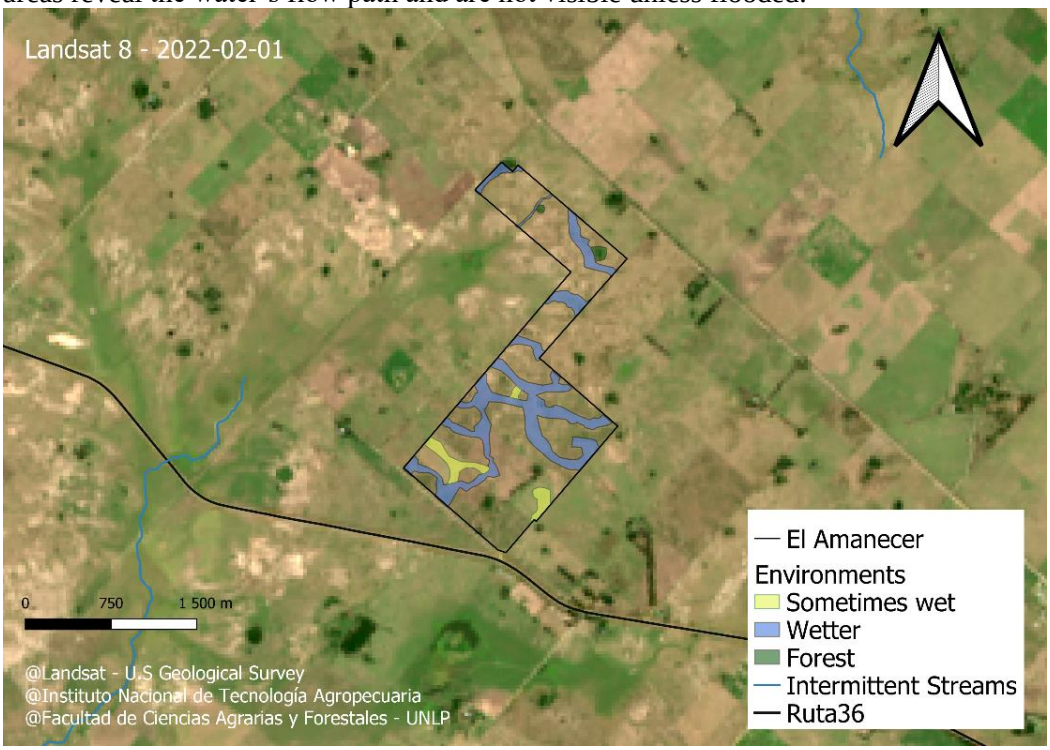

Figure 15: El Amanecer and the field's predefined environments. The environments are based on INTA's analysis of satellite images of floods. The different colours marks wetter and drier environments within the field. The parts of El Amanecer which does not flood has not got any assigned colour. The yellow areas are not as often submerged as the blue marked area. The yellow areas reveal the water's flow path and are not visible unless flooded.

The illustrative mosaics are visualized on top of a Landsat-8 satellite image from February 2022 generated in QGIS Python console, see Appendix E. Forests appears dark green on satellite images and is therefore sometimes hard to distinguish from water surfaces. The mosaic for El Amanecer has been corrected after field visits, where QField was used for orientation.

5. Results and Discussion

The driving factors analysed in the thesis are presented and discussed in relation to field measurements or literature in this section to evaluate how the rainfall, physical characteristics, and the land-use contribute to the runoff generation.

5.1 Rain Analysis

In this section precipitation data is analysed to describe the general precipitation pattern for the seasons and to find possible trends due to climate change. The magnitude of a 100-year event and 20-year event is also estimated with data from the weather station, CHRIRPS and satellite images to quantify heavier precipitation.

5.1.1 CHIRPS Trend Analysis

The seasonal variability of the rainfall in the Punta Indio area during the last 40 years (only January, February, and Marsh for 2022) are presented in Figure 16. The seasonal rainfall during the years is constant with no big precipitation differences between the seasons. Spring (October, November, and December) is the exception and has higher peaks than the other seasons. Looking at the precipitation patterns over the year it rains more during the period October – March. The trends of how the precipitations changes over time is shown with the dotted lines in the plot. During the time of the field visits, summer 2022, it was drier than the trend, but not considerably.

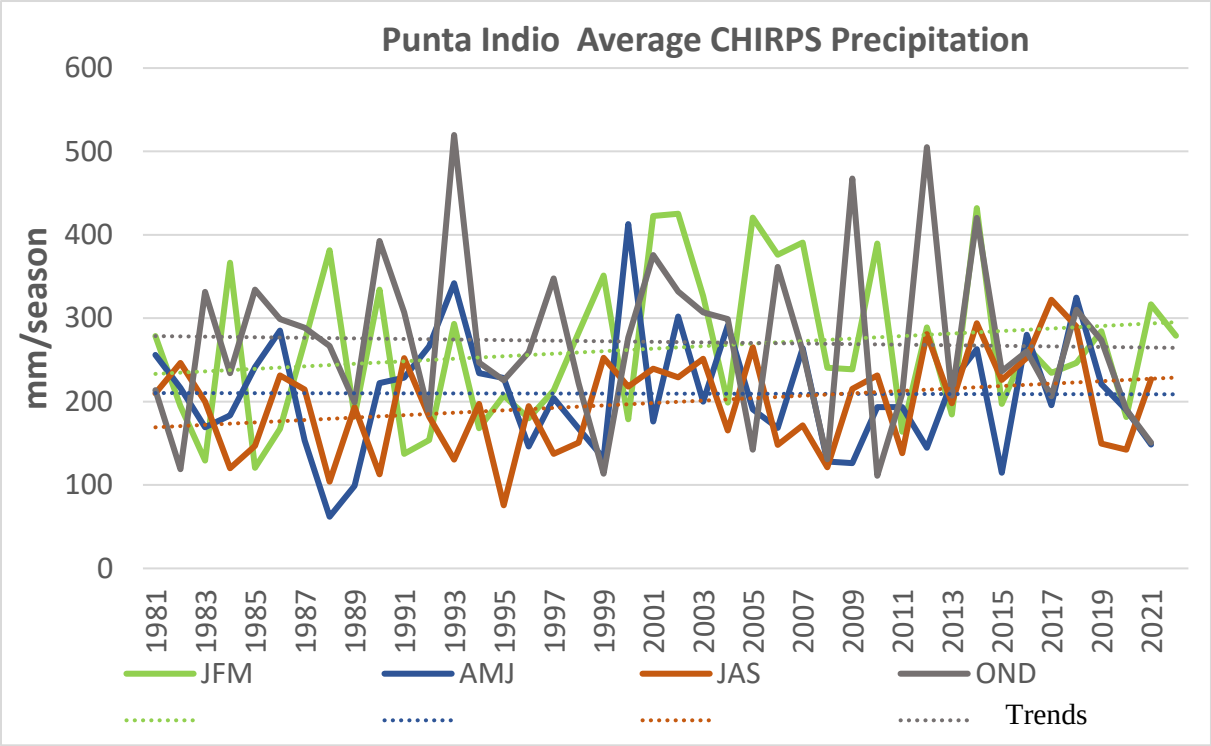

Figure 16: In the figure above the seasonal variability is shown. The precipitation data originates from CHIRPS daily rainfall data. JFM stands for January, February, and Marsh, AMJ stands for April, May, and June, JAS stands for July, August, and September, and OND stands for October, November, and December.

The trends (dotted lines in graph above) are not statistically significant. According to the Mann-Kendall test the seasonal climate is not rainier or less rainy now compared to the past 40 years in the Punta Indio area, see Table *3*.

Table 3: Results from Mann-Kendall test on trends in precipitation per season from 1981 – 2021 in the Punta Indio area. Precipitation data is from CHIRPS (2022).

Season of the year	P -value	Significant Trend (yes/no)
JFM	0.1	No
AMJ	0.7	No
JAS	0.05	No
OND	0.6	No
Mm/year	**0.3**	**No**

Just as in previous studies carried out in Pampas (D'Andrea *et al.*, 2019) no precipitation trends could be discovered in the Punta Indio area in Pampa Deprimida. The precipitation data used in this part of the study is only from remote sensing to prevent that differences in measuring techniques influence the results. The CHIRPS has also the longest series of continuous measurements of rainfall available in this study.

The weather stations around the area of the field study sites are sparse and the relevant (closest) ones are located along the coast (D'Andrea *et al.*, 2019) and since climate might be different in the inlands no conclusion about precipitation trends for the region can be drawn. CHIRPS is suitable for seasonal trend analysis of longer time scales (Rivera, Hinrichs and Marianetti, 2019) and also for the terrain found in Pampas, hence the results are reliable. The

analysis assumes that the seasons have not shifted the last 40 years. If they have changed maybe other trends would have emerged.

5.1.2 100-year Flood

In Punta Indio, the exceedance probability of a 145 mm/day event is 1 % every year (100-year event), see clarification of the frequency analysis based on exceedance probability in Table 4. A storm of the size 125 mm/day would be expected every 20 years. The exceedance probability of a 100-year storm event is once in a hundred years, but the 100-year storm event has been exceeded twice since 1980 in Punta Indio. The annual maximum precipitation series is not normally distributed, see Figure 17, and right skewed, see histogram in Appendix G.

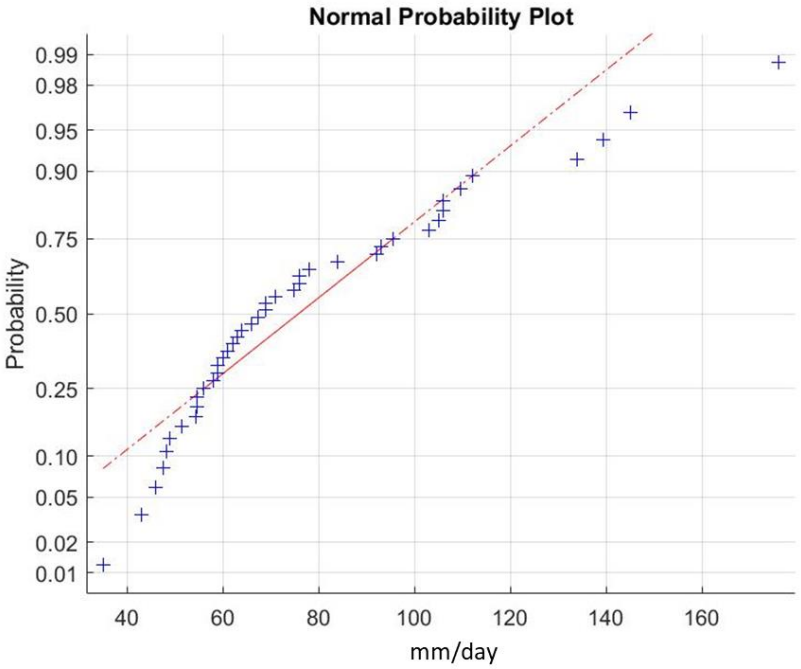

Figure 17: Normal Probability-plot of annual maximum precipitation series in Punta Indio from 1980 to 2021 using MATHLAB's normplot() function. The years that no rain data was available from the Punta Indio weather station, data from CHIRPS was used. The maximum daily precipitation each year between 1980-2021 [mm/day] is on the x-axis. Maximum daily precipitation series is in Appendix A.

The normal probability plot for the flooding events is in Appendix H. An event with an 5 % risk of occurring every year covers 9 % of land with water and the 100-year flood covers 11 % of the land with water.

Table 4: Size of a 100 – year storm event and a 20– year storm event according to the graph above. The 100 – year flood extent and 20 – year flood extent is also presented in the table.

Event	Annual exceedance probability [%]	Magnitude
100-year storm	1 %	145 mm/day
20-year storm	5 %	125 mm/day
100-year flood/ water extent	1 %	11 % water cover in the landscape*
20-year flood/ water extent	5 %	9 % water cover in the landscape*

*2 % or less water coverage is normal water coverage in the area. 2 % water coverage is when the perennial stream network has water (see Appendix I, '2019-07-03')

Both the 20-year flood and the 100-year flood are destructive since a normal water extent in the area around the field sites is estimated to be about 2 %, see Appendix I.

The precipitation data contains few higher precipitation records. Only four years have had at least one day with precipitation over 120 mm, which is high and outstanding compared to the other years. Since the data is not normally distributed the determination of the magnitude of the 100-year precipitation event hard to estimate from the graph. The normal distribution line differs approximately 15 to 30 millimetres from the highest precipitation values recorded in 40 years. It is possible that another distribution, for instance, the Gumble distribution for extreme values, would fit the series of maximum daily precipitation better and hence give a more precise value of the magnitude of the 100-year event.

Similarly, the 100-year flood extent is hard to calculate since there are only 22 years of data since the start of the Landsat program. The data of the greatest water extent each year is not normally distributed. The values do not follow the normal distribution curve which is probably also due to the limited number of events captured with satellite images. Since the data is not normally distributed the results are not very reliable and data collection from more years would be necessary. To be able to do a proper flood frequency analysis discharge data from Río Samborombón would be needed. With discharge data from the waterways the catchments response to precipitation can be measured more frequently than what can be mapped by the satellites that passes in orbits every second week.

5.2 Field Measurements at Campo Don Joaquín

The field measurements and observations at Don Joaquín was done to obtain an overview of the site, to perform necessary measurements which results was used in the calculation of the surface runoff with the SCS-CN and to compare the soil moisture calculated with the TWI to field data.

A general description of Don Joaquín's characterisitcs is presented in the Table 5. Don Joaquín's is part of the widely stretched grasslands of Pampas and has various vegetative cover where the soils are partly barren. However, there are no signs of erosion caused by water in the fields. No impermeable layer was found in the pits.

Table 5: Field observation in the vicinity of the three groundwater wells in Don Joaquín.

Groundwater well:	**Bajo**	**Media loma**	**Loma**
Land-Use	Cattle	Cattle	Next to corn field (left to rest)
Vegetation cover	Green grass	Grass	Almost barren
Signs of soil erosion, rills		No	
Depth of well until clay was encountered. In meters measured from the ground.	3,4 m	4,1 m	4,4 m
Groundwater levels Feb-April 2022	No groundwater was found in the wells. No water is found in the intermittent streams in the vicinity of the fields, see Figure 14 and Figure 15.		
Soil characteristics observed in field pits	Dry crust (0-2cm) Finer particles	Finer particles	Finer particles

During the study no groundwater levels were measured since no water was found in the wells. This is strange since it did rain during the period the wells were checked. Since the groundwater level was so low, lower than three meters, there was probably an ongoing drought autumn 2022 with low groundwater recharge. The drought probably effected the plant growth, the vegetation cover was sparse. Plants get water stressed when the soil moisture depletes due to the drought (Van Loon, 2015). Another explanation to the lack of water in the groundwater wells can be that they were plugged with soil from the sides which would stop the water penetrating the well. This could be the case since groundwater levels are usually found within 1-2 meters below the ground surface (Auge, 2004). Looking at the satellite images from the period of the field visits, see Figure 14, there is no free water surface in the waterways in the vicinity of the field and due to that it is not possible to extrapolate the groundwater levels in the field from free water surfaces. Hence, the ground levels were probably low at the time of the visit.

5.2.1 Infiltration Capacity Measurements

In soils where infiltration capacities are low, for instance due to trampling of cattle or the characteristics of the soil, water from precipitation can cause overland flow since it does not infiltrate the soil.

The infiltration experiments in Don Joaquín gave a high infiltration rate and infiltration capacity (160 mm/h) at ‘bajo’, Figure 18. A lot of water was added per time, and it infiltrated quickly. The infiltration capacity at loma and media loma are not as high and fall into the category of loams. The calculated infiltration capacities are the mean infiltration rates after two hours of trials, when the soil is water saturated. At the beginning of the trial, loma the infiltration rate is higher at loma than at media loma.

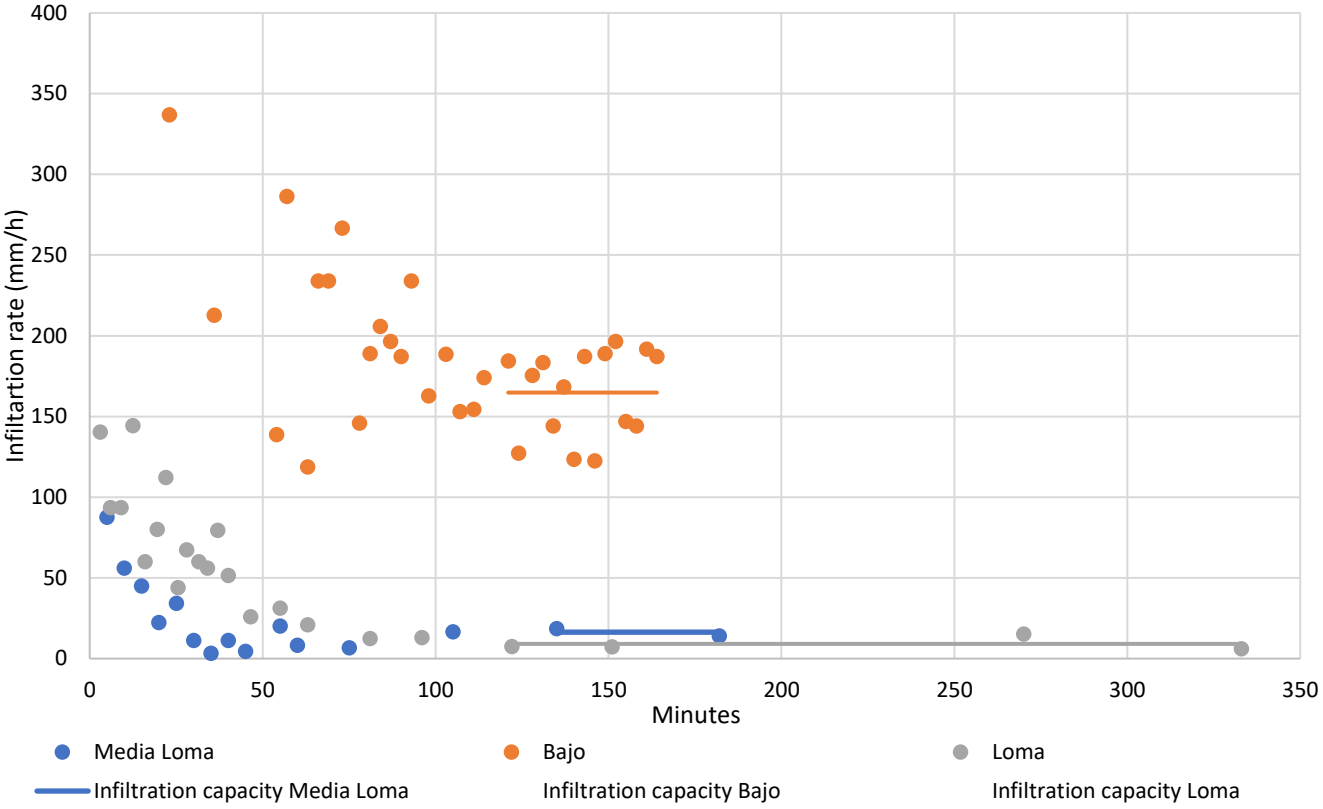

Figure 18: The infiltration rate plotted against time. The infiltration capacity (constant infiltration rate or near-saturated hydraulic conductivity) is the mean of the infiltrations rates after about 120 minutes trial (two hours) marked with a line in the diagram.

The calculated values for the infiltration capacities (the lines in Figure 18) are shown in Table 6.

Table 6: Infiltration capacity and corresponding soil type according to trials and to soil maps.

Local elevation/location in Don Joaquín:	**Bajo**	**Media loma**	**Loma**
Infiltration capacity from field trials	160 mm/h*	16 mm/h	9 mm/h
Soil type according to Infiltration capacity/constant infiltration rate (Eijkelkamp, 2015)	-	Loam	Clayey Loam

*Unrealistically high

The infiltration rate at bajo never stabilizes and is unreasonably high. According to literature higher vegetative cover, which can be observed in bajo in comparison to media loma and loma, indeed leads to higher infiltration rates (Wang *et al.*, 2013). However, the results from the trial at bajo is unrealistic since soils of finer textures were spotted in the observation pit which would impede such a high infiltration capacity. It is possible that bigger pores or cracks in the soil were present and able to rapidly transport the added water down through the soil horizon. It is, however, more likely that the experimental setup failed and that the infiltration rings were not deep enough into the soil, causing water to leak through the sides horizontally.

At bajo the water infiltrated so fast, over 150 mm/h, that the bins ran out of water. The experiment was interrupted while more water was collected which makes the results unreliable. The infiltration rate at bajo could in theory be higher than at media loma and loma because of the higher vegetation cover that besides the cracks, protects the topsoil from direct impact of rainfall. The forces from the raindrops hitting the barren soil directly would decrease the water penetration at media loma and loma. However, in contrary to what would be expected a dry crust, possibly created by heavy rainfall on barren ground was found in the ground surface in the observation pit at bajo, even though it is in general 'greener' than media loma and loma.

The water added during the first two hours of the trial is saturating the soil pores with water. Depending on the soil the time and amount of water demanded for saturation varies. In this trial the time it took for the infiltration rate to settle was about two hours. However, the infiltration rate never stabilized to a constant infiltration rate (less than 10 % difference in infiltration rate between measurements). This is probably due to inaccurate measuring methods. That some water leak horizontally in the soil profile did not affect the results as water were kept as a column in the rings. With other equipment for measuring the volume of added water, an impact-absorbing hammer, and a proper driving plate for entering the rings into the ground results would be more representative and probably not fluctuate as much. The difficulties in entering the rings perpendicularly might have caused fissures which would increase the resulting infiltration rates. The fluctuations in the infiltration rate could also be due to the soil not being saturated yet. Different soils need different time for saturation. If the experiment would have been carried out for a longer time, the infiltration rate might have stabilized resulting in a more accurate value of the infiltration capacity.

As mentioned, three measurements were done in Don Joaquín, whereof one measurement gave unreasonable results and the other two were done over a hundred of meters apart. For this reason, it is not possible to determine the infiltration capacity for the three different spots (bajo, media loma and loma). However, an approximate infiltration capacity for the soils of Don Joaquín can be estimated.

5.2.2 Soil Moisture

The soil moisture was measured two times in Don Joaquín at three locations with different elevation, one of the times was after a bigger rainfall event. The mean soil moisture in the topsoil in the lower elevation *bajo* is higher than at the higher elevation's *media loma* and *loma* both days of trials, see Figure 19 and Figure 20. However according to the t-Test: Paired Two Sample for Means the difference is not significant between the three elevations. The spread among the soil moisture samples taken at each depth and elevation (next to the groundwater wells) is presented by the measured soil moisture in the figures.

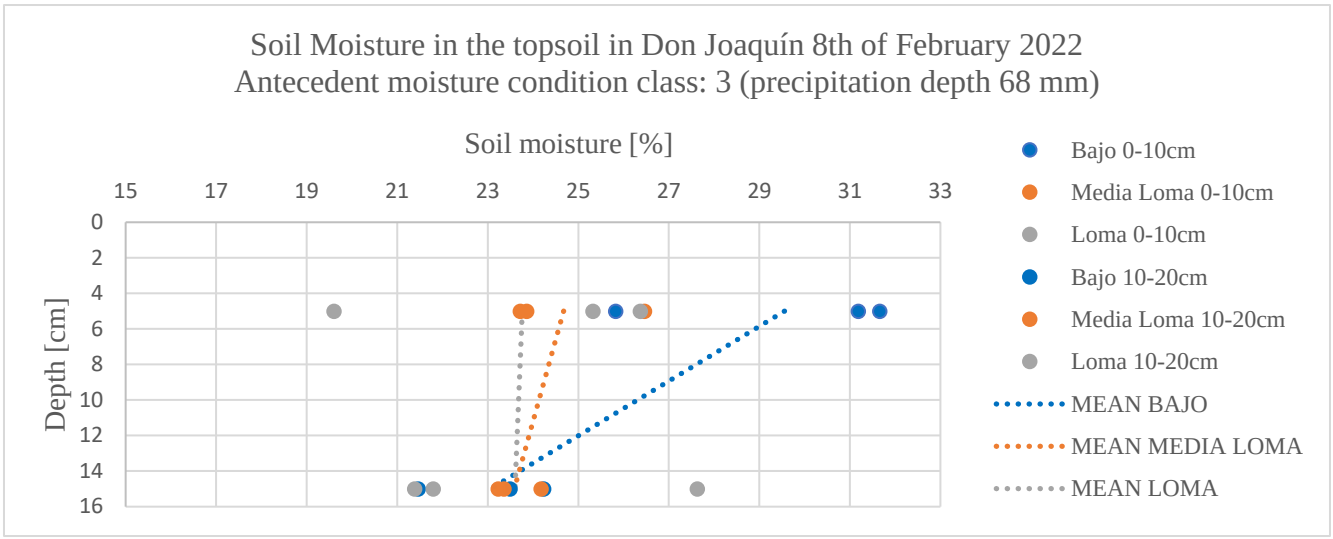

Figure 19: Soil moisture in the topsoil at three spots in Don Joaquín at different elevations.

It was noted in the field on the 19th of February (AMC class 1, AMC: 1.1 mm) that the soil was drier than on the 8th of February (AMC class 3, AMC: 68 mm). The topsoil (0-10cm) is significantly drier the 19th compared to the measurements conducted earlier the same month at the same elevation, except at media loma.

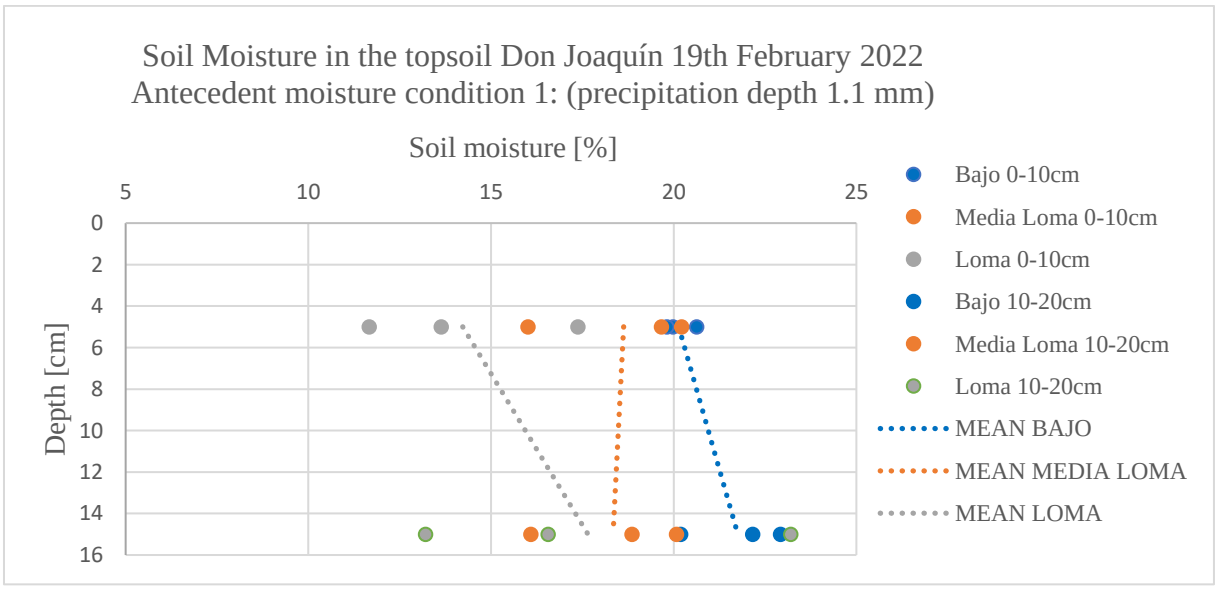

Figure 20: Soil moisture in the topsoil (0-20) at three spots in Don Joaquín at different elevations.

The soil moisture in % differs between the dates that has distinct antecedent conditions, and the results would state that the soil moisture in the landscape is dependent on earlier precipitation (AMC). The paired t-test was used instead of other tests since it compares observations before and after an event or treatment. The difference is significant between the day with low AMC and the day for which it had rained a lot before, however the difference in percentage is not so big comparing to the difference in antecedent precipitation (67 millimetres). Antecedent moisture condition is a term to explain soil moisture, how much water that is stored in the soil from precipitation the previous 5 days, however the translation from rain depth to actual change in soil moisture can be small even though it has rained.

On a smaller scale the results cannot prove that soil moisture depends on small elevation differences in the landscape since the soil moisture between loma, media loma and bajo are not significant according to the t-test. Not considering that there is no significant difference in soil moisture between the three elevations, the mean soil moisture in the lower elevation bajo is more humid than the higher elevations media loma and loma. This aligns with the theory of the TWI and that the soil moisture is higher in the locally lower, and flatter parts of the landscapes. The denser vegetation cover in the locally lower part of Don Joaquín (bajo) could also contribute to and be due to the increased soil moisture. Higher vegetative covered soils has been found by Wang et al. (2013) to have higher water holding capacity due to the topsoil's higher organic content which isolates from the heat that increases evapotranspiration. Furthermore, the vegetation's ability to increase the soil's infiltration capacity and making the soil's bulk density less dense increases the soil moisture and decreases the magnitude of surface runoff responses by retaining water in the soil (Wang *et al.*, 2013). On the other hand, high vegetation cover decrease soil moisture by evapotranspiration (Van Loon, 2015). These arguments also hold for the low soil moisture in the locally highest spot within the trial, loma, where the soil was barren. Except from different vegetative covers and elevation differences the soil types at the three spots can affect the soil moistures. In this thesis the soil characteristics were not investigated to such an extent that conclusions about how the soil type can affect soil moisture can be drawn.

5.3 Upslope Areas

The soil moisture in water ways and how much water fluctuates through the fields depend on the upslope area. The fields upslope areas are shown in Figure 21 and Figure 22 and they are relatively small. The two field study sites are on the ridge between the two basins of Río Samborombón and Río de La Plata, and drain in Río Samborombón. The darker spots in the maps are trees which has not been removed from the digital terrain. Don Joaquín connects to the perennial stream network via a straight drainage channel and a stream. El Amanecer's upslope area drains via an intermittent stream. The slopes within the fields are flat, ranging from 0-3%.

Don Joaquín
Area Don Joaquín: 426 ha
Area watershed: 2940 ha

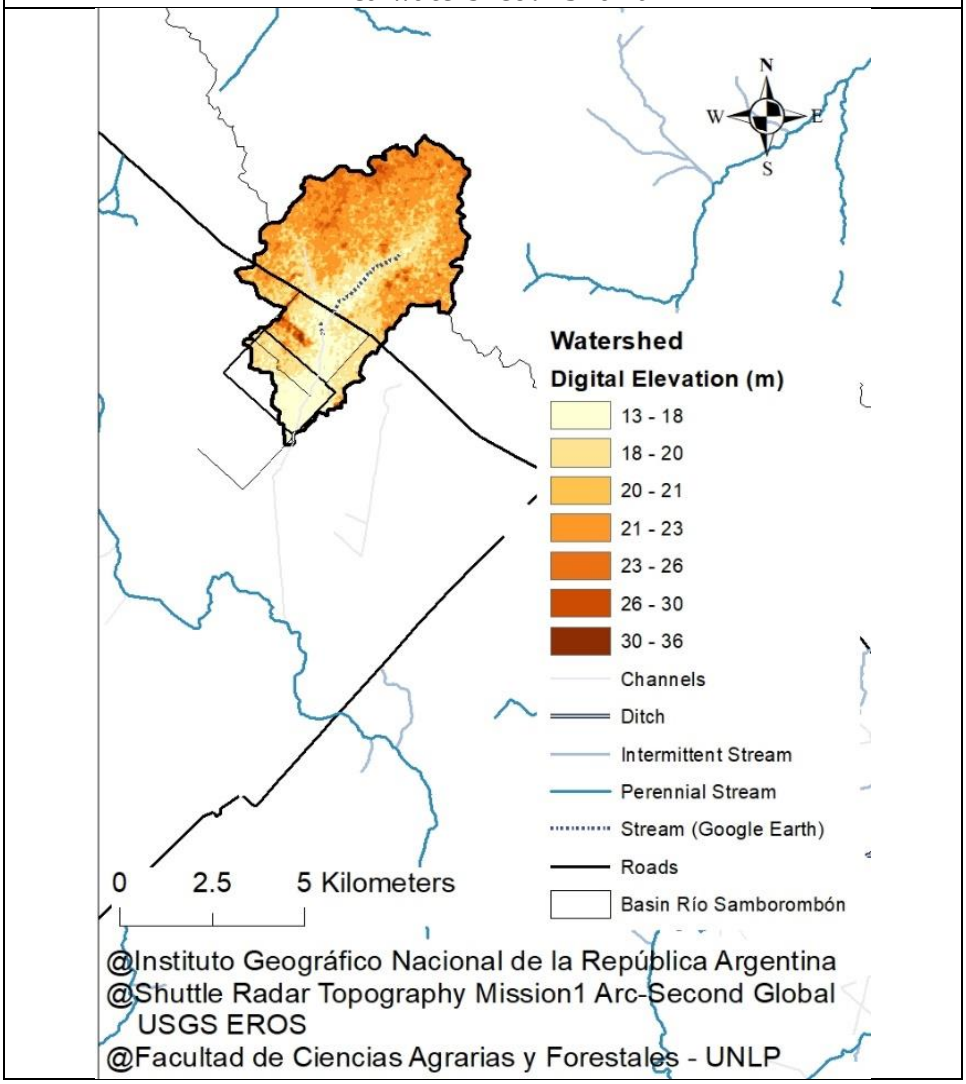

Figure 21: The upslope area of Don Joaquín with its outlet at the southern edge just outside of Don Joaquín (the lowest point). The dashed blue line is a smaller stream. The perennial stream is darker blue and collects the water from the intermittent streams, the channels, and the upslope area.

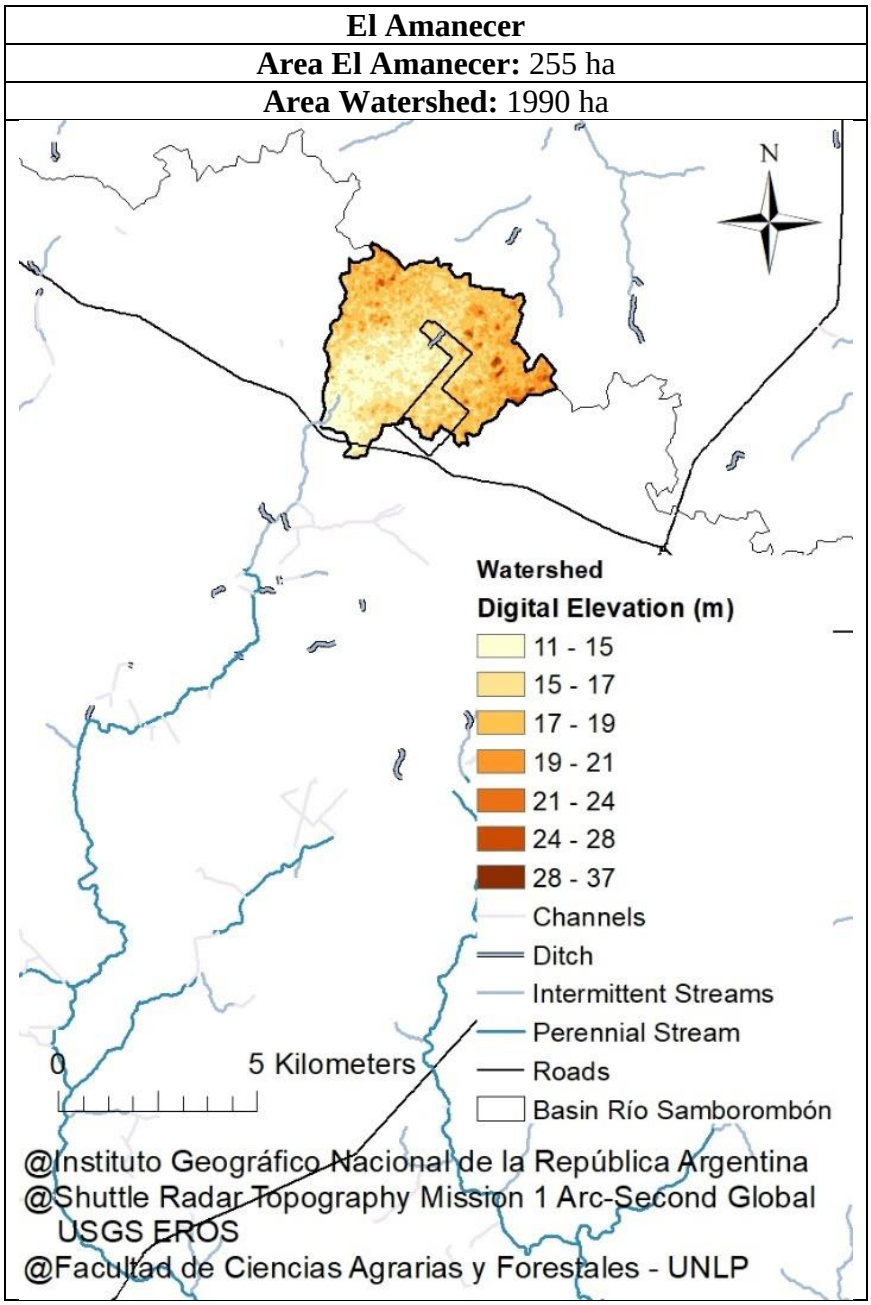

Figure 22: The upslope area of El Amaencer with its outlet at the southwestern edge. The perennial stream is darker blue and collects the water from the intermittent streams, the channels, ditches, and the upslope area.

The upslope areas of Don Joaquín and El Amanecer are both on the edge of the basin of Río Samborombón. Therefore, they have less problems with water accumulations then other fields that are located closer the mainstream, Río Samborombón. The distance to the river affect flood risks of the land (Farhadi *et al.*, 2021). The upslope areas of the two field study sites are also relatively small and therefore the magnitude of the runoff from precipitation is smaller than from bigger basins. Due to the flat landscape the two field study sites have ponding water anyway since water transports slowly in the gentle slopes within the fields which are about 0-3 %. The channels shape with a wide and flat cross section further decreases the water

transportation from the fields as water spreads over a greater surface. The channels are also grass covered which further reduces its speed.

The upslope areas for Don Joaquín and El Amanecer are calculated with SRTM digital elevation with low resolution. With higher resolution digital elevation, and more importantly, a digital elevation model where the tree canopy and houses are extracted, a more accurate delineation of the upslope areas could have been made. A digital elevation model of smaller resolution probably would not improve the representation of the landscapes structure considerably since the terrain is so flat, however streams and ditches might be overseen with the large resolution DEM.

5.4 Water Extents in Pampas

The field sites are not located in the worst flood affected area of Pampa Deprimida which is the lower central-eastern parts. The east-central parts were inundated the 7th of September 2014 to the extent shown in black and blue in Figure 23 and Figure 24 respectively. The 5 days antecedent precipitation for this date was 59 mm in Punta Indio.

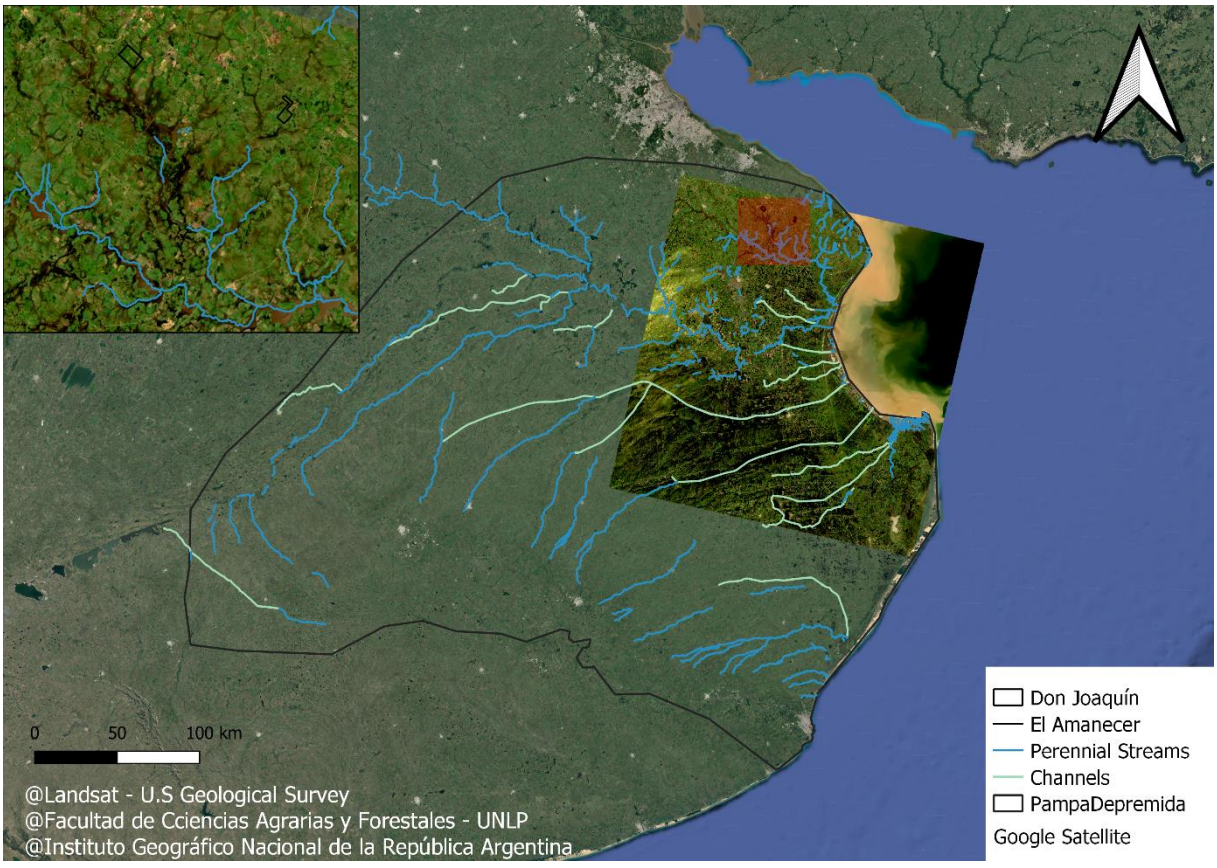

Figure 23: An RGB composite of the northeastern Pampa deprimida region the 7th of September 2014. The two field study sites are spotted in the inset map. Source: Landsat-8 image courtesy of the U.S. Geological Survey, and the waterway network from Instituto Geografico National.

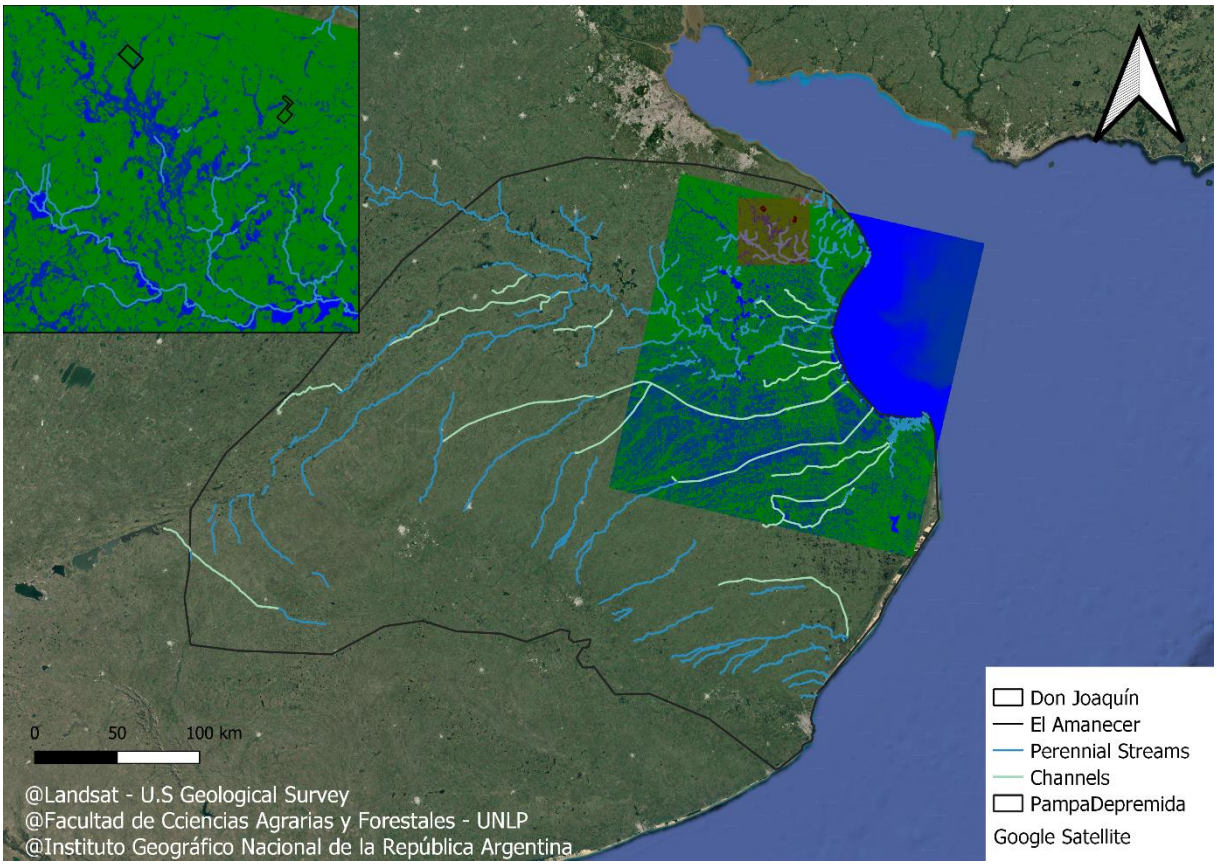

Figure 24: The same satellite photo as in Figure 23 but with different band combinations (MNDWI) visualizing the water extent as a mosaic in the landscape. Blue is the superficial water, and the bare ground is green. Source: Landsat-8 image courtesy of the U.S. Geological Survey, and the waterway network from Instituto Geografico National.

Pampa deprimida is a large region and images over the whole area from the same event does not exists since the satellite passes in orbits and captures images in rows every second week. Furthermore, the cloud cover must be limited if the images should be of use. If clouds are captured by the satellites, they appear as land (green) in the mosaic by the MNDWI and the shadow of the cloud appears as water (blue). The clouds are therefore a source of error when looking at water extents from past events. Images with cloud covers can be sorted out after defined coverage in percentage with the code editor, a 10 % coverage is generally accepted when looking for images. Apart from that the method of examining satellite images to produce flood risk maps is effective since it is probable that water accumulates in the same spots as before unless constructions or drainage channels has changed the water's path.

The MNDWI was chosen in this study instead of other options, such as NDWI. This since it has been shown to include water covered vegetation as water both in this study as well as in other studies (Soltanian, Abbasi and Riyahi Bakhtyari, 2019).

5.4.1 TWI

The topographic wetness index indicates where soil moisture is higher in the landscape with the help of digital elevation, considering the slopes and the elevation. Higher values correspond to higher soil moisture and are found in the local depressions.

The TWI delineate the area in the landscape where water accumulated on the 7th of September 2014 (according to the MNDWI) and the stream network. The exceptions from this are "tails"

where the soil moisture would be higher according to the TWI but is not according to the mosaic of wet environments that are presented for comparison in Figure 14 along with the MNDWI for the image. The TWI classification, 15 – 27, are not absolute values with units, and the values are only comparable with each other within the raster. According to the TWI map the soil moisture is higher at loma than at media loma, which does not match with the results from the field measurements, see Figure 19.

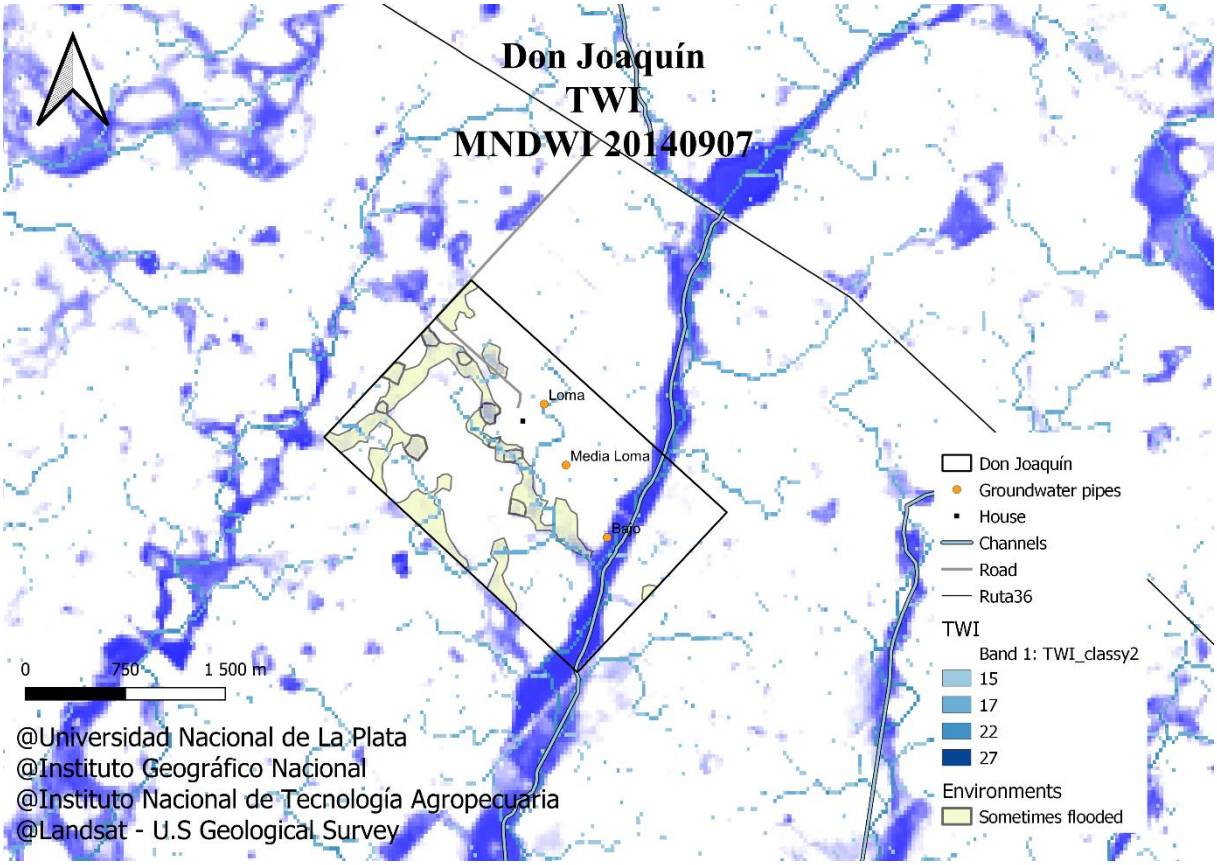

Figure 25: The Topographic Wetness Index, TWI, in the landscape around Don Joaquín. The TWI raster visualizes how the water flow and can indicate where water accumulates. The calculated wetness is compared to the environments of wetter areas presented in mosaic and the water extent the 7th of September 2014 calculated with the MNDWI.

The TWI was chosen in this study to highlight areas with higher risk of inundation since the method only requires free and open-source data and has been shown to be more accurate than other methods within smaller basins (Haas, 2010). The many subbranches with lower TWI are not precise, for instance next to the groundwater well loma (orange dot closest to the house in the map) the soil moisture is supposed to be wetter according to the local topology and slopes (TWI), but according to the soil moisture measurements it is drier. Errors like this could be since the digital elevation used in the calculation of the TWI includes buildings and trees, which causes greater slopes and lower TWI where soil moisture would be higher. That loma is a drier spot is further verified by satellite images, it has not been flooded earlier according to the predefined environments. The higher values of the TWI, 22-27, represent the water path well, and the lower values could be deleted from the map since they are not precise, however they were not deleted in this map for the visualization of the water paths.

In Figure 25, the TWI is evaluated as flood risk mapping parameter by comparing it to actual events and measured values from the field site. Since the water extent is visualized with a satellite image and the extracted MNDWI, it cannot be interpreted as the exact water extent. For example, in Figure 14, in the division between the wet and drier environments compiled by looking at various RGB images, the water extent was overestimated since smaller forests was overlooked as water since forests are dark in the images as well as the water. To compare the calculated soil moisture and the MNDWI based on satellite images can nevertheless be smart since water does not always flow along the slope gradient parallel to the soil surface, which is assumed when using the TWI. If there are impermeable layers in the soil, such as clay, infiltrated water can flow in other directions than what the digital terrain data and the TWI assumes (Haas, 2010). The TWI can therefore, together with the MNDWI, be included in management and planning.

The resolution of the raster, both for the MNDWI, and the digital terrain from the SRTM, is about 30 meters which means that precise information about smaller characteristics as pits and ponds is lost. However, since the variations are few in the plain landscape the lower resolution does not affect the accuracy of the TWI much. The MNDWI however misses smaller streams which the big grids from the satellite images cannot capture. The TWI complement the MNDWI since it marks where the smaller stream networks go, even though the resolution for the digital terrain is just as low.

The limitations of using the TWI as a soil moisture parameter lays in its steady state calculation, whereas soil moisture fluctuates depending on antecedent precipitation which is a driving factors for floods. However, the TWI is good for mapping relative soil moisture in smaller basins since it does not demand much input data and can be done fast and free in GIS-programs, for example QGIS, as well as in ArcGIS.

5.4.2 Water Extents Relation to Precipitation

The relation between precipitation, the season of the year and water extent/floods is analysed in Figure 26, Figure 27 and Figure 28.

Plotted in Figure 26 are the flood extents from the events captured by satellite images from the year 2000 to 2022. The antecedent moisture precipitation is on the y-axis and the flood extents are represented by the sizes of the circles. The colours of the circles correspond to the season of the year. According to the figure the three greatest water events all occurred in the wintertime and the greatest water extent, in 2014, did not have high antecedent soil moisture according to precipitation records.

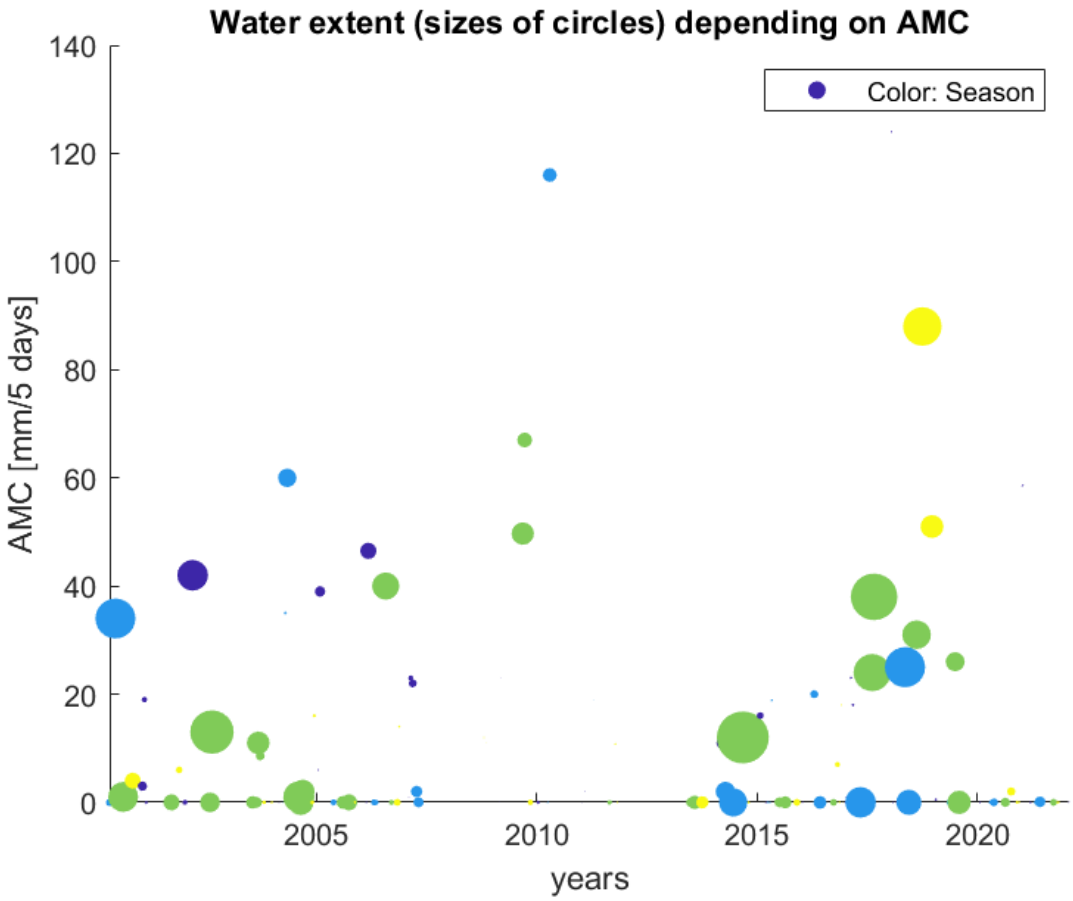

Figure 26: The size of the circles is proportional to the size of the water extent and plotted against the antecedent moisture condition. The water extents are calculated by the Instituto Nacional de Tecnología Agropecuaria in Google Earth Engine with the MNDWI. The green bubbles represent winter events, yellow spring, purple summer, and blue autumn.

Plotted in Figure 27 are the flood extents from the events captured by satellite images from the year 2000 to 2022. The event precipitation is on the y-axis and the flood extents are represented by the sizes of the circles. The colours of the circles correspond to the season of the year. The worst floods had more than 30 mm rain in one day, however some events with big extents have low event precipitation.

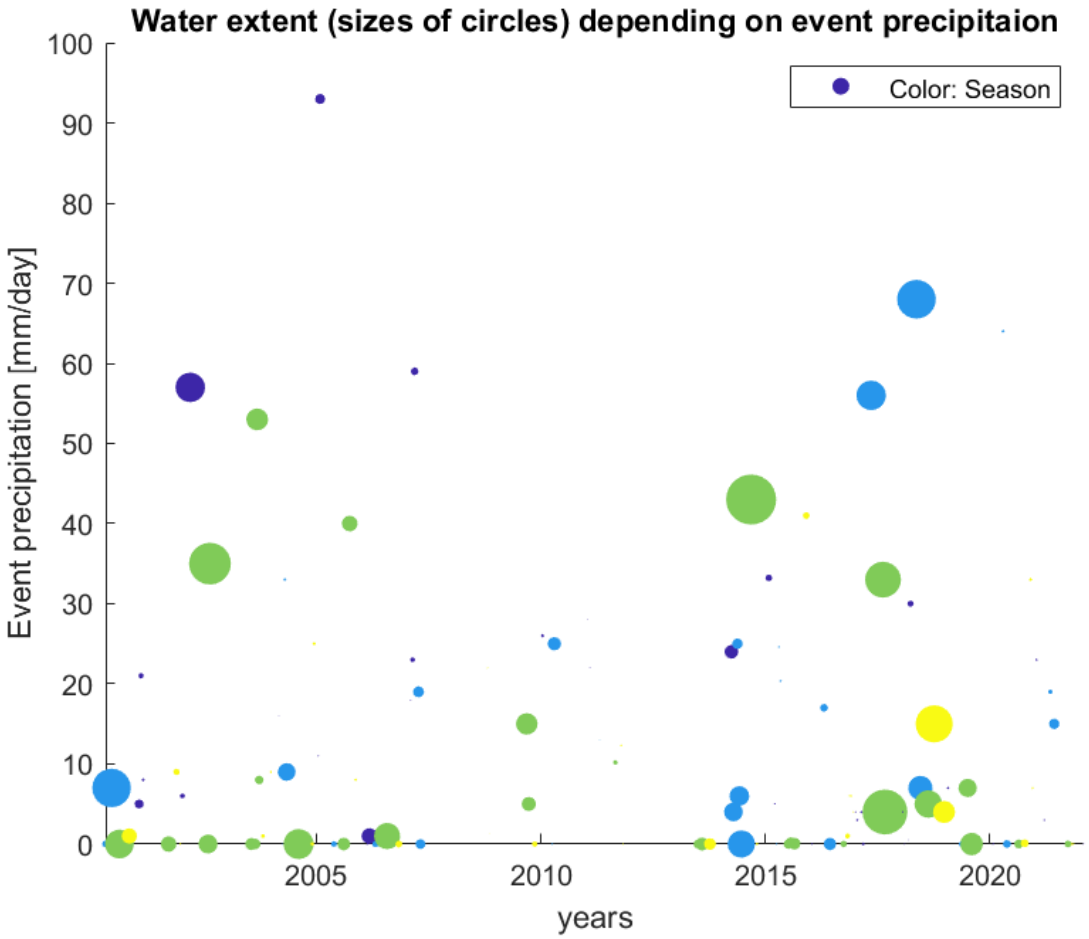

Figure 27: The size of the circles is proportional to the size of the water extent and plotted against the event precipitation. The water extents are calculated by the Instituto Nacional de Tecnología Agropecuaria in Google Earth Engine with the MNDWI. The green bubbles represent winter events, yellow spring, purple summer, and blue autumn.

According to the graphs the greatest flood event occurred in winter 2014. During the winter evapotranspiration is lower due to lower temperatures and plants consuming less water, which increases soil moisture. According to Figure 16 precipitation is also higher in the winter; this does however vary greatly between different years. Both these factors increase the risk of flooding. 2014 was also one of the years with the highest annual precipitation (1400 mm/year), see Figure 6, which probably mean that the groundwater levels were shallow and the soil water storages full causing higher intense runoff. Investigating the flood occurrence in relation to shallow groundwater levels would need to be analysed further.

The precipitation's effect on the flood extent is visualized in Figure 28, the sizes of the circles represent the area of the water extent. The biggest water extent (that has been captured by satellites) is not the event with highest antecedent precipitation nor the highest event precipitation. However, all events with water extents larger than 6 % water coverage has either high AMC or event precipitation or both. AMC, event precipitation and water extent for each event is presented in Appendix B.

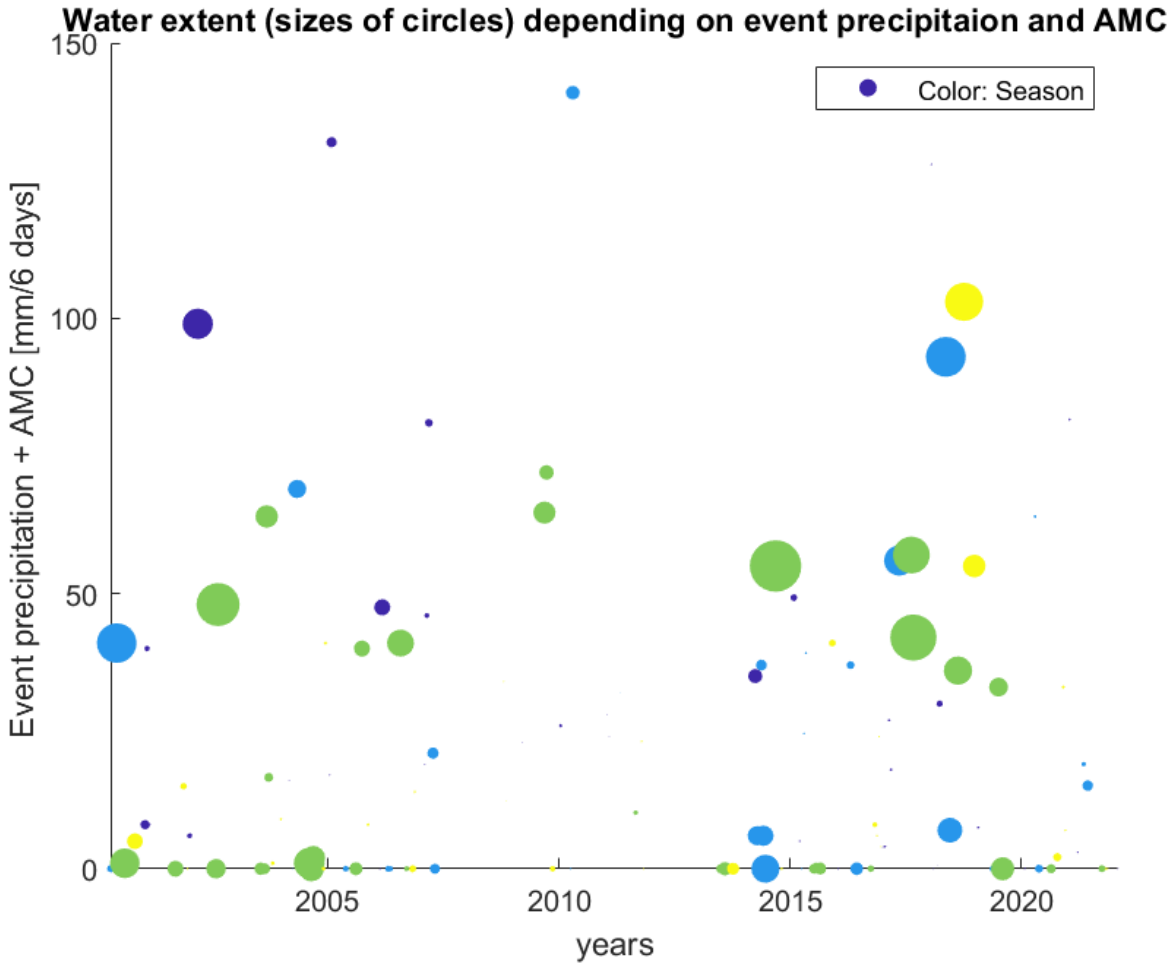

Figure 28: The sizes of the circles visualize the water extent in the landscape after corresponding precipitation for all events. The green bubbles represent winter events, yellow spring, purple summer, and blue autumn.

According the study by Ares, Varni, Chagas, et al. (2020) the antecedent soil moisture conditions, combined with other factors, have an effect on the hydrological response, the runoff. However, in this thesis the area of the water extent was used instead since no runoff data was available. Just as the other study of Pampas, this study claims that several factors are involved in creating hydrological responses in these flat fertile landscapes. The event with largest water extent occurred in 2014, which covered 16 % of the landscape (bigger than the calculated 100-year flood), had an AMC of 43 mm (considered normal conditions during the vegetative season) but the event precipitation was only 15 mm, which is much less than the magnitude of a 20-year event (125 mm/day). The 2014 event cannot be explained by heavy rainfall nor saturated conditions (wet conditions).

The relation between the accumulated water in the landscape around the two field sites and the precipitation is hard to tell from the events studied. One factor of the precipitation that has not been studied which could explain the big water extents in the landscape is the intensity. If the intensity is higher than the infiltration capacity, water ponds on the soil surface. High intense rainfall with big raindrops also decreases the infiltration capacity since it damages the soil's aggregated structures. The intensity could not be studied since the precipitation is measured on daily basis. It is possible that events with high water extent are events with high

intense rainfall, probably over 16 mm/hour, which is the measured infiltration capacity in Don Joaquín. With the data available within the thesis, it is also unsure which day the event precipitation corresponds to, hence what was thought to be antecedent conditions might be the rainfall causing the flood.

The events with water extents greater than 2 % (in this thesis accounted as "normal" water events) available for analysis are few. This is because large floods do not occur on yearly basis. Furthermore, all flood events cannot be captured since the satellites do not pass by frequently enough. The cloud cover further decreases the number of images available and images including clouds are a source of error. The clouds make the area of water appear bigger or smaller depending on the size of the cloud.

There are no precipitation gauges south of the field sites close enough to include in a method for estimating the precipitation in the field study sites (D'Andrea *et al.*, 2019). Since the AMC is based on precipitation from Punta Indio, which lays outside the area of the calculated water extent, results are less accurate. However, during flooding in Pampa deprimida, see Figure 13, large areas are affected at the same time. Hence, the precipitation data and the water extent can be considered linked, unless the precipitation over Punta Indio is very local.

In this thesis CHIRPS lowest time scale for precipitation, daily, is used to complement the precipitation data from the weather station. The CHIRPS data has a resolution of about 5 kilometres, since the mean precipitation was downloaded the heavy precipitation events are surely underestimated compared to what would have been measured at the weather station. This problem has been highlighted by others (UC Santa Barbara, 2021). This made the precipitation relation to the floods harder to distinguish.

5.4.3 Estimated Surface Runoff with SCS-CN method

The water extents of past events relation to precipitation were evaluated in the previous sections, in this section the SCS-CN method is used to find the runoff coefficient for the fields and the past events are used to evaluate the SCS-CN method's ability to foresee floods. Land-use, infiltration capacity and AMC are in-data in the method to obtain an estimation of the direct runoff following a storm precipitation (in this study the event precipitation).

According to the SCS-CN method higher antecedent moisture condition and higher curve number lead to higher runoff. According to the SCS-CN method no surface runoff is produced in the fields of Don Joaquín and El Amanecer if it has rained less than approximately 5, 15 and 33 mm depending on the previous days' rainfall, AMC class 3, 2 and 1 respectively.

The runoff coefficient for the fields depends on the antecedent moisture condition classes, the land-use, the infiltration capacities, the soil characteristics, and the vegetative cover. According to the curves in the graph in Appendix D, the three surface runoff coefficients for the three different scenarios are approximately 0.3, 0.6 and 0.8, see Table 7.

Table 7: The initial abstraction and the calculated surface runoff coefficient for storm events in Pampa deprimida depending on the antecedent conditions. The AMC classes are 1, 2 and 3: AMC class 1 (<25.5 mm), AMC class 2 (35.5 mm – 53.3 mm) and AMC class 3 (>53.3 mm).

CN	AMC class	Initial abstraction (mm)	Surface Runoff Coefficient
56	1	33	30 %
74	2	15	60 %
87	3	5	80 %

The surface runoff coefficients calculated from the SCS-CN graph are higher compared to what have been found in other studies in Argentina, where the runoff coefficient was found to be 1.6% (Ares *et al.*, 2020). The runoff coefficients found with the SCS-CN method is closer to the runoff coefficient found in other studies in flat agricultural landscape, 40 % (Goel, 2011).

The AMC and the event precipitation, in Figure 29, are precipitation depths measured at the weather station in Punta Indio complemented with CHIRPS. The estimation of the surface runoff is based on the curve number and a higher curve number gives higher surface runoff. For curve number 74 (see the path of the blue circles in Figure 29, or more clearly in Appendix D) the high event rainfall of about 60 mm during normal soil moisture conditions gave a high estimated surface runoff. The water extent for that event was also high. The event with the highest expected surface runoff did not have a great water extent. For curve number 56 (see the path of the yellow circles in Figure 29) the surface runoff was not expected to be high considering the AMC for the event. However, many of these events had large water extents and event precipitation over 30 mm/day.

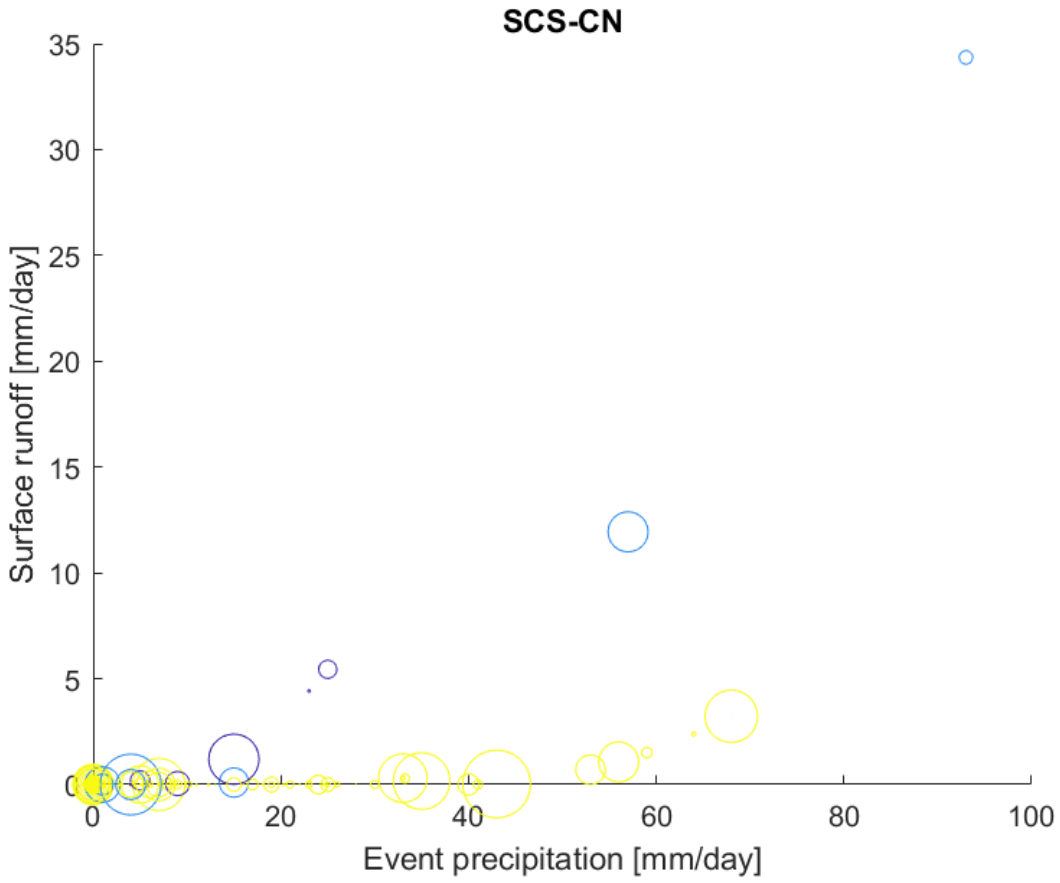

Figure 29: The correlation between runoff and event precipitation according to the SCS-CN method. The sizes of the circles represent the water extent for the events calculated with the MNDWI from satellite images. The three groups are AMC class 3 (purple), AMC class 2 (blue) and AMC class 1 (yellow).

Storm precipitation under 5 mm during wet conditions (AMC class 3, purple), under 15 mm during normal conditions (AMC class 2, blue) and under 33 mm during dry conditions (AMC class 1, yellow) is according to the SCS-CN method lost through interception in the plants canopy and through infiltration and not contributing to direct runoff. That is called the initial abstraction and up until that rain depth a storm precipitation does not cause runoff. The initial abstraction for the method is 20 % of the retention factor, S, regardless the local conditions that day. This is a simplification, even though vegetation and infiltration are considered in the selection of the curve number, vegetational cover and infiltration rates changes through years.

The infiltration rate in non-saturated soil is higher, see Figure 18. The water penetrates the soil surface faster during dry conditions when infiltration rates are lower, and the system can "absorb" more water before surface runoff is created than during wet conditions. That explains why the estimated surface runoff for the yellow circles (AMC class 1) were so small. However, those event precipitations correspond to larger water extents, hence the method cannot foresee surface runoff within the fields of this study.

In this study the event precipitation is daily precipitation, does not say much about the intensity of the rainfall. Therefore, it is hard to know whether the events with higher precipitation are actual storms, considering the unknown time interval for the rain events. Comparing the event precipitation's depth with the depth of a storm event with a return period

of 20 years (125 mm/day) few events in SCS-CN study would be considered storm events. Hence, trying to validate the method with the selected past events is not fair since the events are not storms.

The limits for the classification of the antecedent soil moisture are based on the vegetative growing season since mean temperatures in Punta Indio rarely goes under 6 ℃, see mean temperature in Punta Indio in Figure 4. However, if the classification of AMC would consider vegetative dormant season for the winter months, the AMC class for these events would be higher since evapotranspiration is lower in the wintertime and soil moisture were then actually higher. Since Punta Indio lays by the coast, it is possible that the temperatures are milder there during the wintertime than in the inlands, where the area of the water extent was extracted. Hence, it is possible that the estimated surface runoff is underestimated for the winter months.

The curve number chosen from Table 2 determines how much of the precipitation that becomes surface runoff. The curve number method is not so sensitive and it's used broadly and widely (De Paola, Ranucci and Feo, 2013). However, since the results only relay on one parameter, the curve number, the estimated surface runoff would be different if the curve number were chosen differently. In this study the curve number depends on measured infiltration capacities and on the observed land-cover in a quite homogenous agricultural landscape. However, the infiltration capacity can vary within the fields due to, for example, soil compaction from cattle trampling, causing more surface runoff than expected.

The SCS-CN could not explain the floods for the events in the study, comparing the expected surface runoff and the observed water extent from satellite images. That does not mean that the SCS-CN method is wrong, however, it is not suitable for foreseeing floods in Pampas with the measurement techniques used within the thesis. That the method is not appropriate could also be since the two ways of measuring floods, runoff versus flood extent, are not comparable.

On the other hand, since the SCS-CN method is so widely used and demand few in-data parameters it would be suitable to consider as a method to foresee floods, or at least the principle since it is simple. The SCS-CN method which estimates surface runoff is much cheaper than implementing expansive equipment for measuring discharge to make hydrographs for inundation predictions. The method is also adjusted for smaller subbasins with agricultural land-use (USDA-NRCS, 2019).

5.4.4 Floods

The driving factors behind the flooding investigated in this study are the precipitation; event precipitation, antecedent precipitation and different physical characteristics as the infiltration capacity and the terrain. From the SCS-CN method the surface runoff can be estimated with precipitation data and knowledge about the land-use. No clear correlations could be found between precipitation and surface runoff or water extents in general.

Looking into the small scale processes, as for instance after a 53 mm event rainfall recorded in Punta Indio, the local water extent changes quickly within a two week period, see the difference in water extent between Figure 30 and Figure 31.

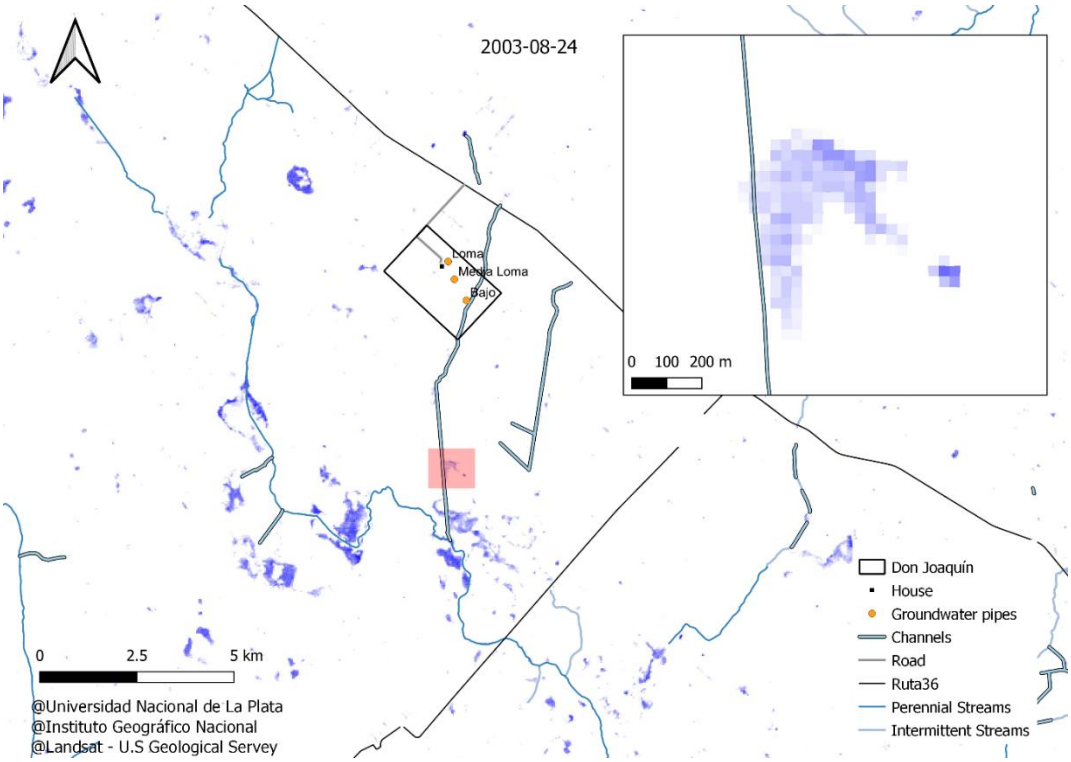

Figure 30: Before a 53 mm/day event rainfall in Don Joaquín Pampa deprimida. The stream network is shown with blue lines and the blue patches are accumulated water. The inset map shows an example of how the water extent changes quickly on a local scale after a rain event, compare with Figure 30.

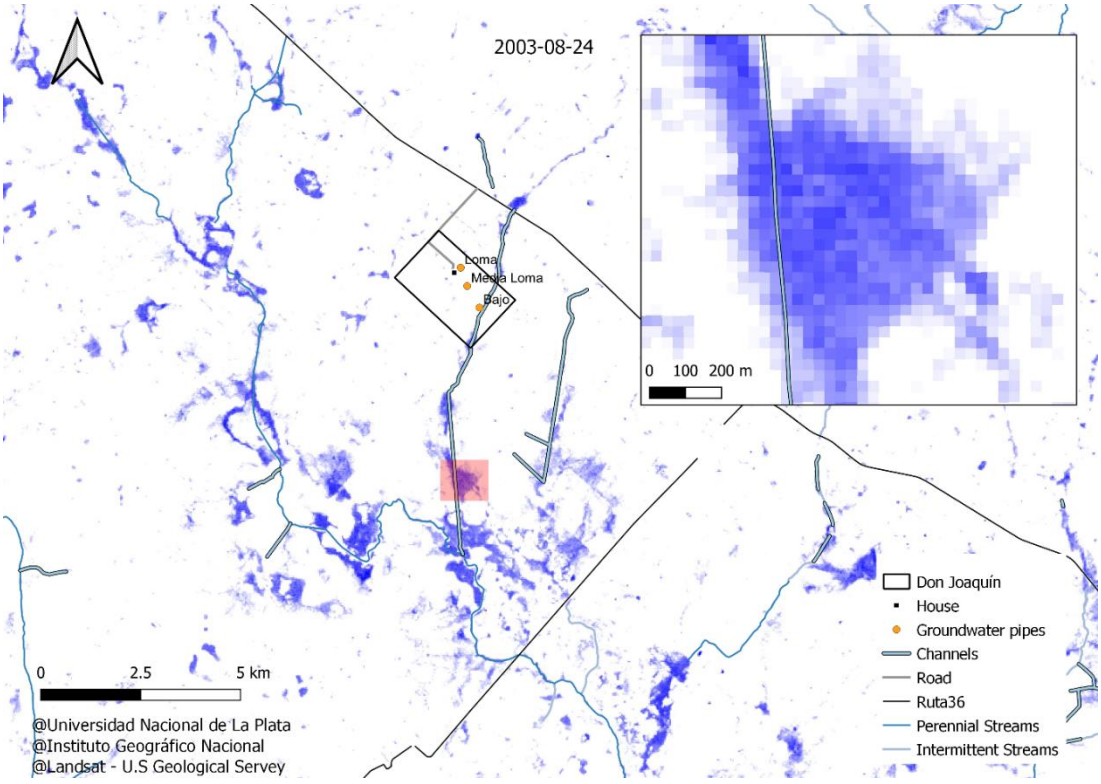

Figure 31: After a 53 mm/day event rainfall in Don Joaquín Pampa deprimida. The stream network is shown with blue lines and the blue patches are accumulated water. The inset map shows an example of how the water extent changes quickly on a local scale after a rain event, 53 mm/day. The rain depth before the event precipitation was 11 mm (AMC class 1).

From the study of all events, it has been unclear whether floods depend on heavy event precipitation. In September 2003 it is possible that the heavy rainfall of 53 mm was the triggering factor of the water accumulation, however, other factors could also have played a role in the flood outbreak. For instance, as Pampa Deprimida is a lower region it can act as outflow area and receive groundwater from distant areas. To further analyse whether Pampa deprimida is an outflow area and affected by rainfall from other regions an isotope analysis of the runoff water could be conducted. The results could distinguish whether the runoff depend on mostly event water or the baseflow (Fischer, van Meerveld and Seibert, 2017). Another factor that has not been included in the thesis is the tide, as the terrain of Pampa deprimida is close to sea level, around 17 meters above sea level in Don Joaquín and El Amanecer, it can have a periodical effect on the water levels in the water ways. No such influences were seen during the field visits in February-April 2022, however during wetter conditions it could contribute to the flood pushing it and raising it.

6. Conclusions

The water extent in Pampa deprimida fluctuates strongly on yearly basis. No trends of changing precipitation patterns could be seen in the study and to make better predictions of floods with precipitation data local measurements with shorter time lapses are necessary. Don Joaquín and El Amanecer have small upslope areas on the ridge of the basin of Río Samborombón and their distance to the river, higher elevation and small watersheds saves them from the largest floods which are found in the lower points in the landscape with gentler slopes. The TWI is a good parameter for visualizing flood risk along with satellite images that can show the width of the water extent. To minimize the risk of surface runoff during storms, the management of the land is of importance to maintain good soil structure. Maintenance of the vegetational cover increase the infiltration into the soil and balances the hydrological responses.

References

Abba, A.M., Zufiaurre, E., Gado, P.A., Codesido, M. and Bilenca, D.N. (2015) 'Distribución de tres especies de armadillos en la región pampeana comprendida en la provincia de Buenos Aires, Argentina', *Mastozoologia Neotropical*, 22(2), pp. 359–365.

Alconada-Magliano, Margarita María (2021) 'Intensified Land and Water Use'. Edited by Margarita María Alconada-Magliano. Available at: https://doi.org/10.1007/978-3-030-65443-6.

Ameghino, F. (1884) *Las secas y las inundaciones en la Provincia de Buenos Aires*. Primera Ed. La Plata: Secretaria de politica ambiental.

Ares, M.G., Varni, M. and Chagas, C. (2020) 'Runoff response of a small agricultural basin in the argentine Pampas considering connectivity aspects', *Hydrological Processes*, 34(14), pp. 3102–3119. Available at: https://doi.org/10.1002/hyp.13782.

Ares, M.G., Varni, M., Chagas, C. and Usunoff, E.J. (2020) 'Runoff response of a small agricultural basin in the argentine Pampas considering connectivity aspects'. Available at: https://doi.org/10.1002/hyp.13782.

Arreghini, S., De Cabo, L., Seoane, R., Tomazin, N., Serafini, R. and De Iorio, A.F. (2007) 'A methodological approach to water quality assessment in an ungauged basin, Buenos Aires, Argentina', *GeoJournal*, 70(4), pp. 281–288. Available at: https://doi.org/10.1007/s10708-008-9134-z.

Auge, M. (2004) 'Regiones hidrogeológicas'.

Awadallah, A.G. and Tabet, D. (2015) 'Estimating flooding extent at high return period for ungauged braided systems using remote sensing: a case study of Cuvelai Basin, Angola', *Natural Hazards*, 77(1), pp. 255–272. Available at: https://doi.org/10.1007/s11069-015-1600-6.

Bergendal, G., Håstad, M. and Råde, L. (1967) *Statistik och sannolikhetslära*. Biblioteksförlaget AB, Stockholm.

Beven, K.J., Kirkby, M.J. and Kirkby, A.J. (1979) 'A physically based, variable contributing area model of basin hydrology / Un modèle à base physique de zone d'appel variable de l'hydrologie du bassin versant) A physically based, variable contributing area model of basin hydrology / Un modèle à base physique de zone d'appel variable de l'hydrologie du bassin versant A physically based, variable contributing area model of basin hydrology', *Hydrological Sciences Journal*, 24(1), pp. 43–69. Available at: https://doi.org/10.1080/02626667909491834.

Blume, T., Zehe, E. and Bronstert, A. (2007) 'Rainfall-runoff response, event-based runoff coefficients and hydrograph separation', *Hydrological Sciences Journal*, 52(5), pp. 843–862. Available at: https://doi.org/10.1623/hysj.52.5.843.

Bona, L. (2021) 'Tendencias recientes en los cultivos de exportación y la producción ganadera en la provincia de Buenos Aires. Una mirada desde sus regiones productivas', *Ciencia, Docencia y Tecnología*, 32(62 may-ago), pp. 1–39. Available at: https://doi.org/10.33255/3262/775.

Bruce, J.P. (2017) 'Meteorology and Water Resources', *Water Resources of Canada*, pp. 111–115. Available at: https://doi.org/10.3138/9781442653863-016.

Capas SIG | Instituto Geográfico Nacional (no date). Available at: https://www.ign.gob.ar/NuestrasActividades/InformacionGeoespacial/CapasSIG (Accessed: 17 February 2022).

Carter, T.R., Hulme, M., Crossley, J.F., Malyshev, S., New, M.G., Schlesinger, M.E. and Tuomenvirta, H. (2000) 'Climate Change in the 21st Century - Interim Characterizations based on the New IPCC Emissions Scenarios', *The Finnish Environment 433*, p. 148 pp.

Cicore, P.L., Sánchez, H.R., Peralta, N.R., Franco, M., Castro, Aparicio, V.C. and Costa, J.L. (2015) *Delimitación de ambientes edáficos en suelos de la Pampa Deprimida mediante la conductividad*

eléctrica aparente y la elevación. Available at: http://www.scielo.org.ar/scielo.php?script=sci_arttext&pid=S1850-20672015000200007&lng=en&tlng=en (Accessed: 2 June 2022).

D'Andrea, M.F., Rousseau, A.N., Bigah, Y., Gattinoni, N.N. and Brodeur, J.C. (2019) 'Trends in reference evapotranspiration and associated climate variables over the last 30 years (1984–2014) in the Pampa region of Argentina', *Theoretical and Applied Climatology*, 136(3–4), pp. 1371–1386. Available at: https://doi.org/10.1007/s00704-018-2565-7.

De Frente al Campo (2021). Available at: https://www.defrentealcampo.com.ar/region-pampeana-caracteristicas-flora-y-fauna/ (Accessed: 16 February 2022).

Degano, M.F., Rivas, R.E., Carmona, F., Niclòs, R. and Sánchez, J.M. (2021) 'Evaluation of the MOD16A2 evapotranspiration product in an agricultural area of Argentina, the Pampas region', *Egyptian Journal of Remote Sensing and Space Science*, 24(2), pp. 319–328. Available at: https://doi.org/10.1016/j.ejrs.2020.08.004.

Eijkelkamp (2015) 'Double Ring Infiltrometer Manual', *Double Ring Infiltrometer*, pp. 1–9. Available at: https://en.eijkelkamp.com/products/field-measurement-equipment/double-ring-infiltrometer.html.

Farhadi, H., Najafzadeh, M., Mohammadi, B. and Zhang, Y. (2021) 'Flood Risk Mapping by Remote Sensing Data and Random Forest Technique'. Available at: https://doi.org/10.3390/w13213115.

Farr, T.G. *et al.* (2007) 'The shuttle radar topography mission', *Reviews of Geophysics*, 45(2). Available at: https://doi.org/10.1029/2005RG000183.

Fischer, B.M.C., van Meerveld, H.J. (Ilja. and Seibert, J. (2017) 'Spatial variability in the isotopic composition of rainfall in a small headwater catchment and its effect on hydrograph separation', *Journal of Hydrology*, 547, pp. 755–769. Available at: https://doi.org/10.1016/j.jhydrol.2017.01.045.

Goel, M.K. (2011) 'Runoff coefficient', *Encyclopedia of Earth Sciences Series*, Part 3, pp. 952–953. Available at: https://doi.org/10.1007/978-90-481-2642-2_456/TABLES/1.

Google Earth Engine (no date). Available at: https://earthengine.google.com/platform/ (Accessed: 10 June 2022).

Grabs, T., Seibert, J., Bishop, K. and Laudon, H. (2009) 'Modeling spatial patterns of saturated areas: A comparison of the topographic wetness index and a dynamic distributed model', *Journal of Hydrology*, 373(1–2), pp. 15–23. Available at: https://doi.org/10.1016/j.jhydrol.2009.03.031.

Gray, D. and Burke, C. (1983) 'Occurrence Probabilities of Antecedent Moisture Condition Classes in Indiana'.

Güçlü, Y.S. (2018) 'Multiple Şen-innovative trend analyses and partial Mann-Kendall test', *Journal of Hydrology*, 566(September), pp. 685–704. Available at: https://doi.org/10.1016/j.jhydrol.2018.09.034.

Haas, J. (2010) 'Soil moisture modelling using TWI and satellite imagery in the Stockholm region', (March).

Herzog, M., Striker, G.G., Colmer, T.D. and Pedersen, O. (2016) 'Mechanisms of waterlogging tolerance in wheat-a review of root and shoot physiology'. Available at: https://doi.org/10.1111/pce.12676.

Hosseinzadehtalaei, P., Tabari, H. and Willems, P. (2020) 'Climate change impact on short-duration extreme precipitation and intensity–duration–frequency curves over Europe', *Journal of Hydrology*, 590(March), p. 125249. Available at: https://doi.org/10.1016/j.jhydrol.2020.125249.

Hümann, M., Schüler, G., Müller, C., Schneider, R., Johst, M. and Caspari, T. (2011) 'Identification of runoff processes - The impact of different forest types and soil properties on runoff formation and floods', *Journal of Hydrology*, 409(3–4), pp. 637–649. Available at: https://doi.org/10.1016/j.jhydrol.2011.08.067.

INDEC-Instituto-Nacional-de-Estadística-y-Censos (2019) *Censo Nacional Censo Nacional Agropecuario Agropecuario, 2018*.

Instituto Geográfico Nacional (no date) *Introducción | Instituto Geográfico Nacional*. Available at: https://www.ign.gob.ar/NuestrasActividades/Geodesia/ModeloDigitalElevaciones/Introduccion (Accessed: 3 June 2022).

Johnson, A.I. (1963) 'A Field Method for Measurement of Infiltration', *Geological Survey Water-Supply Paper*, 1544-F, p. 27.

Kim, J., Johnson, L., Cifelli, R., Thorstensen, A. and Chandrasekar, V. (2019) 'Assessment of antecedent moisture condition on flood frequency: An experimental study in Napa River Basin, CA', *Journal of Hydrology: Regional Studies*, 26, p. 100629. Available at: https://doi.org/10.1016/J.EJRH.2019.100629.

Van Loon, A.F. (2015) 'Hydrological drought explained HYDROLOGICAL DROUGHT IN CONTEXT', *WIREs Water*, 2, pp. 359–392. Available at: https://doi.org/10.1002/wat2.1085.

Marteinsdóttir, B., Barrio, I.C. and Svala Jónsdóttir, I. (2017) 'Assessing the Ecological Impacts of Extensive Sheep Grazing in Iceland', *Icelandic Agricultural Sciences*, 30, pp. 55–72. Available at: https://doi.org/10.16886/IAS.2017.07.

National Geographic Society (2018) *Köppen Climate Classification System | National Geographic Society*, *Neional Geographic*. Available at: https://education.nationalgeographic.org/resource/koppen-climate-classification-system (Accessed: 16 September 2022).

OECD (2019) *Water_Governance_in_Argentina, OECD Studies on Water*. Available at: https://doi.org/10.1787/bc9ccbf6-en.

Palmero, F., Carcedo, A.J.P., Haro, R.J., Bigatton, E.D., Salvagiotti, F. and Ciampitti, I.A. (2022) 'Modeling drought stress impacts under current and future climate for peanut in the semiarid pampas region of Argentina', *Field Crops Research*, 286(June), p. 108615. Available at: https://doi.org/10.1016/j.fcr.2022.108615.

De Paola, F., Ranucci, A. and Feo, A. (2013) 'ANTECEDENT MOISTURE CONDITION (SCS) FREQUENCY ASSESSMENT: A CASE STUDY IN SOUTHERN ITALY †', *IRRIGATION AND DRAINAGE Irrig. and Drain*, 62, pp. 61–71. Available at: https://doi.org/10.1002/ird.1801.

Paredes Trejo, F.J., Barbosa, H.A., Peñaloza-Murillo, M.A., Alejandra Moreno, M. and Farías, A. (2016) 'Intercomparison of improved satellite rainfall estimation with CHIRPS gridded product and rain gauge data over Venezuela', *Atmosfera*, 29(4), pp. 323–342. Available at: https://doi.org/10.20937/ATM.2016.29.04.04.

Parvez, M.B. and Inayathulla, M. (2019) 'Estimation of surface runoff by soil conservation service curve number model for upper Cauvery Karnataka', *Int. J. Sci. Res. in Multidisciplinary …* [Preprint], (November). Available at: https://doi.org/10.13140/RG.2.2.30526.23366.

Pereyra, F.X. and Ragas, D.B. (2021) 'Los suelos de la pampa ondulada', *Anales Segemar* [Preprint].

Pourali, S.H., Arrowsmith, C., Chrisman, N., Matkan, A.A. and Mitchell, D. (2016) 'Topography Wetness Index Application in Flood-Risk-Based Land Use Planning', *Applied Spatial Analysis and Policy*, 9(1), pp. 39–54. Available at: https://doi.org/10.1007/S12061-014-9130-2.

Rivera, J.A., Hinrichs, S. and Marianetti, G. (2019) 'Using CHIRPS Dataset to Assess Wet and Dry Conditions along the Semiarid Central-Western Argentina'. Available at: https://doi.org/10.1155/2019/8413964.

Soltanian, F.K., Abbasi, M. and Riyahi Bakhtyari, H.R. (2019) 'Flood monitoring using NDWI and MNDWI spectral indices: A case study of Aghqala flodd-2019, Golestan province, Iran'. Available at: https://doi.org/10.5194/isprs-archives-XLII-4-W18-605-2019.

Soulis, K.X. and Valiantzas, J.D. (2012) ‘SCS-CN parameter determination using rainfall-runoff data in heterogeneous watersheds-the two-CN system approach’, *Hydrology and Earth System Sciences*, 16(3), pp. 1001–1015. Available at: https://doi.org/10.5194/hess-16-1001-2012.

UC Santa Barbara (2021) *CHIRPS: Rainfall Estimates from Rain Gauge and Satellite Observations | Climate Hazards Center - UC Santa Barbara, Univeirsty of California*. Available at: https://www.chc.ucsb.edu/data/chirps (Accessed: 11 August 2022).

USDA-NRCS (2019) *National Engineering Handbook, Part 630 Hydrology*. U.S. Department of Agriculture (USDA). Available at: https://www.nrcs.usda.gov/wps/portal/nrcs/detailfull/national/water/manage/hydrology/?cid=stelprdb1043063 (Accessed: 1 June 2022).

Wang, C., Zhao, C.Y., Xu, Z.L., Wang, Y. and Peng, H.H. (2013) ‘Effect of vegetation on soil water retention and storage in a semi-arid alpine forest catchment’, *Journal of Arid Land*, 5(2), pp. 207–219. Available at: https://doi.org/10.1007/s40333-013-0151-5.

Xu, M., Fralick, D., Zheng, J.Z., Wang, B., Tu, X.M. and Feng, C. (2017) ‘The Differences and Similarities Between Two-Sample T-Test and Paired T-Test’, *Shanghai Archives of Psychiatry*, 29(3), p. 184. Available at: https://doi.org/10.11919/J.ISSN.1002-0829.217070.

Appendix

Appendix A: Yearly Maximum Daily Precipitation in Punta Indio

The rain values with decimals are values from CHIRPS, the other values (whole numbers) are from the weather station in Punta Indio (pluviometry type B).

Table 8: Maximum daily precipitation every year since 1980-2021 in Punta Indio. Missing daily precipitation data is replaced with daily rainfall data from CHIRPS for an area around Punta Indio.

Year	Maximum Daily precipitation from Punta Indio [mm/day]*
'1980-01-01'	139.500000000000
'1981-01-01'	59
'1982-01-01'	62
'1983-01-01'	76
'1984-01-01'	112
'1985-01-01'	69
'1986-01-01'	54.5000000000000
'1987-01-01'	61
'1988-01-01'	74.8000000000000
'1989-01-01'	60
'1990-01-01'	109.600000000000
'1991-01-01'	67.3714000000000
'1992-01-01'	35.0344000000000
'1993-01-01'	95.5902000000000
'1994-01-01'	54.4437000000000
'1995-01-01'	54.5847000000000
'1996-01-01'	51.3053000000000
'1997-01-01'	48.2721000000000
'1998-01-01'	47.5211000000000
'1999-01-01'	45.8991000000000
'2000-01-01'	49
'2001-01-01'	176
'2002-01-01'	103
'2003-01-01'	66
'2004-01-01'	134
'2005-01-01'	93
'2006-01-01'	145
'2007-01-01'	59
'2008-01-01'	78
'2009-01-01'	69
'2010-01-01'	106
'2011-01-01'	63
'2012-01-01'	56
'2013-01-01'	76
'2014-01-01'	92
'2015-01-01'	43
'2016-01-01'	105
'2017-01-01'	84
'2018-01-01'	71

'2019-01-01'	106
'2020-01-01'	64
'2021-01-01'	58

Appendix B: Events

The events used for the SCS-CN method, the frequency analysis, and the distribution of different events through the years compared to the AMC are presented in Table 9. The column "Agua" refers to the area of the water extent, classified with the MNDWI and appears as blue in Figure 13. The column "sin agua" is the area appearing as green in the satellite images classified not to be water with the MNDWI. The events are not all flooding events. The blue marked in Table 9 signifies the greatest water cover that year captured with a satellite images.

Table 9: Event precipitation and AMC (Punta Indio weather station and CHIRPS) for the events in the study (satellite images) and their estimated water extents calculated with the MNDWI by INTA (2022).

Event: Date of image capturing	**Sin agua***	**Agua ***	**Water %**	**Event precipitation** [mm] ***	**AMC** [mm] ****
2000-04-25	53 321	178	0.3	0.0	0.0
2000-06-12	48 564	4 935	9.2	7.0	34.0
2000-08-15	50 732	2 766	5.2	0.0	1.0
2000-11-03	52 707	791	1.5	1.0	4.0
2001-01-22	53 228	271	0.5	5.0	3.0
2001-02-07	53 397	102	0.2	21.0	19.0
2001-02-23	53 463	35	0.1	8.0	0.0
2001-09-19	52 692	806	1.5	0.0	0.0
2001-11-22	53 357	142	0.3	9.0	6.0
2001-12-24	53 482	16	0.0	0.0	0.0
2002-01-09	53 410	88	0.2	6.0	0.0
2002-03-14	50 590	2 908	5.4	57.0	42.0
2002-08-05	52 289	1 210	2.3	0.0	0.0
2002-08-21	47 681	5 817	10.9	35.0	13.0
2003-07-23	52 999	500	0.9	0.0	0.0
2003-08-24	53 125	374	0.7	0.0	0.0
2003-09-09	51 907	1 592	3.0	53.0	11.0
2003-09-25	53 249	249	0.5	8.0	8.6
2003-10-27	53 448	50	0.1	1.0	0.0
2003-12-30	53 476	23	0.0	9.0	0.0
2004-03-03	53 494	5	0.0	16.0	0.0
2004-04-04	53 494	5	0.0	0.0	0.0
2004-04-20	53 466	32	0.1	33.0	35.0
2004-05-06	52 450	1 048	2.0	9.0	60.0
2004-06-07	53 228	271	0.5	0.0	0.0
2004-08-10	50 500	2 999	5.6	0.0	1.0
2004-08-26	51 517	1 982	3.7	0.0	0.0
2004-09-11	51 738	1 761	3.3	0.0	2.0
2004-11-30	53 450	49	0.1	0.0	0.0
2004-12-16	53 453	46	0.1	25.0	16.0
2005-01-17	53 489	9	0.0	11.0	6.0

2005-02-02	53 157	341	0.6	93.0	39.0
2005-05-25	53 383	115	0.2	0.0	0.0
2005-08-13	52 952	546	1.0	0.0	0.0
2005-09-30	52 678	821	1.5	40.0	0.0
2005-11-17	53 466	32	0.1	8.0	0.0
2006-02-21	53 488	10	0.0	0.0	0.0
2006-03-09	52 680	819	1.5	1.0	46.5
2006-04-26	53 374	125	0.2	0.0	0.0
2006-05-12	53 406	93	0.2	0.0	0.0
2006-07-31	51 218	2 281	4.3	1.0	40.0
2006-09-17	53 412	87	0.2	0.0	0.0
2006-11-04	53 336	163	0.3	0.0	0.0
2006-11-20	53 476	22	0.0	0.0	14.0
2007-02-08	53 494	4	0.0	18.0	1.0
2007-02-24	53 415	84	0.2	23.0	23.0
2007-03-12	53 292	207	0.4	59.0	22.0
2007-04-13	53 090	408	0.8	19.0	2.0
2007-04-29	53 173	325	0.6	0.0	0.0
2008-10-24	53 493	6	0.0	22.0	12.0
2008-11-09	53 496	3	0.0	1.4	11.0
2009-02-13	53 498	0	0.0	68.0	0.0
2009-03-01	53 497	1	0.0	0.0	0.0
2009-03-17	53 497	1	0.0	0.0	23.0
2009-09-09	51 946	1 553	2.9	15.0	49.7
2009-09-25	52 817	682	1.3	5.0	67.0
2009-11-12	53 398	101	0.2	0.0	0.0
2010-01-15	53 453	45	0.1	26.0	0.0
2010-04-05	53 487	11	0.0	0.0	0.0
2010-04-21	52 897	601	1.1	25.0	116.0
2011-01-18	53 496	2	0.0	28.0	0.0
2011-02-03	53 495	3	0.0	22.0	2.0
2011-04-24	53 496	2	0.0	13.0	18.9
2011-08-30	53 428	71	0.1	10.2	0.0
2011-10-17	53 487	12	0.0	12.3	10.8
2011-11-02	53 491	7	0.0	0.0	0.0
2013-07-02	53 232	266	0.5	0.0	0.0
2013-08-03	52 918	580	1.1	0.0	0.0
2013-08-19	53 261	238	0.4	0.0	0.0
2013-10-06	53 031	467	0.9	0.0	0.0
2013-11-23	53 485	13	0.0	0.0	0.0
2014-03-31	52 862	637	1.2	24.0	11.0
2014-04-16	52 324	1 174	2.2	4.0	2.0
2014-05-18	53 124	375	0.7	25.0	12.0
2014-06-03	52 203	1 296	2.4	6.0	0.0
2014-06-19	51 028	2 471	4.6	0.0	0.0
2014-09-07	45 180	8 319	15.5	43.0	12.0
2014-10-25	53 475	24	0.0	0.0	0.0
2015-01-29	53 343	155	0.3	33.2	16.0
2015-03-18	53 485	13	0.0	5.0	0.0
2015-04-03	53 486	13	0.0	0.0	0.0

2015-04-19	53 484	15	0.0	24.6	0.0
2015-05-05	53 480	18	0.0	20.4	18.8
2015-07-08	53 180	319	0.6	0.0	0.0
2015-07-24	53 267	232	0.4	0.3	0.0
2015-08-25	53 029	470	0.9	0.0	0.0
2015-11-29	53 339	159	0.3	41.0	0.0
2016-01-16	53 489	9	0.0	0.0	0.0
2016-03-04	53 498	1	0.0	0.0	0.0
2016-04-21	53 286	212	0.4	17.0	20.0
2016-06-08	52 980	518	1.0	0.0	0.0
2016-09-28	53 348	151	0.3	0.0	0.0
2016-10-30	53 415	83	0.2	1.0	7.0
2016-11-15	53 482	16	0.0	6.0	0.0
2016-12-01	53 488	11	0.0	6.0	18.0
2016-12-17	53 492	6	0.0	4.0	0.0
2017-01-02	53 489	9	0.0	4.0	0.0
2017-01-18	53 477	22	0.0	3.0	1.0
2017-02-19	53 474	24	0.0	4.0	23.0
2017-03-07	53 465	33	0.1	0.0	18.0
2017-05-10	50 602	2 897	5.4	56.0	0.0
2017-08-14	49 228	4 270	8.0	33.0	24.0
2017-08-30	46 797	6 702	12.5	4.0	38.0
2018-01-21	53 485	13	0.0	4.0	124.0
2018-02-06	53 489	9	0.0	0.0	0.0
2018-03-10	53 495	3	0.0	0.5	0.0
2018-03-26	53 365	133	0.2	30.0	0.0
2018-05-13	48 508	4 990	9.3	68.0	25.0
2018-06-14	51 554	1 944	3.6	7.0	0.0
2018-08-17	50 971	2 527	4.7	5.0	31.0
2018-10-04	48 926	4 572	8.5	15.0	88.0
2018-12-23	51 872	1 626	3.0	4.0	51.0
2019-01-24	53 473	25	0.0	7.0	0.5
2019-05-16	53 381	117	0.2	0.0	0.0
2019-07-03**	52 375	1 123	2.1	7.0	26.0
2019-08-04	51 787	1 711	3.2	0.0	0.0
2019-09-21	53 371	127	0.2	0.0	0.0
2020-01-27	53 486	11	0.0	0.0	0.0
2020-04-16	53 465	33	0.1	64.0	0.0
2020-05-18	53 284	214	0.4	0.0	0.0
2020-08-22	53 232	266	0.5	0.0	0.0
2020-10-09	53 273	225	0.4	0.1	2.0
2020-11-26	53 458	40	0.1	33.0	0.0
2020-12-12	53 480	18	0.0	7.0	0.0
2021-01-13	53 478	20	0.0	23.0	58.6
2021-03-18	53 484	14	0.0	3.0	0.0
2021-05-05	53 432	66	0.1	19.0	0.0
2021-06-06	53 137	361	0.7	15.0	0.1
2021-09-26	53 332	166	0.3	0.0	0.0
2021-10-28	53 472	26	0.0	0.0	0.0
2021-11-13	53 490	8	0.0	0.0	0.0

2022-02-01	53 492	5	0.0	0.0	0.0

* (INTA, 2022)
** Normal water extent in the landscape, approximately 2 % water cover.
***Not the same date as event date
****Data from Punta Indio weather station and CHIRPS.

Appendix C: MATLAB code for frequency analysis, AMC, SCS-CN

```
%% Precipitation & Flood analysis in Punta Indio
% 100-year storm event
% 100-year flood event
% AMC vs. water extent
% Event precipitation vs. water extent

Table =readtable('PuntaIndio_prec_1980.xlsx'); % daily temp & prec.
TimeTable = table2timetable(Table);
precPunta = Table.prec_mm(1:15142); % prec from weather station
precCHIRPS=Table.CHIRPS(1:15142);   % prec from Punta Indio area
datesPunta=TimeTable.Date(1:15142); % has to be in date form in Excel
%% Mean monthly temperature in Punta Indio 1980-2021
tempPunta = Table.TempMed(1:15142);
for u =1:length(tempPunta)
    if tempPunta(u) ==-99.9
        tempPunta(u) =NaN;
    end
end
tempData=timetable(datesPunta, tempPunta);
monthlyavg = groupsummary(tempData, "datesPunta", "monthofyear", "mean");
mean_tempPunta=table2array(monthlyavg(:,3));
figure, plot(mean_tempPunta)
set(gca, 'xtick',1:12,...
    'xticklabel', {'Jan', 'Feb', 'March', 'April', 'May', 'June', 'July', 'Aug', 'Sep',...
    'Oct', 'Nov', 'Dec'})
ylabel('Mean Temperature °C')
title('Mean temperature 1980-2021')
%% Complete the missing precipitation Punta Indio data with the CHIRPS data
PrecPIandCHIRPS = precPunta;
 for  i =1:length(precCHIRPS)
        if precPunta(i) == -99.9
       PrecPIandCHIRPS(i)=precCHIRPS(i);
        end
 end
%% Calculate the 100 -year storm event
% with data from Punta Indio complemented with CHIRPS daily data
% since some days and years doesn't have rain record
% Find the maximum daily rainfall for every year
RainData = timetable(datesPunta, PrecPIandCHIRPS);
CHIRPSData =timetable(datesPunta, precCHIRPS);
YearMax = retime(RainData, 'yearly', 'max');

% Sort the maximum daily rainfall every year in descending order
MaxYearlyPrec = timetable2table(YearMax);
Prec_max_sorted=sortrows(MaxYearlyPrec,2,'descend');
MaxYearlyPrec_array=table2array(Prec_max_sorted(:,2));
% Make a normprobplot, read 100 year event from 0.99 y-axis
figure(1)
normplot(MaxYearlyPrec_array)

%% Normal distrubution over maximum daily rainfall event each year
tjoho = fitdist(MaxYearlyPrec_array, 'Normal'); % run in command window to obtain mu and
sigma.
mu2 = 77.9386;
sigma2= 30.9837;
y2 = normpdf(MaxYearlyPrec_array, mu2, sigma2);
figure(2)
plot  (MaxYearlyPrec_array, y2);
xlabel('Maximum daily precipitation for every year')
title('Normal distrubution curve of the maximum daily precipitation each year')
% Make histogram to see skewness right/left
figure (3)
histogram(MaxYearlyPrec_array, 13);
xlabel('Maxiumum daily precipitation per year (mm/day)')
ylabel('count')
```

```
title('Histogram')

 %%  precipitation per year (mm/year)
YearSum = retime(RainData, 'yearly', 'sum');
YearSum2 = retime(CHIRPSData,'yearly', 'sum');
SumYearlyPrec =timetable2table(YearSum);
SumYearlyPrec2=timetable2table(YearSum2);
Prec_sum_sorted =sortrows(SumYearlyPrec, 2, 'ascend');
SumYearly_array= table2array(Prec_sum_sorted(:,2));

figure (4)
plot(YearSum.datesPunta,YearSum.PrecPIandCHIRPS)
hold on
plot(YearSum2.datesPunta,YearSum2.precCHIRPS)
legend('Precipitation (Punta Indio & CHIRPS)', 'CHIRPS', 'Location', 'southeast');
title('Yearly precipitation') % rain data from CHIRPS and Weather station
xlabel('Years')
ylabel('mm/year')
% Normal distrubution
% pd = fitdist(SumYearly_array, 'Normal'); % run in command window to obtain mu and sigma.
mu = 1005;
sigma= 232.291;
y = normpdf(SumYearly_array, mu, sigma);
figure(5)
plot  (SumYearly_array, y);
xlabel('Yearly precipitation')
title('Normal distrubution curve of the yearly precipitation')
%% data from INTA, Instituto Nacional de Tecnología Agropecuaria
T =readtable('engine_agua2000-2022.xlsx');
TT = table2timetable(T);
agua = T.agua(1:132);
datesEngine=TT.date(1:132);
%% Flood / Superfical water extent frequency
agua_percent=(agua./53498)*100;
FloodData = timetable(datesEngine, agua_percent);
YearMaxFlood= retime(FloodData, 'yearly', 'max');

% sort the max flood extent (m2) in descending order
MaxYearlyFlood = timetable2table(YearMaxFlood);
Flood_max_sorted=sortrows(MaxYearlyFlood,2,'descend'); % no data 2012
MaxYearlyFlood_array=table2array(Flood_max_sorted(:,2));
% Make a normprobplot, read 100 year event from 0.99 y-axis
figure(5)
normplot(MaxYearlyFlood_array)
%% Is the Pampa deprimida climate defined as growing season all around the year?
% Look at the amount of days each year with a temperature under 6 degrees.
% Temperature-Med data is from Punta Indio Weather station

TemperatureMed = TimeTable.TempMed(1:15476);
DaysUnder6 = TemperatureMed ;

for g = 1:length(DaysUnder6)
    if not(TemperatureMed(g) ==  -99.9) && TemperatureMed(g) <= 6
                DaysUnder6(g) = 666;
    end
end
numberofdaysunder6 = sum(DaysUnder6==666,'all');
% in avarage only approx 6 days a year with lower mean temp than 6degrees.
% --- > assume all days a year are 'growing season' for the AMC classification

%% SCS-CN and AMC
% Land use for area around Don Joaquín and El Amanecer
% is Grass lands/pasture and the hydrologic the soil group is
% from field measurements (decided upon infiltration measurements) group A,
% However since it is known that the soils consists of finer texture ->
% soil group C is considered.

% The CN value for the area around Don Joaquín and
% El Amanecer is ..... -> 74
% the rainfall depth is the cumulative rainfall 6 days prior the event
% plus the rainfall that date

CurveNumber_AMC2 = 74;
CurveNumber_AMC1 = CurveNumber_AMC2 /( 2.281 - 0.01281* CurveNumber_AMC2);
CurveNumber_AMC3 = CurveNumber_AMC2 /( 0.427 + 0.00573* CurveNumber_AMC2);

%%Event rainfall
```

```
EventRainfall=zeros(1,132);

I=zeros(1,132);
for v=1:length(datesPunta)
    for b = 1:length(datesEngine)
        if datesEngine(b) == datesPunta(v)
           [EventRainfall(b), I(b)] = max([PrecPIandCHIRPS(v) PrecPIandCHIRPS(v-1)...
            PrecPIandCHIRPS(v-2) PrecPIandCHIRPS(v-3) PrecPIandCHIRPS(v-4)]);
         end
     end
end
%% 5-days AMC before event precipitation
AMCevent= zeros(1,132);
for w=1:length(datesPunta)
   for u=1:length(datesEngine)
         if datesEngine(u) == datesPunta(w)
         AMCevent(u) = PrecPIandCHIRPS(w-I(u))+ PrecPIandCHIRPS(w-I(u)-1)+PrecPIandCHIRPS(w-
I(u)-2)...
             +PrecPIandCHIRPS(w-I(u)-3)+PrecPIandCHIRPS(w-I(u)-4);
         end
   end
end

%Transpose
AMCevent_T=AMCevent.';
%round
AMCevent_T_round=round(AMCevent_T);

% replace zeros by 1 to be able to plot the circles in the scatter plot
AMCevent_T_round_1=AMCevent_T_round;
for j = 1:length(AMCevent_T_round)
     if AMCevent_T_round(j)==0
        AMCevent_T_round_1(j)=1;
     end
end
%% Divide the antecedent moisture  into AMC classes 1, 2 or 3

AMCclasses = AMCevent_T;

for d =1:length(AMCevent)
    if AMCevent(d) <35.5
        AMCclasses(d) = 1;
    elseif AMCevent(d) < 53.3
        AMCclasses(d) = 2;
    else  % over 53.3 mm rain
        AMCclasses(d) = 3;
    end
end
% make color string to tell the season
Season=discretize(month(datesEngine), 1:3:13, 'categorical', {'summer','autumn', 'winter',
'spring'});
figure(6)
scatter(datesEngine, AMCevent_T, agua_percent *20, Season, 'filled')
hold on
legend('Color: Season')
xlabel('years')
ylabel('AMC [mm/5 days]')
title('Water extent (sizes of circles) depending on AMC')
hold off
%% Water extent and event prec
Season=discretize(month(datesEngine), 1:3:13, 'categorical', {'summer','autumn', 'winter',
'spring'});
figure(7)
scatter(datesEngine, EventRainfall_T, agua_percent *20, Season, 'filled')
hold on
legend('Color: Season')
xlabel('years')
ylabel('Event precipitation [mm/day]')
title('Water extent (sizes of circles) depending on event precipitaion')
hold off
%% Water extent due to event prec and AMC
Season=discretize(month(datesEngine), 1:3:13, 'categorical', {'summer','autumn', 'winter',
'spring'});
figure(8)
scatter(datesEngine, EventRainfall_T+AMCevent_T, agua_percent *20, Season, 'filled')
hold on
legend('Color: Season')
```

```
xlabel('years')
ylabel('Event precipitation + AMC [mm/6 days] ')
title('Water extent (sizes of circles) depending on event precipitaion and AMC')
hold off
%% replace zeros by 1 to be able to plot the circles in the scatter plot
EventRainfall_T=EventRainfall.';
EventRainfall_T_1=EventRainfall_T;
for j = 1:length(EventRainfall)
     if EventRainfall_T(j)==0
        EventRainfall_T_1(j)=1;
     end
end

%% retention
S = zeros(1,132);

for u = 1:length(AMCevent)
    if AMCclasses(u) == 1
        S(u) = (25400/CurveNumber_AMC1) -254;
    elseif  AMCclasses(u) == 2
        S(u) = (25400/CurveNumber_AMC2) -254;
    else
        S(u) = (25400/CurveNumber_AMC3) -254;
    end
end
% Surface runoff
SurfaceRunoff = zeros(1,132);
for r =1:132
    if S(r) ==(25400/CurveNumber_AMC1) -254 && EventRainfall(r) < 33 %33 mm is initial
abstraction
          SurfaceRunoff(r) = 0;
    elseif S(r) ==(25400/CurveNumber_AMC1) -254 && EventRainfall(r) > 33 %33 mm is initial
abstraction
        SurfaceRunoff(r) = ((EventRainfall(r) - 0.2*S(r))^2)/ (EventRainfall(r)+0.8*S(r));
    elseif  S(r) == (25400/CurveNumber_AMC2) -254 && EventRainfall(r) < 15 %15mm is initial
abstraction
        SurfaceRunoff(r) = 0;
    elseif S(r) == (25400/CurveNumber_AMC2) -254 && EventRainfall(r) > 15 %15mm is initial
abstraction
        SurfaceRunoff(r) = ((EventRainfall(r) - 0.2*S(r))^2)/ (EventRainfall(r)+0.8*S(r));
    elseif S(r) == (25400/CurveNumber_AMC3) -254 && EventRainfall(r) < 5 %5mm is initial
abstraction
        SurfaceRunoff(r) = 0;
    else
        SurfaceRunoff(r) = ((EventRainfall(r) - 0.2*S(r))^2)/ (EventRainfall(r)+0.8*S(r));
    end
end
%%  SCS-CN  template
RainSCS=1:100; % 1 - 100 mm
AMCclasses_scs= randi([1 3],1,100);

S_SCS=zeros (1,100);
 for h=1:100
    if AMCclasses_scs(h) == 1
        S_SCS(h) = (25400/CurveNumber_AMC1) -254;
    elseif  AMCclasses_scs(h) == 2
        S_SCS(h) = (25400/CurveNumber_AMC2) -254;
    else
        S_SCS(h) = (25400/CurveNumber_AMC3) -254;
    end
end
SurfaceRunoff_scs=zeros(1,100);
for g=1:100
    SurfaceRunoff_scs(g) = ((RainSCS(g) - 0.2*S_SCS(g))^2)/ (RainSCS(g)+0.8*S_SCS(g));
end

%%
figure(9)
scatter(EventRainfall, SurfaceRunoff, agua./15, S, 'filled')
xlabel('Event precipitation [mm]')
ylabel('Surface runoff [mm]')
text(10, 110, 'Sizes of the circles represent the water extent in the landscape')
title('SCS-CN')
hold on
plot(RainSCS, SurfaceRunoff_scs, '.');
hold off
```

```
%% prec relation to water extent
figure (10)
% water extent as percetnage

scatter(agua_percent, AMCevent+EventRainfall, 'o');
xlabel('Water extent [%]')
ylabel('Antecedent Moisture Condition + Event precipitation [mm/6 days]')
hold on
plot([0 16],[16 16]) % 16 [mm/h] is infil. capacity media loma
plot([2 2],[0 160])
txt = {'Infiltration capacity 16 mm/h'};
txt2 = {'2% water extent = water in waterways'};
legend('Events', 'location', 'best');
title('Precipitation effect on water extent')
text(9.5, 21,txt)
text(2.1, 130,txt2)
hold off
```

Appendix D: Runoff coefficient

The runoff coefficient was calculated by dividing the estimated surface runoff by the event precipitation from the three scenarios with the different curve numbers, see Figure 32.

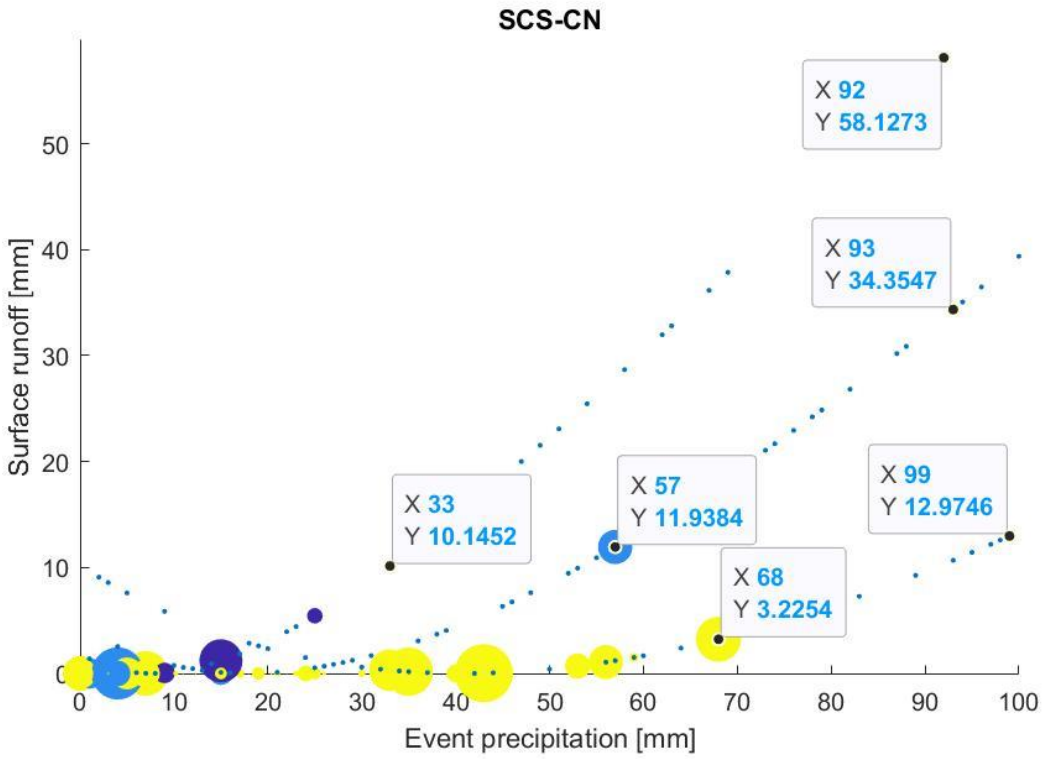

Figure 32: The estimated surface runoff [mm/day] from the precipitation events [mm/day] according to the SCS-CN method. The dotted lines are the curve numbers for AMC class 1, 2 and 3 (CN: 56, 74 and 87) and the filled circles are actual rain events with corresponding water extent (size of circle).

Appendix E: Python console code in QGIS to obtain Landsat-8 satellite Imagery 7th of September 2014 and 1st of February 2022

```
import ee
from ee_plugin import Map

landsat8=  ee.Image('LANDSAT/LC08/C02/T1_L2/LC08_224084_20140907');
landsat81= ee.Image('LANDSAT/LC08/C02/T1_L2/LC08_224085_20140907');
landsat82= ee.Image('LANDSAT/LC08/C02/T1_L2/LC08_224085_20140201');
landsat83= ee.Image('LANDSAT/LC08/C02/T1_L2/LC08_224084_20190703');
```

```
Map.setCenter(-57.65, -35.26, 10);

mndwi=landsat8.normalizedDifference(['SR_B3','SR_B6']);
mndwi2=landsat83.normalizedDifference(['SR_B3','SR_B6']);
mndwi3_without_green=landsat8.normalizedDifference(['SR_B3','SR_B6']);

Map.addLayer(mndwi,{'min':-0.1, 'max':0.1, 'palette':['green', 'blue']},
'mndwi2014', True)
Map.addLayer(mndwi2,{'min':-0.1, 'max':0.1, 'palette':['green', 'blue']},
'mndwi2019', True)
Map.addLayer(mndwi3_without_green,{'min':-0.1, 'max':0.1,
'palette':['white', 'blue']}, 'mndwi20140907', True)

#Define the visualization parameters.
vizParams = {
  'bands': ['SR_B4', 'SR_B3', 'SR_B2'],
  'min': 8000,
  'max': 13000,
  'gamma': [1.4]
};

Map.addLayer(landsat8, vizParams, 'rgblue');
Map.addLayer(landsat81, vizParams, 'rgblue1');
Map.addLayer(landsat82, vizParams, 'rgblue2022');
```

Appendix F: Google Earth Engine script for MNDWI with Landsat 8

Example script from the code editor in Google Earth Engine for visualizing water extent with MNDWI and Landsat-8.

```
Map.centerObject(table, 7);

Map.addLayer(table, {} , 'RegiónDeprimida')

var start = '2014-09-01';
var end   = '2014-09-15';

// Load landsat 8 surface reflectance
 var landsat8 = ee.ImageCollection("LANDSAT/LC08/C02/T1_L2")
     .filterDate(start, end)
     .filterBounds(geometry1) // Region deprimida
     .filterMetadata("CLOUD_COVER","Less_than", 10) //
print(landsat8)
var landsat8_1 = landsat8.median()
print(landsat8_1, 'landsat8')

 // A normal photo RGB - visualization parameter
var RGBvisualize = {bands: ["SR_B4", "SR_B3", "SR_B2"],
  min: 8000, // Range: (min max) from 98% Custom
  max: 13000,
  gamma: 1.4};

var MNDWI= landsat8_1.normalizedDifference(['SR_B3', 'SR_B6']);

print(MNDWI, 'MNDWI');

var MNDWIvisualize=  {min: -0.1, max: 0.1, palette: ['green', 'blue']};

var MNDWIclip = MNDWI.clip(table)
var landsat8_1clip= landsat8_1.clip(table)

Map.addLayer(MNDWIclip, MNDWIvisualize, 'MNDWI');
```

```
Map.addLayer(landsat8_1clip, RGBvisualize, 'satimageDjEa')

var DonJoaquin = ee.FeatureCollection('users/linneasvard/Perimetro');
 Map.addLayer(DonJoaquin, {}, 'DonJoaquin');
var ElAmanecer = ee.FeatureCollection('users/linneasvard/PerimetroEA');
 Map.addLayer(ElAmanecer, {}, 'ElAmanecer');
var channels = ee.FeatureCollection('users/linneasvard/canales_3');

Map.addLayer(channels, {color: '0000FF'}, 'channels');
var riosamborombon =
ee.FeatureCollection('users/linneasvard/rioSamorombon');
Map.addLayer(riosamborombon, {color: '00FFFF'}, 'RioSamborombon');
```

Appendix G: Histogram of maximum daily precipitation per year

In Figure 33 is the distribution and frequency of yearly maximum daily precipitation for Punta Indio. The data is not normally distributed why a regression analysis for testing trend is not an option. The data is based on both CHIRPS and Punta Indio weather station data. There is no significant trend of increased maximum daily precipitation per year in Punta Indio with time (p-value > 0.05, Mann-Kendall test).

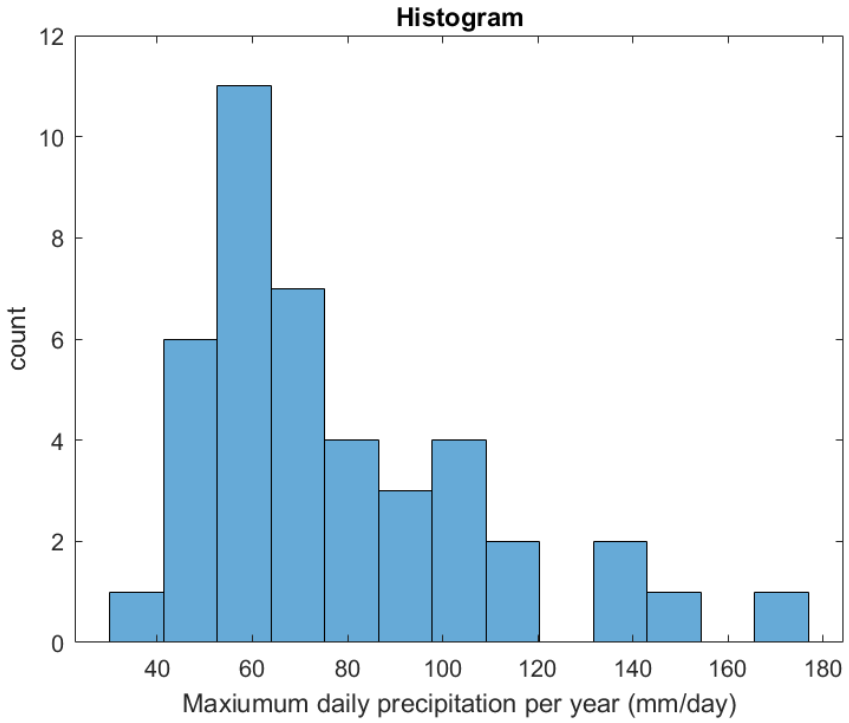

Figure 33: Distribution of yearly maximum daily precipitation series from Punta Indio. The precipitation data is collected at Punta Indio weather station and from CHIRPS. The data is right-skewed.

Appendix H: 100-year flood event

The maximum water event recorded from satellite analysis since the year 2000 (2012 excluded) covers 16% of the surface. According to the normal probability plot, see Figure *34*, an event with 1% exceedance probability year (100-year flood) would cover 6000 m^2 with water which is about 11% of the area. A 'normal' water extent is around 2 % (2019-07-03).

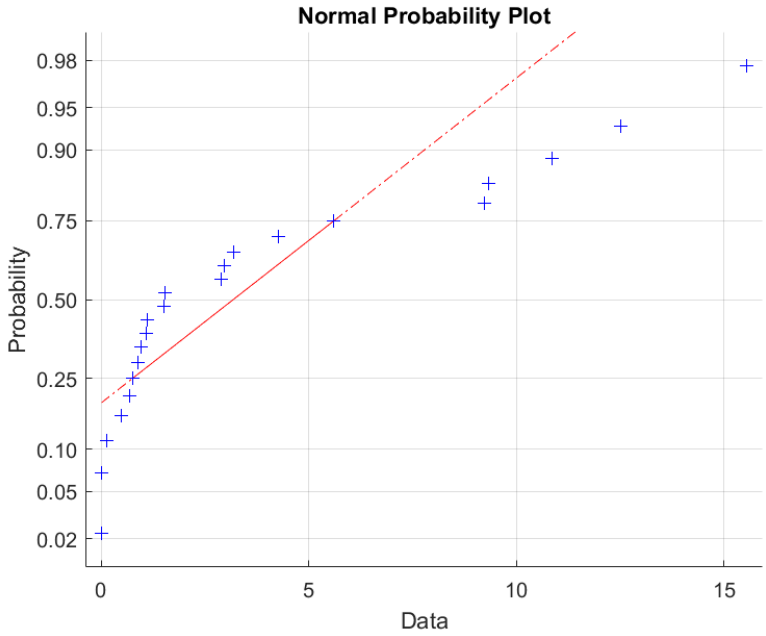

Figure 34: Normal probability plot over the yearly largest water extents series in the Don Joaquín and El Amanecer area since 2000 (no data 2012). The total area is 53498 m^2. On the x-axis is the area of water (blue, in %) from the MNDWI mosaic maps extracted from the satellite images.

Appendix I: Normal water extent in the landscape

A normal percentage of water in the area could be assumed to be around 2%, see Figure 35. The 3rd of July 2019 water was observed in the perennial stream network but not in the flood plains.

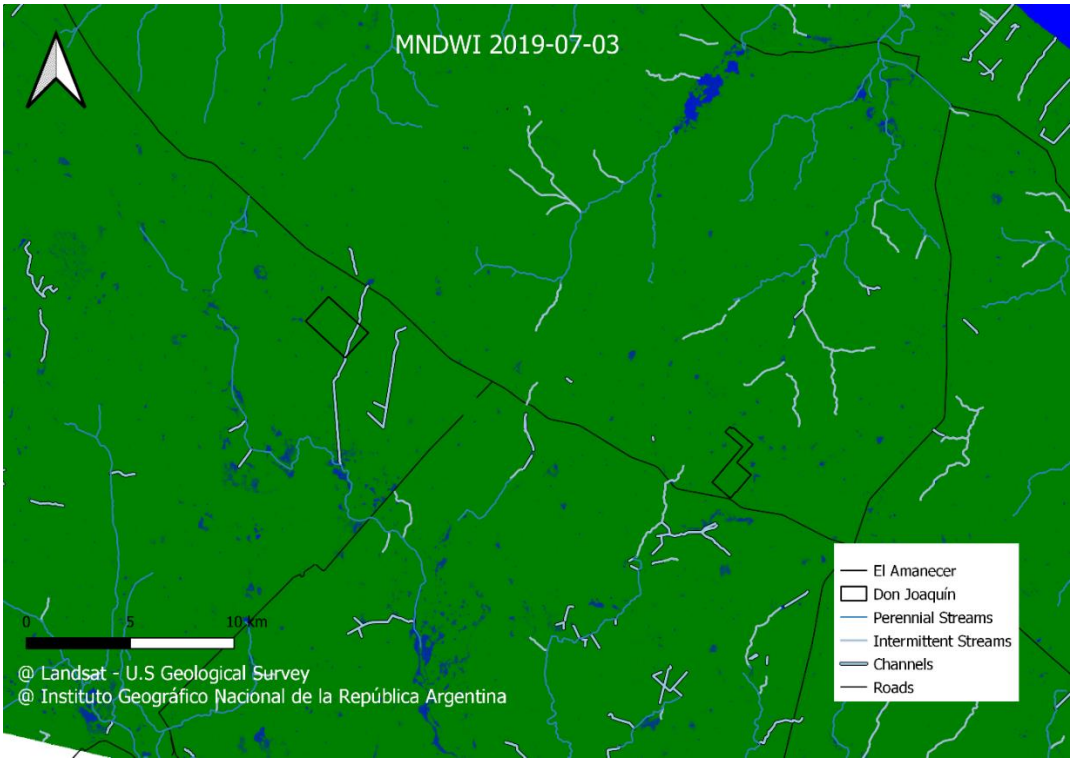

Figure 35: 2 % water (blue) coverage in the landscape around the two field study sites Don Joaquín and El Amanecer. The stream network is shown with blue continuous lines.